AN EXPERIMENTAL INVESTIGATION OF SERRATED FLOW
IN AN ALUMINUM-MAGNESIUM-SILICON ALLOY

By

Paulo Roberto Cetlin

A Thesis Presented to the Graduate Council of the
University of Florida
in Partial Fulfillment of the Requirements for the
Degree of Master of Science in Engineering

UNIVERSITY OF FLORIDA

1972

ACKNOWLEDGEMENTS

I would like to thank above all the chairman cf my
advisory committee, Dr. R. E. Reed-Hill, whose guidance,
support and patience were essential in the completion of
this work. Thanks are also due to the remaining members of
the committee, Dr. E. D. Verink, Jr., Dr. C. A. Ross and Dr.
C. S. Hartley, whose expertise in experimental stress analy-
sis techniques was also fundamental in this investigation.

I am grateful for all help received from the faculty,
staff and fellow graduate students in the Department of
Metallurgical and Materials Engineering, as well as from
Dr. F. N. Rhines, Chairman of the department.

Appreciation is also extended to my fellow students of
the mechanical metallurgy group, Dr. A. T. Santhanam, Mr.
S. N. Monteiro and Mr. A. M. Garde, for their help and dis-
cussions in many points in this work. The cooperation of
Mr. P. Pinheiro and Dr. R. W. Gould was of great value to
me. I would also like to thank Mr. C. F. Pittella, Mr. E.
M. de P. e Silva, Mr. E. O. de Lima and Dr. J. T. Veado for
their constant encouragement and support.

I am indebted to the United States Atomic Energy Com-
mission for its financial support of this investigation,
through project ORO-AT-(40-1)-3262.

TABLE OF CONTENTS

LIST OF TABLES

vi

LIST OF FIGURES

Abstract of Thesis Presented to the Graduate Council of the
University of Florida in Partial Fulfillment of the Require-
ments for the Degree of Master of Science in Engineering

AN EXPERIMENTAL INVESTIGATION OF SERRATED FLOW
IN AN ALUMINUM-MAGNESIUM-SILICON ALLOY

By

Paulo Roberto Cetlin

March, 1972

Chairman: Dr. Robert E. Reed-Hill
Major Department: Metallurgical and Materials Engineering

A method involving photoelastic coatings, that depicts

local changes in strain in the gage length of specimens by

changes in color, was used. The strain behavior associated

with different types of serrations was studied and recorded

in a movie. It was confirmed that Type A serrations do in-

deed correspond to the formation of deformation bands at one

end of the specimens and their propagation to the other end.

Secondary serrations were observed during these serrations,

and were found to correspond to localized strain in the

specimens during the early stages of deformation. Type B

serrations were identified with the formation of bands that

do not propagate; these can form at random in the specimen,

in the same region where other bands nucleated before, or

successively ahead of each other. A decrease in the spring

constant of the testing machine makes these bands propagate

very fast over small distances, after their formation.

INTRODUCTION

The curves obtained on recorders of common tensile testing machines are usually load-time ones, and are often smooth. However, some materials develop load-time curves with irregularities when tested under certain conditions. These irregularities can also be observed in load-elongation curves and other kinds of plots, but their shapes would be different for plots involving elongation or strain as one axis. When such phenomena are present, one says that the material exhibits discontinuous flow, serrated yielding or serrated flow. The irregularities are called serrations. For example, this happens in commercial purity aluminum[1] and several of its alloys,[2-4] and also for other materials.[5,6] The following factors affect this phenomenon: strain rate and temperature of test, grain size, composition and heat treatment of the material, testing machine stiffness and, finally, the level of strain in the specimen.

Substitutional alloys will be treated in this investigation. For these materials, serrated flow has been attributed to an interaction between the solute atoms and dislocations, through vacancy assisted diffusion.[7] Other theories[8,9] consider serrated yielding as a result of an inverse relationship between the flow stress and strain rate. Higher

1

strain rates would correspond to lower flow stresses, and serrations would result from mechanical instability of the material.

However, none of these theories can fully account for all experimental results that have been obtained on serrated flow. Thus, it seems obvious that, although they may have correct aspects or even have the right general approach, there is more to the problem than they imply.

It is our belief that further understanding of serrated flow can be obtained only through new and better experimental data about the phenomena in question, especially about the ones that cannot be explained by the current theories. Thus, the purpose of this work is to obtain some new experimental evidence about serrated yielding.

The material used for this investigation was a commercial aluminum-magnesium-silicon alloy, also known under the name of aluminum 6061 alloy. This material was chosen because it presented profuse serrated flow,[10] and because it is also widely used.

Each serration in a load-time diagram, for example, corresponds to a localized strain in the gage length of the specimen being tested. Up to now, the study of this local strain behavior has been done by clamping extensometers to the specimens,[3,5] attaching strain gages to its gage length,[1] and by visual observation of these local strains[11] whenever the deformation associated with the serrations was big enough to cause surface markings. We have endeavoured to

obtain a new direct method for the observation of the local-
ized strains associated with different types of serrations
reported in the literature.[2,3,5,6] This method should be
used to show what would be the difference between these
types. In other words, it should be used to recognize new
features associated with serrated flow and to scrutinize
concepts already introduced in the literature.

Some other results were also obtained during the pro-
cess of obtaining the desired serration shapes in aluminum
6061 alloy. They shall be reported in this work.

A new method fulfilling the above requirements was in-
deed developed. Furthermore, it was used to obtain some
new aspects of serrated flow, and permitted a broad evalu-
ation of previous results. This is reported in detail in
the next chapters.

CHAPTER I

PREVIOUS INVESTIGATIONS: THEIR ACCOMPLISHMENTS AND LIMITATIONS

1.1. The Phenomenon

The first report on serrated yielding was made by LeChatelier[12] (1909) in mild steel, in the range of temperatures 80-250°C; in 1923, Portevin and LeChatelier[13] communicated a similar phenomenon in duraluminum (Al - 4.8 percent Cu) at room temperature. After these works, many other occurrences of the phenomenon were reported, as is the case of 70/30 brass at 450°C, and nickel at 300°C[14] (1941).

Lüders,[15] in 1860, reported the appearance of large-scale markings on the surface of strained mild steel sheet. These markings were later studied systematically by Hartmann,[16] and are well known as "Lüders lines," stretcher strains, or Hartmann or Piobert lines. Portevin and LeChatelier[13] also reported that the serrated curves they obtained were characterized by the appearance of Lüders lines on the surface of their specimens, and that each oscillation of stress was accompanied by propagation of the markings along the specimen.

The next important contribution was due to McReynolds[1] (1949), who worked with commercial purity aluminum, high purity aluminum and Al-Cu alloys. His work was performed with a dead-weight loading apparatus, and strain was recorded by means of several resistance strain gages attached to different regions along the gage length of the tensile specimen. A typical stress-strain curve obtained is shown in Fig. 1, for commercial purity aluminum. His conclusions point out that:

- High purity aluminum does not present serrated yielding. Therefore, impurities are necessary for discontinuous flow.

- There is always some smooth deformation before the initiation of serrated flow. This pattern has been found, in fact, for almost all substitutional alloys exhibiting serrated yielding.

- The steps in the curve were found to be the result of successive propagation of waves of plastic deformation along all or part of the specimen length; there is practically no plastic strain between the occurrence of these waves. Under varying conditions, waves may be either very sharp or extended and velocities range from a few millimeters to around 100 cm/sec.

- At a given strain rate, the phenomenon is always observed in a fixed temperature range, for each material. The stress-strain curves tend to be smooth outside this interval.

By now, it should be pointed out that serrated yielding can be observed in interstitial and substitutional solid solutions, in single crystals and polycrystals. We shall center our attention on polycrystalline substitutional solid solutions, though reference to other systems shall be used whenever necessary.
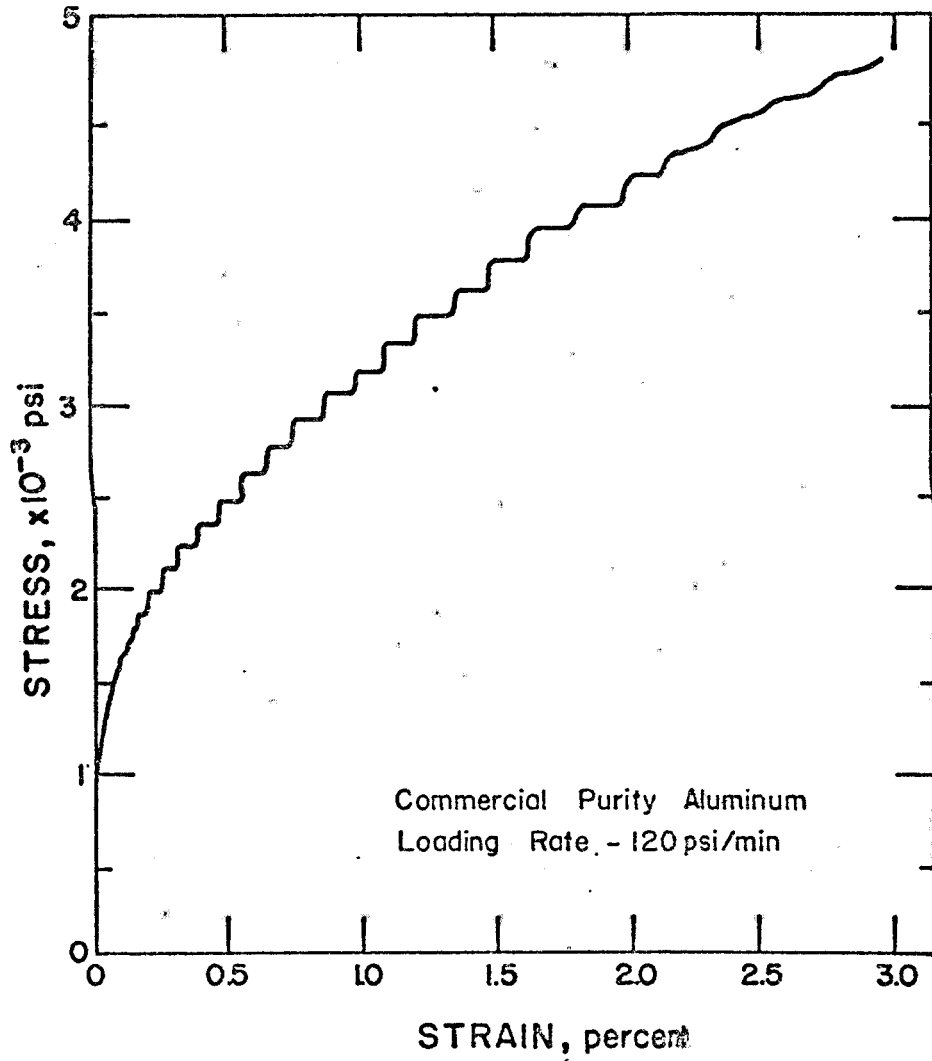
Fig. 1. Typical stress-strain curve for dead-weight loading of commercial purity aluminum.[1]

Lubahn,[10] working with aluminum 6061 alloy strained in a hard machine, indicated that the discontinuous flow exhibited different characteristics under different conditions of strain rate, amount of strain and heat treatment. In his work, he used solution treated specimens aged for different times and then tested. Figure 2, for example, shows schematically four of the curves obtained. Finally, he associates serrated yielding with the simultaneous occurrence of aging and straining in the material, that shall be called dynamic strain aging from now on. In a later paper[4] Lubahn analyzed dynamic strain aging in a broader sense, and concluded that:

- Dynamic strain aging occurs only in an interval of temperature, and its effects are most pronounced at some intermediate temperature in this interval.

- For the same material, four effects are maximized at this temperature:

    a. a yield point tends to appear in the material,

    b. the material is strengthened,

    c. discontinuous yielding is present, and

    d. the strain rate sensitivity of the material is exceptionally low.

The work of Russel[17] with copper-tin alloys confirmed Lubahn's assertion that the type of serration depended on many factors, among them, strain. Russel identified two distinct types of serrations for tests in a hard machine and named them Type A and Type B. They are shown in Fig. 3, and we shall also use this notation. Figure 4 shows that for a
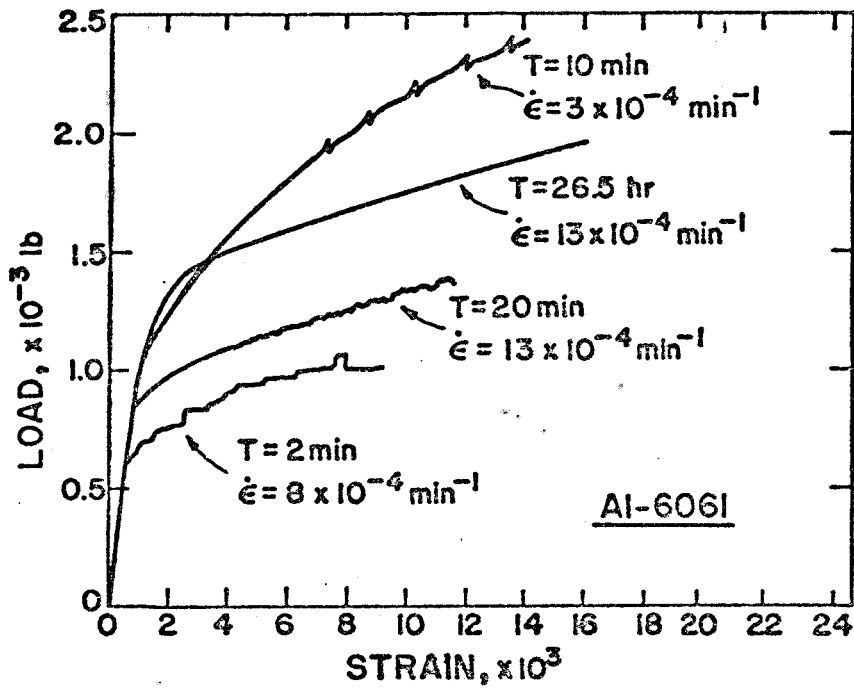
Fig. 2. Influence of heat treatment, strain rate and amount of strain on serrated flow of Al 6061 alloy. T = aging time at room temperature after solution treating and quenching.[10]
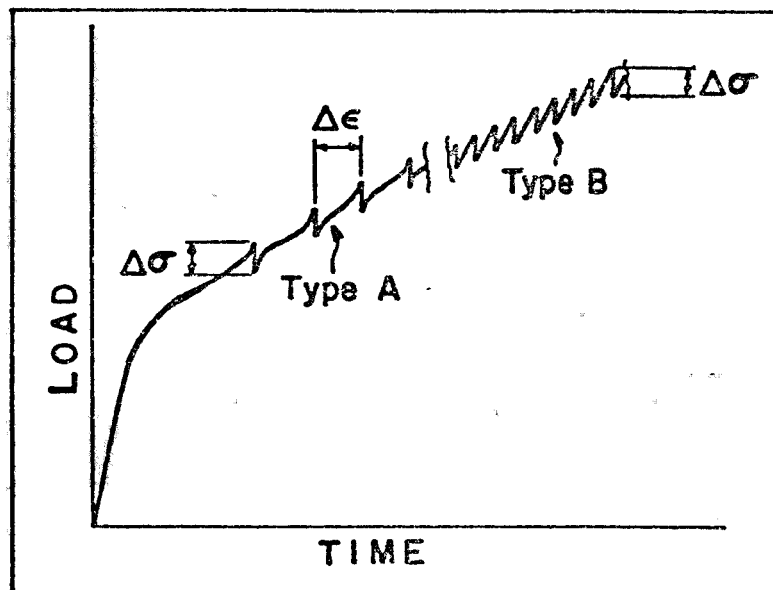
Fig. 3. Type A and Type B serrations.
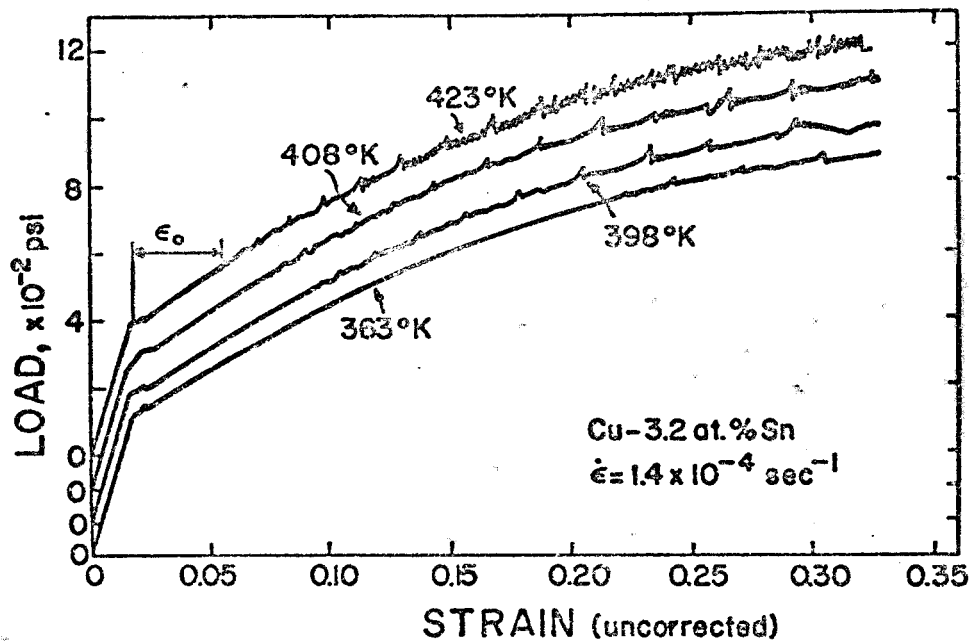
Fig. 4. Influence of temperature on serrated yielding.[17]

given strain rate, the type of serrated yielding depends on the temperature. Besides, as the temperature is increased, the smooth initial part of the curve decreases, and Type A serrations slowly transform themselves into Type B serrations, that also start earlier.

Another important feature in Russel's work is the observation that grain size also influences serrated flow. If $\Delta\sigma$ is the load drop for both Type A and Type B serrations (Fig. 3), it was observed that for the same level of strain, $\Delta\sigma$ increased with grain size. Besides, according to his concepts, Type A serrations would correspond to the successive nucleation (at the peaks) and propagation (in the region between peaks) of a deformation band along the gage section, while Type B serrations would correspond again to a band sweeping the gage section, but in a discontinuous, jerky way.

Concerning Type B serrations, other authors[18] have also associated it with the random nucleation of deformation bands along the gage section.

One can now summarize the factors that affect serrated yielding: level of strain, tensile apparatus mechanical characteristics, temperature, strain rate, grain size, heat treatment and composition. Some of these factors are deeply interrelated, but we shall try to analyze in greater detail each one separately.

1.1.1. The Effect of Strain

The effect of strain most easily perceived is that it can cause a change in the character of the serrations.[1,5,17,18] Figure 1, for example, shows that the strain associated with each step increases with the total strain. Figure 4 shows that in a test performed in a hard machine, an increase in strain may cause a change from smooth flow to Type A serrated flow, which in turn may change to Type B serrated flow. The curve for 423°K is a very good example. Munz and Macherauch[5] have in fact observed five different regions of serrated flow in a single load-time curve for α-brass. However, these observations are strongly temperature and strain rate dependent.

If $\Delta\sigma$ is the load drop at each Type A serration, and $\Delta\varepsilon$ is the strain between serrations (Fig. 3), it has been observed that both $\Delta\sigma$ and $\Delta\varepsilon$ increase with strain.[3,17] Figures 5 and 6 illustrate this behavior for aluminum 6063 alloy.[3] In the case of Type B serrations, it has also been observed that the load drops increase with strain.[19]

Another effect that has also been reported as a result of strain is the establishment of strain gradients along the gage section[3] as a result of Type A serrated flow. First, deformation bands tend to start at the same end of the gage section of the tensile specimen.[3,5] They also cause more strain in the opposite end of the specimen, where they die away. The effect is cumulative, so that the gradient keeps
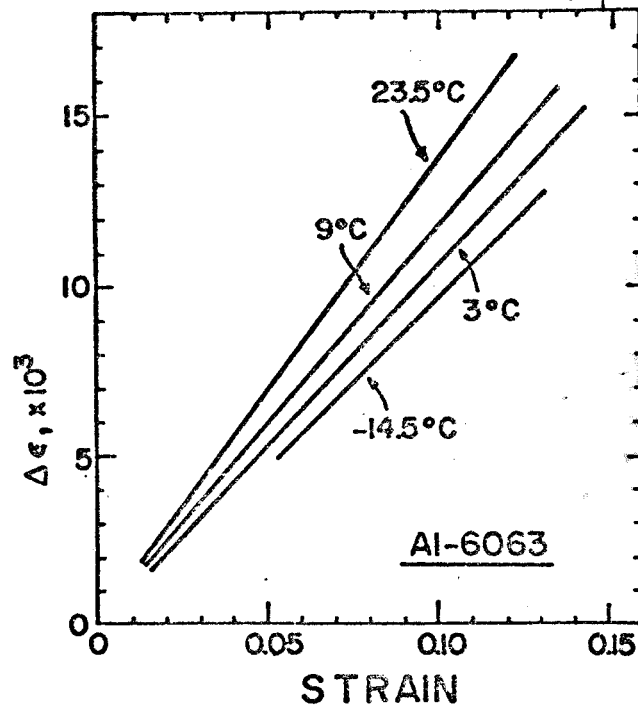
Fig. 5. The effect of strain and temperature on the strain between two successive Type A serrations.[3]
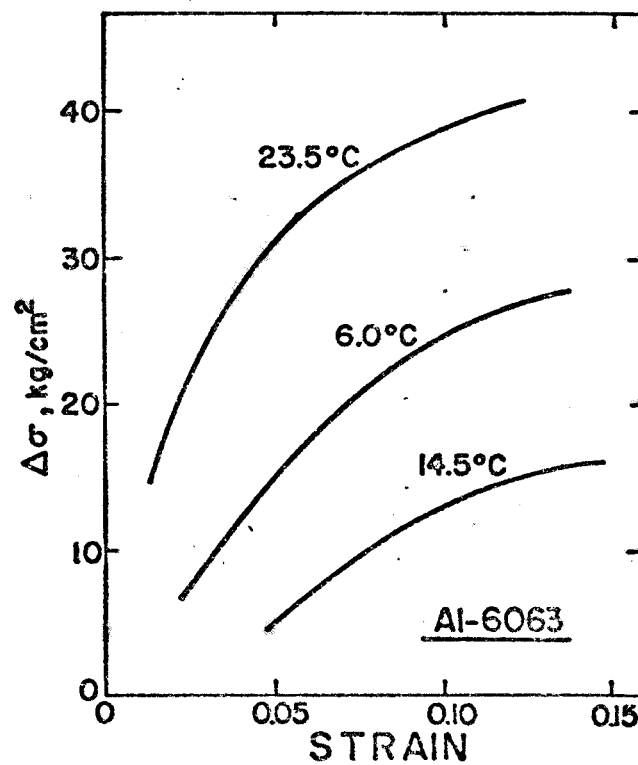
Fig. 6. The effect of strain and temperature on the load drop of Type A serrations.[3]

increasing. This is shown in Fig. 7, where the strain is plotted as a function of distance along the gage section, for different average strains.

1.1.2. The Effect of the Mechanical Characteristics of the Tensile Apparatus

The curve shown in Fig. 1 is typical for serrated flow resulting from straining in a "soft" dead-weight loading machine. If one now considers a relatively rigid, "hard" machine, serrations have the typical appearance shown in Fig. 4.

Concerning the behavior of commerical purity aluminum, Rosen and Bodner[20] have found that an increasing "hardening" of a soft machine tended to make the serrations less and less obvious, and finally obtained practically smooth curves for a regular, hard, Instron machine.

Considering now Al-Cu alloys, one finds a somewhat different behavior: an alloy of Al - 0.5 percent Cu strained in a soft machine[1] showed the typical stepped curve. However, another alloy Al - 1.0 percent Cu strained in an Instron machine presented load drops characteristic of this type of equipment.[21]

One may conclude that serrated flow does not depend only on the properties of the material being tested, but also on the mechanical characteristics of the loading apparatus.
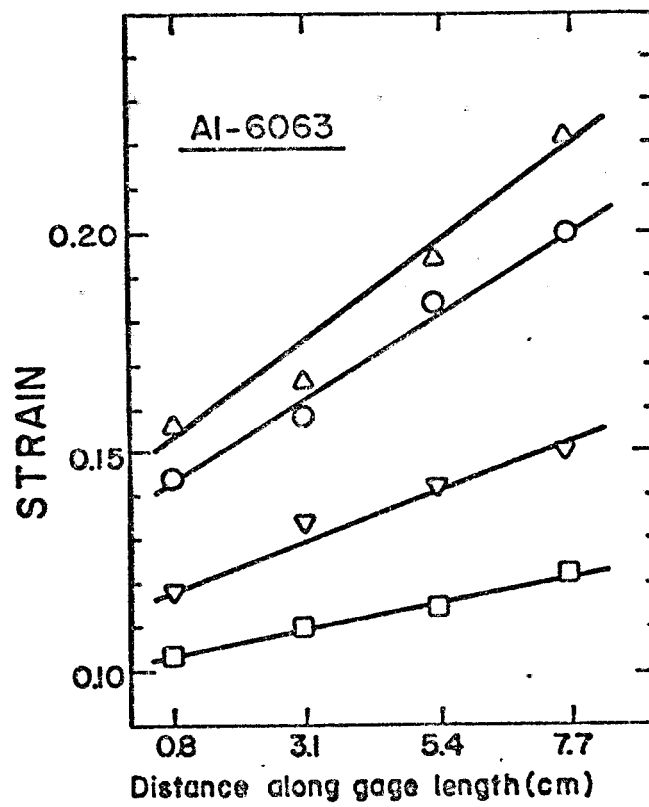
Fig. 7. The variation in strain along the gage length
for various mean strains.[3]

1.1.3. The Effect of Temperature

As it has been stated previously, serrated yielding in a given material occurs only in a certain range of temperatures. Both below and above this range one obtains smooth curves.[1,5,6]

In a soft machine, a change in temperature does not seem to change the character of the serrations.[1] However, when a material is strained in a hard machine, the temperature has a very big influence on the appearance of the curve. One can pick up as a prototype of this behavior the Cu - 1.09 at. percent In alloy discussed by Brindley and Worthington,[6] shown in Fig. 8. In this case, still another kind of serration is identified, the so-called Type C. As the temperature increases, serrations of Type A start appearing earlier and earlier, and finally Type B serrations also start appearing at large strains. As the temperature is further raised, Type B serrations start earlier, and end up covering the whole curve. Finally, Type C serrations start in the same way described before for Type B, then take over the whole curve and disappear, leaving a completely smooth curve at high temperature. Thus, at some temperatures, certain types of serrations might be completely missing. For example, in the 573°K curve of Fig. 8, one has no Type A serrations. A behavior very similar to this was also observed for α-brass.[5]
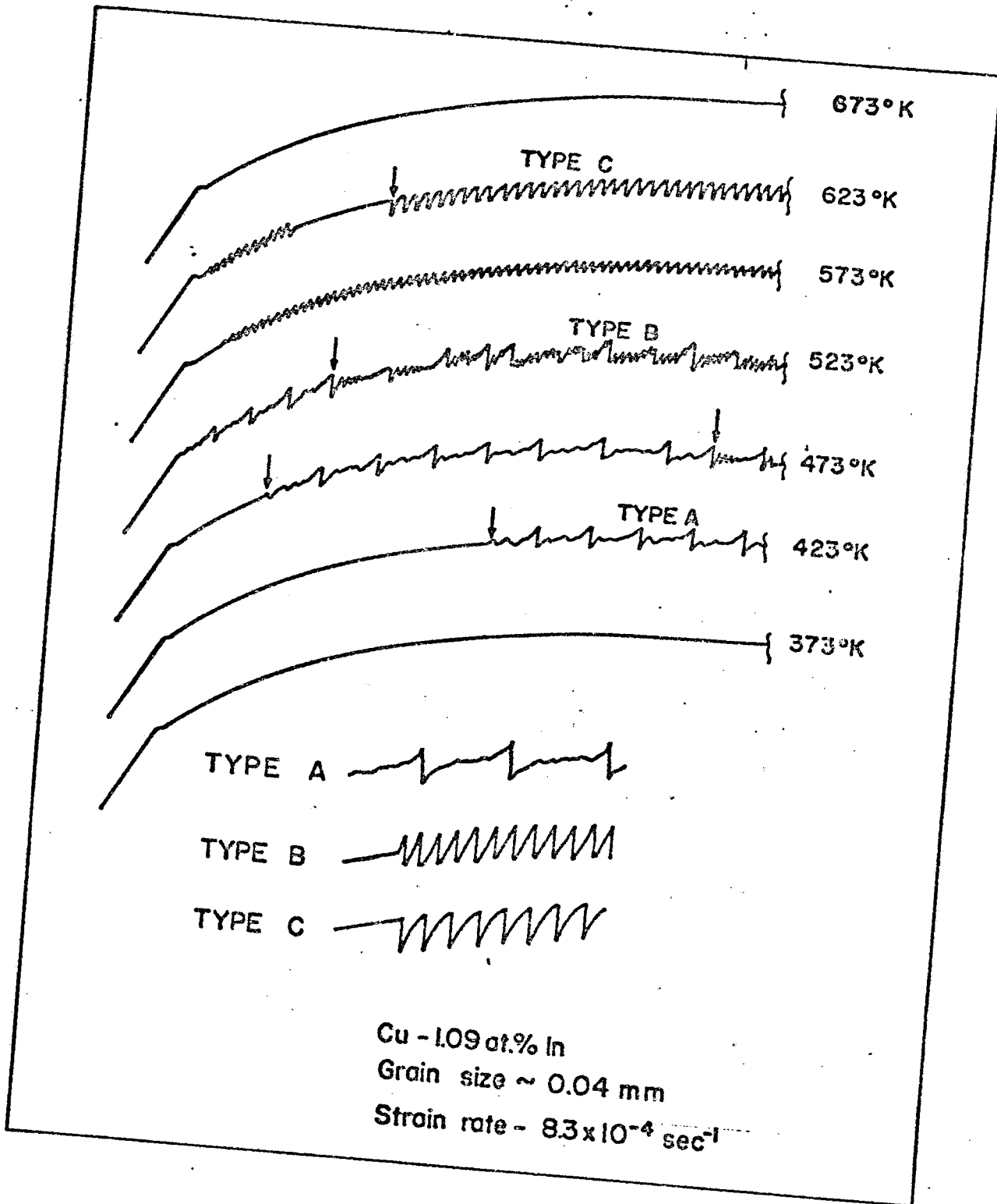
Fig. 8. The influence of temperature on the presence of serrations in a Cu-In alloy.6

Very often stress-strain curves exhibit continuous deformation prior to the initiation of serrated yielding, as discussed before. Temperature has a great influence on this parameter, that we shall call the critical strain, ε_o (see Fig. 4). Figure 9 shows how ε_o changes with temperature for four different materials.[3,5,11,17] As one can see, there is a general tendency for decreasing ε_o with increasing temperature. However, in the case of Al-Mg alloys, there is a sudden reversal of the behavior at high temperatures. The same occurs for α-brass at high temperatures.[5]

Finally, one should consider the effect of temperature on the load drop and on the strain between serrations in Type A discontinuous flow ($\Delta\sigma$ and $\Delta\varepsilon$ in Fig. 3). Figure 5 shows that at constant strain, a decrease in temperature causes a decrease in $\Delta\varepsilon$, and Fig. 6 shows that the same is true for $\Delta\sigma$.

1.1.4. The Effect of Strain Rate

According to Brindley and Worthington,[6] the effect of a large increase in strain rate is roughly equivalent to a small decrease in temperature. However, it seems that a change in strain rate can actually completely change the character of the serrations. This is the case for Al 2024 alloy,[2] where a decrease of strain rate from 1.5×10^{-3} sec^{-1} to 1.5×10^{-5} sec makes the load-time curve go from extremely serrated to practically smooth. A similar phenomenon has been observed for Al 6063 alloy,[22] where a change in strain
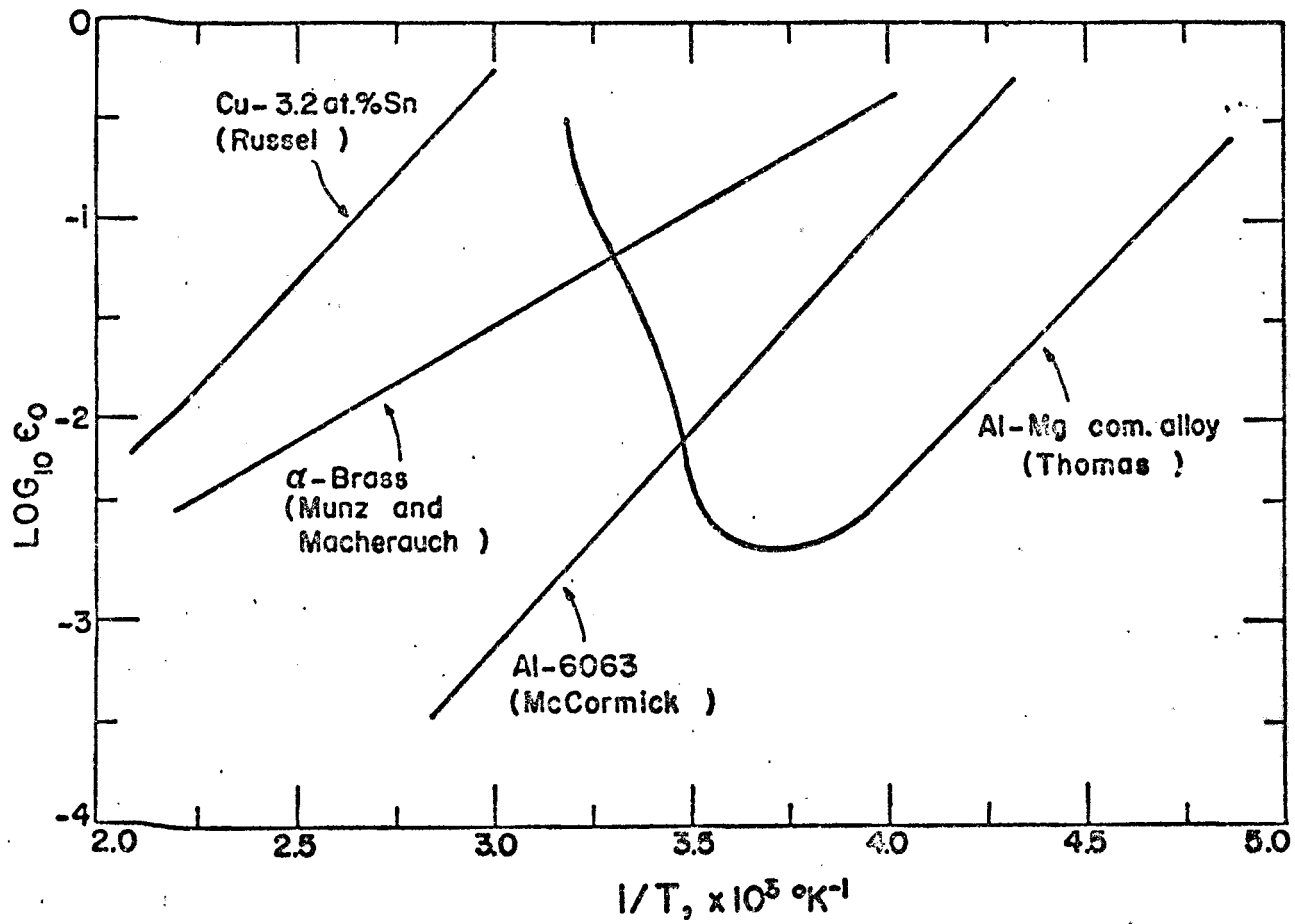
Fig. 9. The influence of temperature on the critical strain ε_o.[3,5,11,17]

rate from 10^{-2} min^{-1} to 10^{-3} min^{-1} makes the load-time curve

go from Type A flow to Type B flow.

In the case of a dead-weight loading apparatus, the rate of loading is more representative than the strain rate. For commercially pure aluminum,[1] a change in the loading rate by a factor of 50 causes relatively small changes, approximately by a factor of 2, in the step sizes and their spacing. However, if such rate changes were performed at temperatures near the limits of the temperature interval where the phenomenon is present, it should be expected that it would have a greater effect on the stress-strain curve.[1]

Another interesting feature is the influence of strain rate on the critical strain to begin serrated flow, ε_o. Figures 10 and 11 show this relationship for several materials. It should be pointed out that the behavior of Al-Mg is the inverse of Cu-Sn and α-brass. On the other hand, Al 6063 presents two kinds of behavior, that have been associated with the change in the character of serrations.[22] The minimum in the ε_o vs strain rate curve for this material corresponds to the point where one switches from Type A yielding to Type B yielding, going down with the strain rate.

If the deformation of α-brass at high temperature is considered,[5] one finds the same kind of behavior described for Al-Mg alloys. In this case, it seems that the strain rate dependence of the critical strain is strongly temperature dependent.
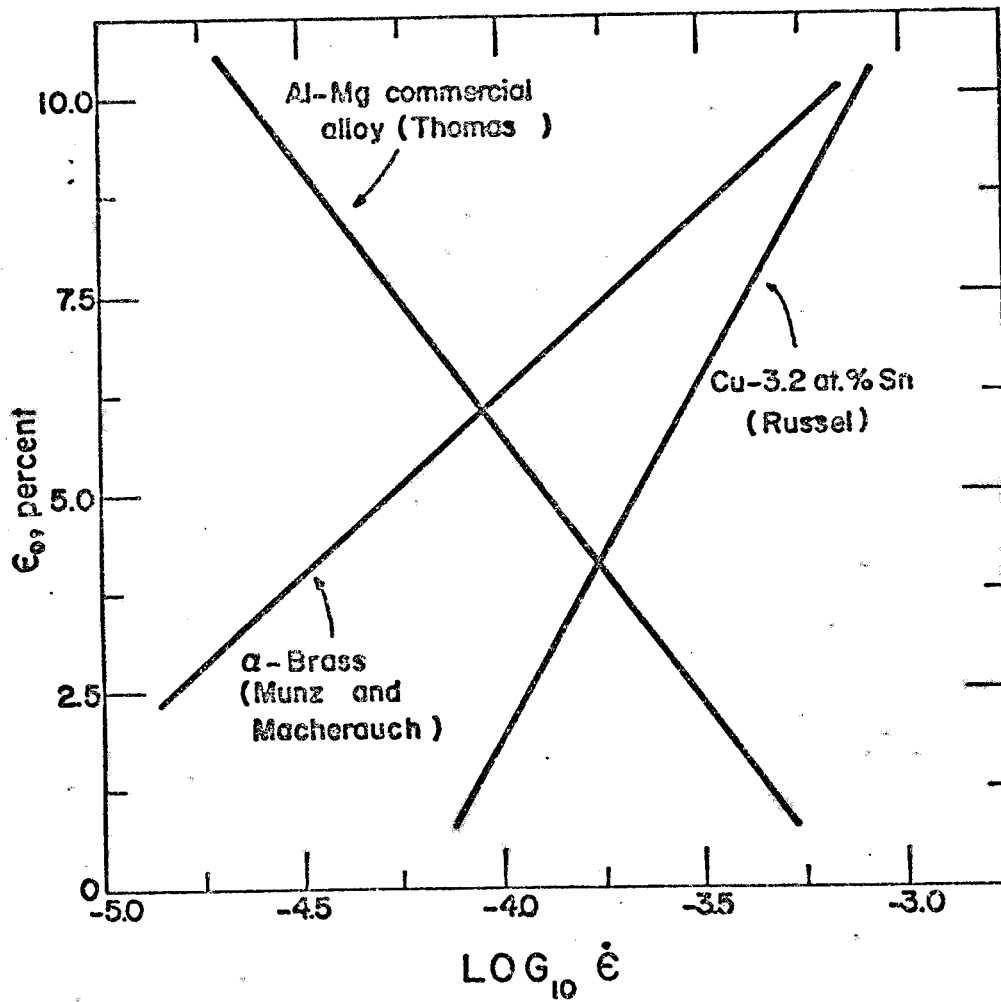
Fig. 10. The influence of strain rate on the critical
strain ϵ_0.[5,11,17]
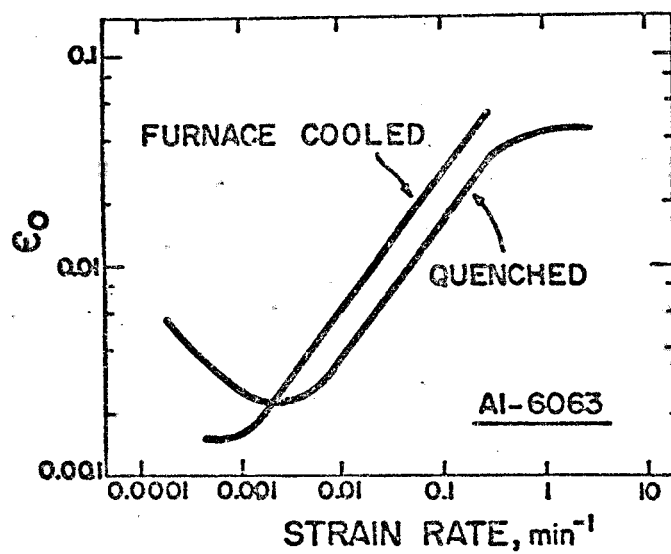
Fig. 11. The influence of strain rate and heat treatment on the critical strain ε_o.[3]

1.1.5. The Effect of Heat Treatment

Serrated yielding can be profoundly affected by heat treatments of the material being tested. For example, Fig. 2[10] shows the difference in the stress-strain curves of aluminum 6061 alloy, solution treated, quenched and then aged for different times.

It seems also that heat treatment can have a very big influence on the critical strain ε_o. Cottrell,[7] for example, attributed the fact that some of Lubahn's[10] curves had very small ε_o to the fact that they were for solution treated and quenched material. However, Cu - 3.2 at. percent Sn alloys[17] submitted to the same heat treatment still presented a reasonable amount of strain before the beginning of serrated yielding.

Solution treating and quenching an Al-Mg alloy[11] produces serrated flow after some smooth deformation. However, if an aging treatment ensues, or if specimens are slowly cooled from the solution treating temperature, an extra region of serrated yielding is observed just after the yield point. Their deformation continues smoothly and lapses back to discontinuous flow after some strain.

In 6063 aluminum alloy, one can observe the effect of heat treatment on the ε_o vs strain rate and $\Delta\varepsilon$ vs strain relationships, in Figs. 11 and 12, respectively.

Rosen[21] reports that the alloy Al - 4.5 percent Cu, annealing at three different temperatures, not only gave
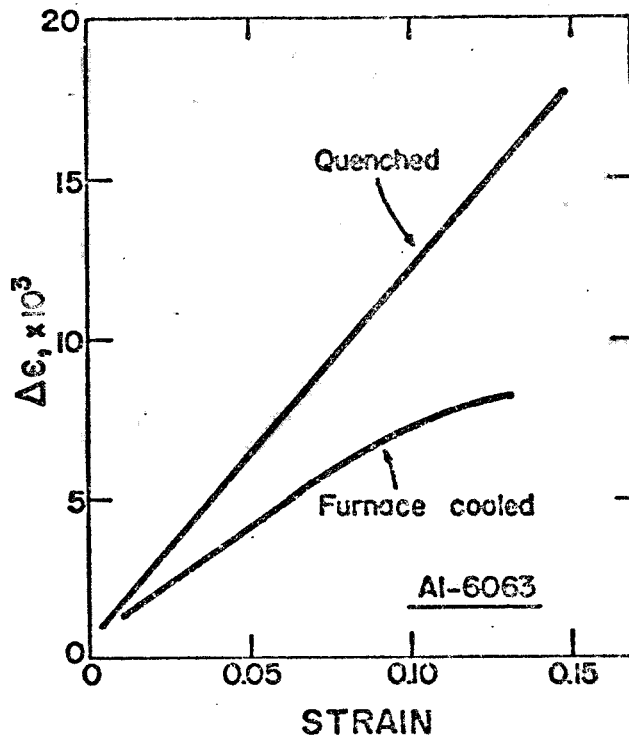
Fig. 12. The influence of heat treatment on
the strain Δε between two successive
Type A serrations.[3]

different serrations for the three different heat treatments, but also presented differences in work hardening. It should be noted that the grain sizes of the specimens are different, but surprisingly, the material with larger grains underwent higher work hardening!

Finally, one can consider the effect of heat treatment on a commercial 2024 aluminum alloy.[2] For specimens strained at room temperature at a strain rate of 10^{-4} $\sec^{-1}$, fully aged specimens gave smooth curves, annealed specimens showed Types A and B serrations, while Type C serrations occurred profusely on solution treated specimens.

1.1.6. The Effect of Grain Size

The grain size affects the critical strain ε_o, the stress at which serrations appear, σ_o (critical stress), and the load drops $\Delta\sigma$ (Fig. 3) of Type B serrations.

Munz and Macherauch[5] point out that σ_o depends only very weakly on the grain size. On the other hand, Thomas,[11] in his work with Al-Mg alloys, states that σ_o is proportional to $d^{-1/2}$, where d is the grain size. However, the constant of proportionality can vary widely with temperature. Besides, he points out that whenever serrated flow started in fine-grained materials, one or several plateaus would be observed in the curve. This did not occur in coarse-grained material.

Concerning the dependence of the critical strain on the grain size, a general statement may be made that it increases

with increasing grain size.[5,6,23] However, the dependence between these two parameters is affected by temperature[5,6,23] and strain rate.[5] Figure 13 shows a plot of $\log \epsilon_0$ vs $\log d$,[23] where the temperature dependence is very clear.

In the case of Type B serrations, a decrease in the amplitude and period of the serrations with increasing grain size has also been reported.[23]

On the other hand, the influence of grain size on the deformation of commercial purity aluminum in a soft machine is somewhat different from the above described behavior.[1] For example, it has been reported that the critical strain ϵ_0 decreases with increasing grain size, while other factors are essentially unmodified by variations in this parameter.

1.1.7. The Effect of Composition

McReynolds[1] compared the behavior of commercial purity aluminum, high purity aluminum and Al-Cu alloys under dead-loading. Tests with high purity aluminum yielded completely smooth curves, while tests with commercial purity material showed curves of the type shown in Fig. 1. The curves for Al-Cu alloys were similar to those for commercial aluminum except that steps began at much smaller strains and were much sharper. Besides, going down to a 0.025 percent Cu alloy, the steps are not sharp and appear only under certain conditions of previous strain and loading rate. In commercial purity material, the steps were associated with a deformation band that swept through the whole length of
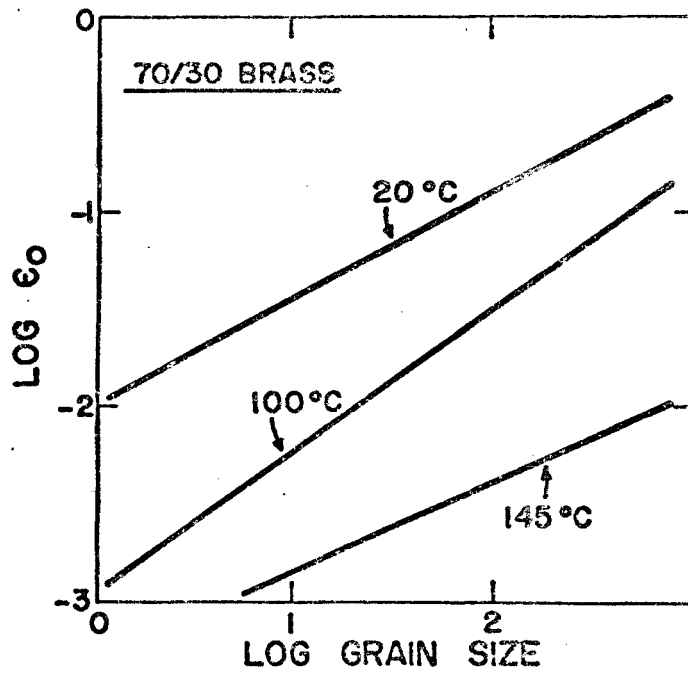
Fig. 13. The influence of grain size on the
critical strain ε_o.[23]

the gage section. On the other hand, in Al-Cu alloys, the corresponding bands tended to propagate only through a limited region of the specimen, and then stopped.

Regarding the deformation in hard machines, it seems that the tendency is for the critical strain to decrease with increasing solute content. This has been observed in Cu-Sn alloys[17] and in α-brasses.[5] This effect is difficult to detect in Rosen's[21] work in Al-Cu alloys, due to differences in grain size for the same composition. However, it is possible to observe in their work an increase in the magnitude of the effect with increasing solute concentration.

1.2. The Theories

Once the phenomena involved with serrated yielding were considered, it should only be expected that attempts would be made to unify and explain the experimental observations. This is indeed true, and in 1953 Cottrell,[7] based on McReynolds'[1] work and some other observations, offered a microscopic model for serrated yielding. Later, other authors[23,24] extended this model to a more general one. From a macroscopic point of view, two models were developed[8,20,25] that take into consideration the mechanical behavior of the material as a whole.

These theories have had success to a limited degree, but have failed to completely describe the phenomena in question. We shall make a quick summary of them and point out

their highlights and deficiencies. However, first of all
we shall discuss some of the principles involved in dynamic
strain aging, to make the whole question clearer.

1.2.1. Dynamic Strain Aging[26]

If one considers an edge dislocation in a substitutional
solid solution, it can be easily seen that substitutional
atoms may be attracted to this dislocation due to the stress
field around it. If the substitutional solid solute has a
lower size than the matrix atoms, it can be attracted by the
stress field where the extra plane lies, for this way it can
decrease the magnitude of the compressive stresses in this
region. A solute atom bigger than the matrix atom would ob-
viously be repelled by these stresses. However, these
larger atoms would decrease the energy associated with the
stress field of edge dislocations, if they position them-
selves below the extra plane of the dislocation. A similar
rationale can be developed for screw dislocations, though in
this case the interaction is weaker.[27]

The result of this is that if the solute atoms have
sufficient mobility they will congregate around these de-
fects, establishing the so-called dislocation "atmospheres."
Now consider a dislocation that is surrounded by an atmo-
sphere and is moving under the action of the applied stress-
es. The atmosphere will obviously try to move with the dis-
location, but it can move only by the thermally activated
movement of the solute atoms, and the velocity with which

it can move may differ from the dislocation velocity. As
a result, there may be a "drag stress" on the dislocation,
slowing it down, and requiring more force to keep it moving.
It is only to be expected that this "drag stress" will de-
pend very much on temperature, that will control the diffu-
sion processes associated with the movement of the atmo-
spheres. At low temperatures, the mobility of the solute
atoms is too low, and they are not able to form the atmo-
spheres or to follow the dislocations. The drag stress is
then small. As the temperature is increased, the atmospheres
will be formed, and will hinder the movement of dislocations,
by lagging behind them. The drag stress will then grow to
a maximum, and after that the temperature is so high that
the solute atoms are able to follow the dislocations, and
besides, the atmosphere decreases by entropy effects. The
drag stress then decreases, and finally disappears at very
high temperatures. Since strain rate and temperature are
interrelated, the same phenomena are observed under a range
of strain rates, from very low (equivalent to high tempera-
tures) to very high (very low temperatures).

Thus, one can explain some aspects associated with dy-
namic strain aging based on this model. First of all, the
fact that it occurs only over a range of temperatures and
its effects are maximized at some intermediate temperature
is a direct consequence of what has been said before. The
strengthening mentioned is obviously related to the drag

stress. The explanation for serrations will be shown in section 1.2.2. Besides, it is obvious that the presence of impurities is essential for the occurrence of dynamic strain aging.

1.2.2. Cottrell's Theory[7]

In his work, McReynolds[1] associated discontinuous yielding with the hardening of the material by precipitation of solute atoms on slip planes. Since this precipitation should be very fast, he made the assumption that motion on slip bands during strain results in lattice vacancies and imperfections that greatly accelerate general diffusion and thus the precipitation of copper aggregates.

When it was realized that most probably serrations were due to the interaction of solute atoms and dislocations,[7] two problems remained to be solved; first, the serrations start only after some plastic deformation; second, in the case of aluminum, for example, the rates of diffusion of alloying elements at room temperature, deduced by extrapolating measurements at high temperatures, are far too small to account for the necessary rates of strain aging.

In his theory, Cottrell[7] suggests that plastic deformation of metals should create vacancies and other defects, that would speed up the diffusion of substitutional atoms. *This concept is similar to McReynolds',[1] stated above.* Thus, in the beginning of the deformation, when diffusion is still slow, the flow is smooth. With increasing strain,

the diffusion coefficient increases, up to a point where the velocity of the solute atoms and the velocity of dislocations reaches a critical value. Serrated yielding would start at this point. Besides, Cottrell points out that in freshly quenched alloys, where plenty of vacancies are available, serrated flow starts immediately after the yield point; in addition, he does not point out what kind of interaction takes place once the critical velocity relationship is reached. One possibility is that as the drag stress increases, the flow stress increases to the point where the dislocations are freed from their atmospheres (unpinning of dislocations); another possibility is that at this point, a sudden multiplication of dislocations occurs, in some highly stressed region. In both cases, the material can suddenly deform easily due to the sudden increase in dislocations available. These new dislocations would then be gradually slowed down, and the process would keep repeating. As one can see, this would correspond to the so-called Type B serrations (Fig. 3). Concerning the distinction between unpinning and multiplication of dislocations, one may consider both of them as processes leading to an increase in the mobile dislocation density, which simplifies the problem.

In his work, Cottrell also derives some quantitative relationships that should hold for the beginning of serrated yielding. One of these relations states that the diffusion coefficient necessary for the beginning depends directly on

the strain rate. Since the diffusion coefficient depends

on strain, the critical strain dependency with strain rate

could be known once the relationship between diffusion co-

efficient and strain were known. This was worked out by

Cottrell again, who finally arrived at the expression

$$\dot{\epsilon} \sim A \, \epsilon_o^{\,m} \, , \qquad\qquad (1)$$

where A is a constant depending on temperature and m is

another constant.

Later, other authors[18,23,24] generalized this theory

to cover other effects. Ham and Jaffrey[24] included the

effect of dislocation multiplication, Charnock[23] introduced

also the grain size dependence of the dislocation density.

Brindley and Worthington[18] tried to extend the theory to

Type A (Fig. 3) serrations. According to them, at the

first stress drop the deformation is confined to a band

which forms across the whole specimen. Immediately prior

to this drop the stress rises above the general level of the

stress-strain curve. During this rise new dislocations are

continuously being produced, the rest of the dislocations

being aged and moving slowly. Since the free dislocations

can most easily take up the strain rate by moving quickly,

the stress then rises until gross dislocation movement

occurs, causing breakout of slip across the whole specimen.

If the deformation in the band associated with this first

stress drop is sufficient to increase the diffusion coeffi-

cient so that fast moving dislocations at the band front

can be fully aged, then little propagation of the band will occur. In order to continue deformation in this case a new band will have to be formed, giving rise to Type B serrations. However, if the increase in the diffusion coefficient is insufficient to fully age the fast moving dislocations at the band front, then the band propagates along the specimen, giving rise to Type A serrations. After the band covers the whole gage length, another band is nucleated, with the ever-present possibility of degenerating into Type B serrations. The fact that Type A serrations are indeed associated with the propagation of a deformation band along the gage length had already received indirect confirmation.[5]

During the propagation of the deformation band in Type A serrations, the load rises, in contrast to other similar phenomena, where the load is constant during propagation (as is the case in steel). This is a phenomenon that Cottrell's theory hasn't been able to explain. It has been attributed to deformation behind the band front,[18] but it's hard to conceive that the material would behave in this way, if it were easier to deform it by propagating the deformation band. It has been observed experimentally that the bands nucleate always at the same end of the specimen and that in this case the other end of the specimen, where the band finally stops, is more work hardened than the end where the band begins.[3,5] Thus, one has a strain gradient along the specimen, and McCormick[3] attributes to this the above-mentioned rising stress between serrations. However,

Cottrell's theory offers no explanation as to why the bands always nucleate in the same region, or why a strain gradient is established along the specimen.

Indirect evidence[5] implies that Type B serrations are associated with either the discontinuous, jerky motion of a deformation band along the gage length,[5] or with the random nucleation of bands in the gage length.[18] Nothing is stated in Cottrell's theory about this.

It has been reported earlier in this chapter (section 1.1.1) that both $\Delta\sigma$ and $\Delta\varepsilon$ (Fig. 3) increase with strain. The fact that $\Delta\sigma$ increases may be rationalized by the fact that at higher strains the diffusion coefficient is higher, pinning and locking of dislocations more efficient, and thus the effect of the decrease in mobile dislocation density should be greater, with a corresponding increase in $\Delta\sigma$. If $\Delta\sigma$ increases by this reason, it is to be expected that $\Delta\varepsilon$ should also increase, because it depends on the dislocation density involved in the process. However, there is no experimental proof of the statements above.

Regarding the mechanical characteristics of the loading apparatus, it should be pointed out that in a dead-loading apparatus, the load almost does not drop when a deformation band is nucleated, and thus the newly freed dislocations do not decelerate. Thus, it is to be expected that bands will propagate once they are formed, as discussed in section 1.1.2.

We shall now analyze together the effect of both strain rate and temperature according to the theory in question, since the two effects are interrelated. As seen in section 1.1.3, increasing temperature tends to promote Type B serrations, which agrees with the theory's predictions. As the temperature is increased, the interaction between dislocations and solute is stronger, for the diffusion is more pronounced. This would correspond to a tendency for formation of Type B serrations, in a coherent picture. Analogously, the critical strain should decrease as temperature increases, for less diffusion needs to be vacancy assisted. As seen in Fig. 9, this is true.

Concerning the influence of the strain rate on the shape of the serrations, a decrease in strain rate (equivalent to increase in temperature) should promote Type B serrations. As mentioned in section 1.1.4, this is indeed the case. Analogously, a decrease in strain rate leads to a decrease in the critical strain (see Fig. 10). However, α-brass at high temperature, Al-Mg alloys, and aluminum 6063 alloy at low strain rates present an inverse relationship, or the critical strain ε_o decreases for increasing strain rate. This is attributed to the fact that for these materials the dislocations are pinned to begin with, and it is not necessary to have vacancy assisted diffusion. Typically, all three present only Type B serrations. The rationale for the critical strain behavior[22] is that in these cases the

dislocation velocity is low enough for the solute atmo-
spheres to be dragged along with the dislocations (or con-
versely, the temperature is high enough to allow a quick
movement of solute atoms). Then, one starts with atmospheres
already around the dislocations, and the critical condition
for onset of serrated yielding is the breakaway from these
atmospheres. Thus, a rise in flow stress is not observed
prior to the yield drop; only the drop occurs. The higher
the temperature and the lower the strain rate, more strain
can be provided by the movement of dislocations with their
atmospheres, and the stress has to be higher to break the
dislocations away from the atmospheres.

Let us now consider how Cottrell's theory applies to
the influence of grain size. As seen in section 1.1.5, in-
creasing grain size tends to increase the critical strain
ϵ_o and to decrease[11] or not affect at all[5] the critical
stress for the beginning of serrated flow, σ_o. It is well
known that bigger grains lead to less work hardening and
thus to a lesser dislocation density and interaction than
smaller grains, for the same strain levels. If one has to
achieve a certain diffusion coefficient by dislocation
interaction, it is to be expected that one shall need more
strain to accomplish this in a large-grained material than
with a fine-grained one. Thus, ϵ_o should increase for big-
ger grains. Regarding the effect on σ_o, Thomas[11] argues
that in aluminum-magnesium alloys it decreases with

increasing grain size, because this causes an increase in the length of individual dislocations, leading to a reduction in the stress required to unlock pinned dislocations, thus accounting for a decrease in σ_o with increasing grain size. However, Munz and Macherauch[5] have observed that σ_o is practically independent of grain size in α-brass, and they argue that if one requires a certain dislocation structure to begin serrated flow, and if a fixed flow stress corresponds to this dislocation structure, there is no reason why σ_o should change with grain size.

However, the influence of grain size on ε_o for the deformation of commercial purity aluminum in a dead loading machine is the inverse of the exposed above.[1] No explanation can be given by Cottrell's theory for this phenomenon.

Regarding the influence of heat treatment, freshly solution-treated alloys should present serrations immediately after yielding (see section 1.1.6). However, this is not the case for many alloys. No explanation is offered by the theory in this case.

The increase in solute concentration should make easier the interaction between dislocations and substitutional atoms, and thus decrease ε_o. This in fact has been observed.

According to Cottrell's theory, the following experiment should be true: strain a specimen well within the serrated yielding region. Unload the specimen and give it a low temperature heat treatment, so that vacancies are

annihilated from the structure, but dislocations are not.
Then, if one loads the specimen again, one should expect to
have some smooth flow before the onset of serrations. How-
ever, this is not observed in the case of α-brass,[5] and the
only explanation that Munz and Macherauch could find for
this abnormality is that, if indeed Cottrell's theory is
valid, the total number of vacancies formed during the
deformation is not decisive for the beginning of dynamic
strain aging. What would really matter would be the instan-
taneous build-up of vacancies around interacting disloca-
tions.

On the other hand, Ham and Jaffrey,[24] using the same
procedure but limiting the pre-strain to the smooth initial
part of the strain, actually found an increase in the total
strain to initiate serrations. However, the increase in
total strain decreased for higher pre-strains, and it could
be possible that no increase would be observed after ser-
rated yielding began.

1.2.3. Sleeswyk's Theory[8]

In fact, this is not a theory, but just some concepts
formulated by the author as conditions for the presence of
discontinuous flow.

Usually, the flow stress for a metal deformed at a
strain rate $\dot{\epsilon}_2$ higher than another $\dot{\epsilon}_1$ is higher than for
this second strain rate. However, for some metals, the in-
verse is true, as shown in Fig. 14. The author argues that
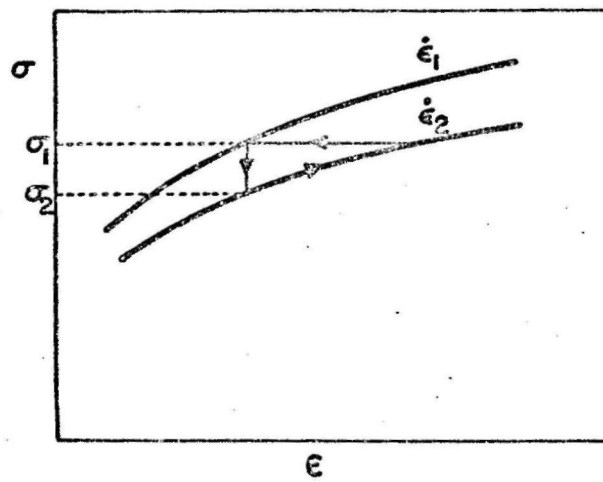
Fig. 14. Behavior described in Sleeswyk's
theory.[8]

in this case, plastic flow is unstable, due to the following: initially, the material is being strained at the strain rate $\dot{\varepsilon}_1$. If, by any chance, a small region of the specimen starts deforming preferentially, the strain rate in it will shoot up, and this region will start behaving as shown for curve $\dot{\varepsilon}_2$, or, in other words, it softens as a result of deformation. This region will then keep deforming until it hardens to the same level of the rest of the specimen. The process is then repeated.

The flaw in this reasoning is that Sleeswyk assumes that the flow stress of a material is a function of only strain, strain rate and temperature. Actually, it is also a function of the strain history of the specimen, and if the conditions proposed by him are simulated in a quick strain rate change test in a material that presents serrations, frequently no load drops are observed as described.

However, his ideas have the merit to point out the fact that the essential requisite for localized deformation to occur in a material is that it must somehow soften as a result of strain.

1.2.4. Rosen and Bodner's Theory[20,25]

The initial theory of these two authors refers to dead weight loading.[20] Later, Bodner[25] extended it for materials strained in hard machines. We shall be primarily dealing with the first theory, which is simpler and affords a good

insight into the principles involved. Only some references
will be made to the second part of it.

In this theory, the factor determining the presence of
discontinuous yielding is a negative flow stress-strain rate
relationship, just like Sleeswyk's theory. Concerning the
objections to this assumption that were made in the last
section, the authors argue that for not very dissimilar
loading histories, the flow stress may be considered as a
function of only strain, strain rate and temperature.[20]
The point is disputable, and may apply only to some materials
and conditions. In the case of work softening, for example,
the flow stress depends crucially on the previous deforma-
tion history.[28]

Let us follow their reasoning. Using an Instron "hard"
machine to determine stress-strain curves of commercial
purity aluminum at several strain rates, they replotted
these curves as flow stress vs strain rate, as shown in Fig.
15. Let us suppose now that we are loading a material in
a dead weight loading machine at a slow strain rate, and we
reach point C_0 in Fig. 15. Then, it is easier for the mate-
rial to strain at a higher strain rate, and since the load
does not drop in this case, the strain rate will shoot up
very quickly, at practically the same strain, following the
horizontal line C_0BA, until it reaches point A. Here, an
increase in strain rate would require an increase in stress.
Since the loading rate is very low, the stress does not
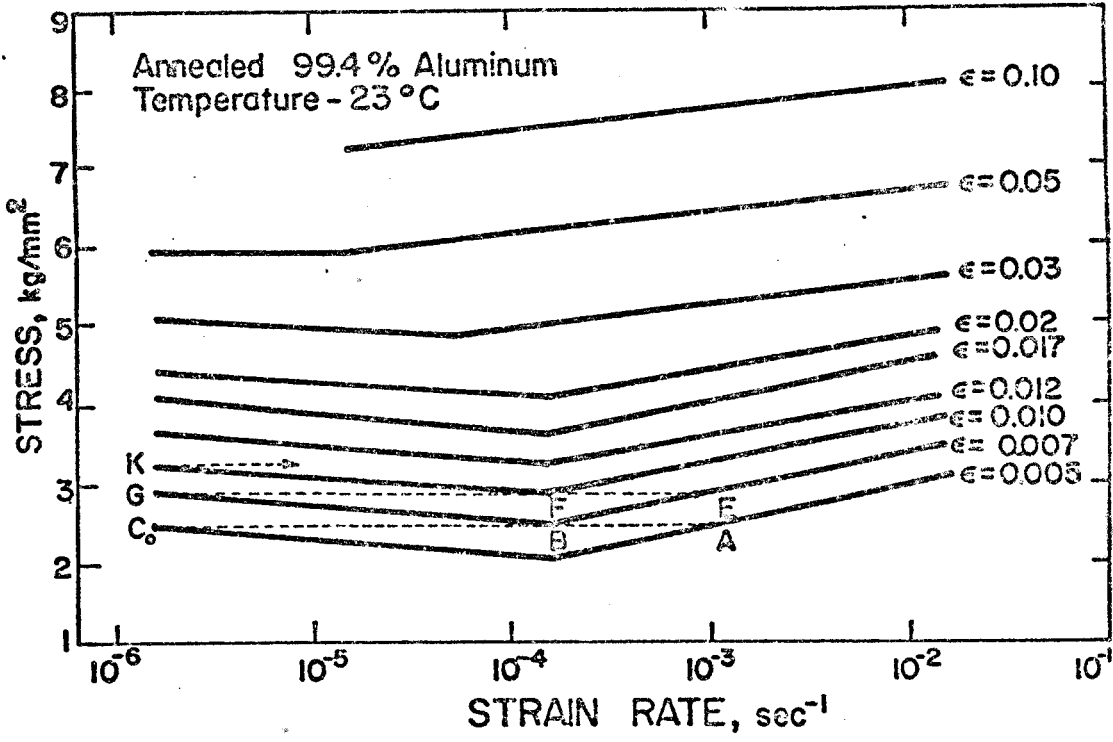
Fig. 15. Behavior described in Rosen and Bodner's theory.[20]

rise sufficiently fast, and the strain rate starts to de-
crease, as a result of work hardening. Consequently, the
strain increases, and the specimen starts following higher
strain plots of flow stress vs strain rate, following the
line AB. The moment this line meets a point like B, the
flow should stop, for its continuation would require a fast
stress rise, which is not available. The specimen then
behaves elastically to point G, where the process is re-
peated. As one can see, the essential characteristic of
the flow stress-strain rate is that it has a negative slope.
When there is no inflexion in the curves, as is the case
discussed above, the strain rate would increase to a point
determined by the mechanical characteristics of the system.
Some modifications are provided to cover the band propaga-
tion discussed previously.[1]

Although the theory, according to the authors, describes
fairly well the behavior of commercial purity aluminum, some
serious problems are present. First of all, according to
Fig. 15 and the reasoning above, the discontinuous flow
should stop as soon as the strain reached a level where no
negative flow stress-strain rate is present any longer.
This does not happen, and the authors themselves state that
serrated flow has been observed at high levels of strain.[20]
Their argument is that most probably the negative flow
stress-strain rate relation extends for a higher strain
range for dead weight loading. Thus, they draw conclusions

from curves obtained from a "hard" machine, knowing that
their results might not be entirely applicable to the the-
ory. Besides, they base their argument of the history
independence of flow stress on results obtained with a hard
machine,[9] while McReynolds,[1] performing strain rate changes
in a dead weight machine, did not report any change in flow
stress with changes in loading rate. Another problem is
that the theory predicts that if a material that presents
steps in its stress-strain curve, under dead weight loading,
is strained in a rigid machine, serrations should not be
present. This is indeed true for commercial purity alumi-
num,[9] but this is not the case of Al-Cu alloys, that present
stepped stress-strain curves under dead weight loading,[1] and
extremely serrated curves when deformed in a stiffer ma-
chine.[25]

The extension of the theory for a hard machine is much
more elaborate, and predicts only a sort of Type C serra-
tion (Fig. 8). No mention is made of other types of ser-
rations.

Concerning the microscopic aspects of the problem,
the authors attribute them to dynamic strain aging,[25] and
conclude that the hypothesis of dislocations breaking away
from impurity pinning points appears to be unnecessary, and
the desired effects can be obtained through only multipli-
cation of dislocations.

1.3. Summary

As seen before, none of the theories presented describe serrated yielding satisfactorily. Cottrell's theory is by far the best one in the current state of affairs. Sleeswyk's ideas can be hardly called a theory, and Rosen and Bodner's theory, if valid at all, presents many shortcomings.

It is our feeling that more empirical results are necessary for clarification of some aspects of the problem. Concerning the formation and propagation of deformation bands upon straining in a hard machine, visual observation is possible only when the deformation associated with them is big enough to cause surface markings. Besides, the nucleation and propagation of a deformation band in Type A serrations has been studied only by indirect means, using an extensometer, and the controversy between the responsibility of Type B serrations being due to random nucleation of deformation bands or to their jerky propagation has not been solved. The reason why the load rises during the propagation of the deformation band in Type A serrations is obscure. The influence of the mechanical characteristics of the equipment is not very clear. For example, stiffening a soft machine leads to the disappearance of serrations in commercial purity aluminum,[20] while this stiffening promotes load drops in Al-Cu alloys.[21]

Thus, we have endeavoured to develop a new method for studying discontinuous yielding, that would lead to further knowledge in this field. Besides, once this method was developed, it should be applied to recognize new features associated with serrated flow and to scrutinize concepts already introduced.

A new method was indeed developed. The next chapters describe it in detail, as well as the results obtained with its use.

CHAPTER II

EXPERIMENTAL METHODS

2.1. Introduction

The material chosen for this work was aluminum 6061
alloy, and tensile tests were performed in an Instron
machine. The majority of tests were made at room tempera-
ture, although a few were run at a low temperature (0°C).
Serrated flow was commonly observed. In order to verify
that this effect was not due to the tensile apparatus, tests
were performed with materials that undergo smooth flow.
This was verified by attaching an extensometer to these
specimens, and registering the result on a separate re-
corder. To check the effectiveness of the Instron recorder,
the output of the machine load cell was introduced in a
separate fast speed response recorder and the result com-
pared with those obtained in the Instron chart. In order
to analyze the effect of changing the mechanical character-
istics of the machine, a few tests were made with a spring
in series with the test specimen. This reduced the machine
stiffness. Since it was observed that misalignments in
gripping the specimens were of importance, self-aligning
grips were made in order to eliminate misalignment effects.

47

Almost all the specimens used were flat, and photoelastic
coatings could be attached to them in order to analyze the
strain behavior of the material. However, a few tests
were performed with round specimens, in order to study the
presence of strain gradients along the gage length.

2.2. Material and Specimens Used

The material was commercial 6061 aluminum alloy, with
the composition shown in Table 1.[29] The specimens were cut
from three plates of different thickness (0.032", 0.250",
0.375") in the rolling direction. After solution treating
and quenching the material of the 0.032" sheet, it showed
the microstructure shown in Fig. 16. The grain size was
~10μ. After annealing, the material of the 0.250" and
0.375" plate showed, respectively, the microstructure shown
in Figs. 17 and 18. Their grain sizes were ~70μ and ~200μ,
respectively. This measurement was made by the linear
intercept method in the last two cases, and by X-ray analy-
sis in the first case.

Complete solution treatment of the material was per-
formed by holding it for one hour at 535°C and water quench-
ing it afterwards.[29] Annealing was completed by heating
the alloy to 413°C for three hours and then furnace cooling
it.

The metallographic procedure used to obtain the micro-
structures seen in Figs. 16, 17 and 18 covered the following

Table 1

Nominal Composition of Commercial 6061 Aluminum Alloy

Element	Content (%)
Mg	0.8 to 1.2
Si	0.4 to 0.8
Cu	0.15 to 0.40
Cr	0.15 to 0.35
Fe	max 0.7
Mn	max 0.15
Zn	max 0.25
Ti	max 0.15
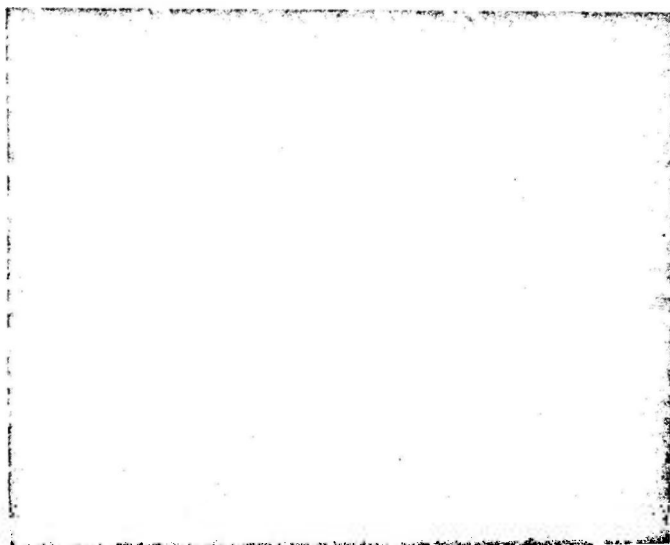
Fig. 16. Microstructure of the solution treated and quenched 0.032" thick sheet. Magnification 110X.
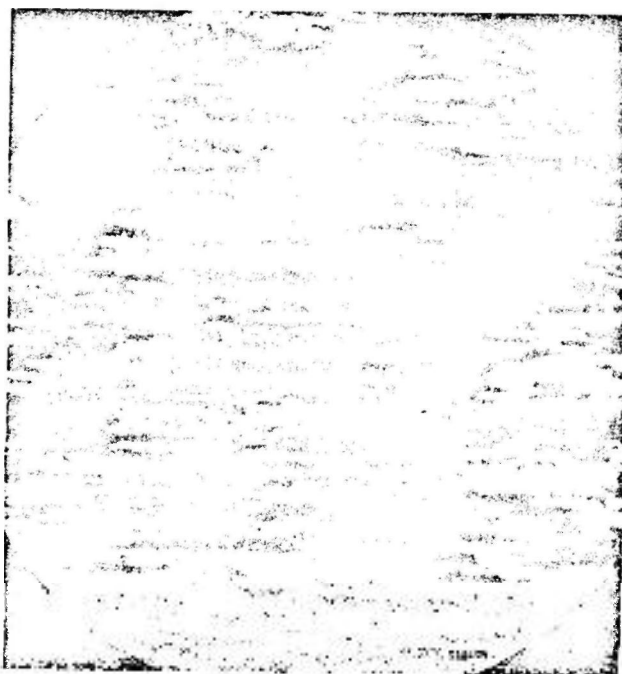
Fig. 17. Microstructure of the annealed 0.250" thick plate. Magnification 50X.
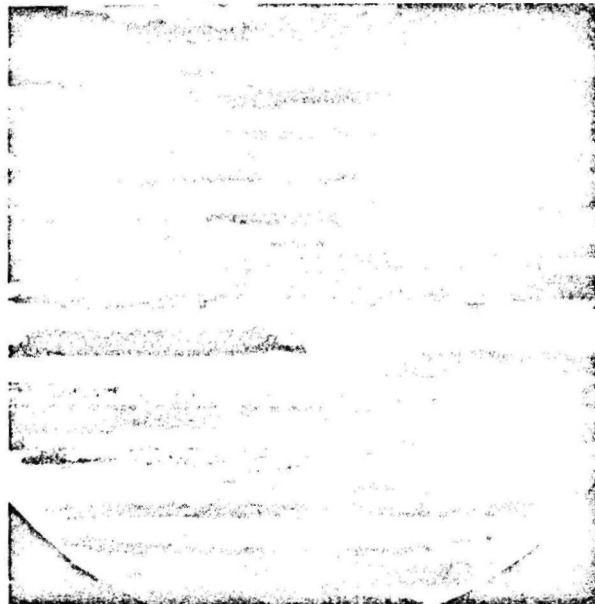
Fig. 18. Microstructure of the annealed 0.375" thick
plate. Magnification 25X.

steps:

1. Grind the cold mounted specimens on silicon carbide wet grinding papers, from grit 240 to 600.

2. Thoroughly wash the specimen under cold running water.

3. Further polish it with 6μ and 1μ diamond paste.

4. Step 2 is repeated.

5. Anodize specimens for 5 minutes, under 30 volts, in the solution

    8.65 ml HF
    3.4 g Boric Acid
    250 ml water.

Specimens of several geometries were used in this investigation. They are shown schematically in Fig. 19. The specimens with holes were machined according to ASTM standards.[30] Specimens of Type 3 (Fig. 19, left column) were used in all the early part of the investigation, particularly in the case of solution treated specimens. However, for tests with photoelastic coatings, specimens of Type 5 were used, for they allowed the use of the self-aligning grips and had a longer gage length, that permitted better viewing of the phenomena in question. The same reason applies in relation to specimens of Type 6 compared to specimens of Types 1 and 2. Specimens of Type 2 have longer gage lengths and grips than specimens of Type 1, which made easier its use. Finally, specimens of Type 4 were used in the low temperature tests and specimens of Type 7 were used in the investigation of the presence of strain gradients

Spec. no.	Specimen Dimensions, in					
	A	B	C	D	R	Thickness
1	0.750	1.00	1.00	0.375	0.250	0.125
2	0.750	2.00	2.00	0.375	0.500	0.125
3	0.500	1.125	1.250	0.220	0.250	0.032

Dimensions – inches
Thickness – 0.032 in

Specimen	Thickness
5	0.032
6	0.125

Dimensions – inches

Dimensions – inches
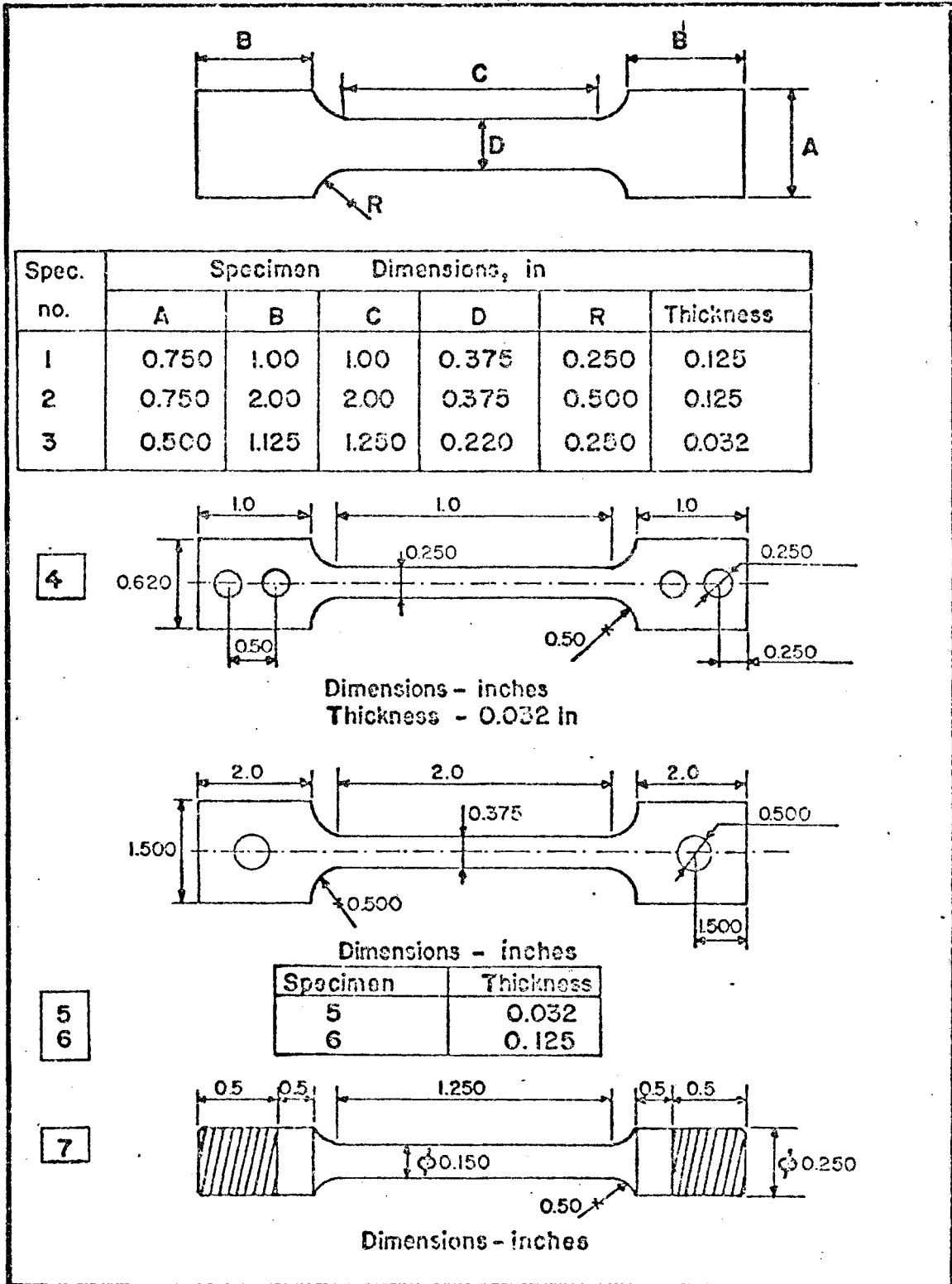
Fig. 19. Geometry of specimens used in this investigation.

along the gage length. Round specimens offer a better symmetry and easier measurement of local strains, and Type 7 was used for this purpose.

2.3. Experimental Apparatus

The tensile tests were performed in a TT-D-L Instron machine, with a capacity of 20,000 pounds. A few tests were performed in a TT-C Instron machine model, that provided a bigger frame when this was necessary. In both cases the load was recorded with an accuracy of 0.5 percent of the load indicated, and the crosshead speed accuracy was better than 0.1 percent for all specified speeds at any load.

The equipment used for performing the tensile tests was as follows. For presentation purposes, it shall be divided into equipment to test flat specimens, round specimens, and specimens with photoelastic coatings.

2.3.1. Flat Specimens

In the majority of cases, a common standard screw grip was used, as shown in Fig. 20. However, this kind of equipment easily leads to small misalignments, which were observed to be of importance. Thus, a self-aligning grip was designed, and is shown in Fig. 21. The four plates in the bottom of this figure are shims used for testing thinner specimens. Figure 22 shows these grips mounted in the Instron.
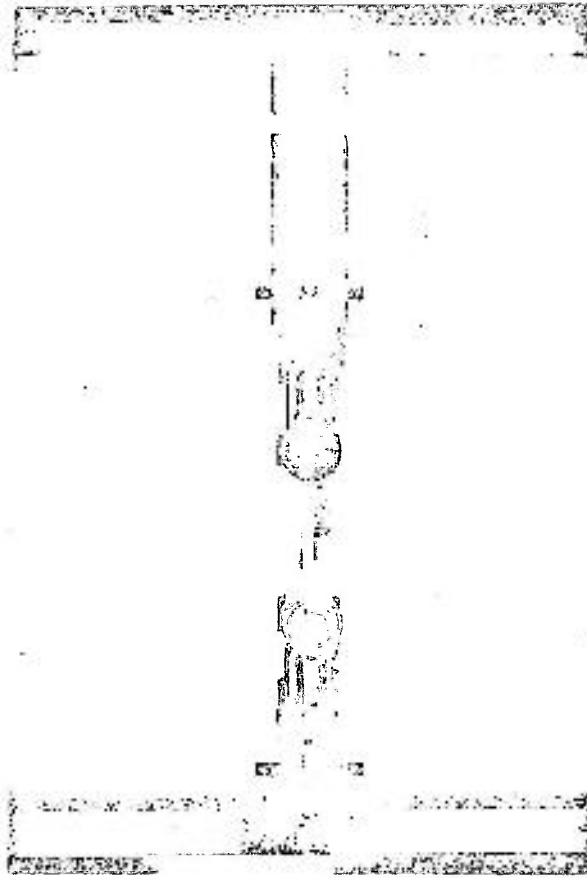
Fig. 20. Screw grip used for testing flat specimens.
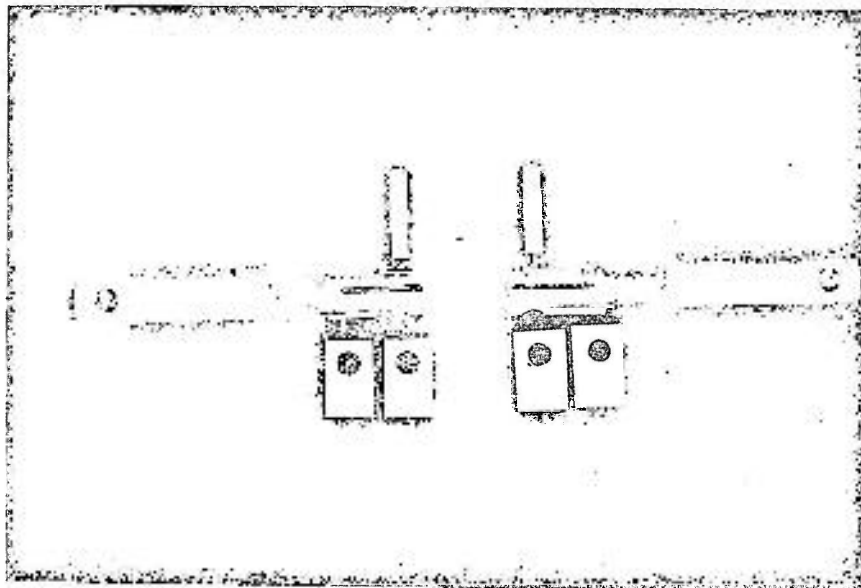
Fig. 21. Self-aligning grips.

56
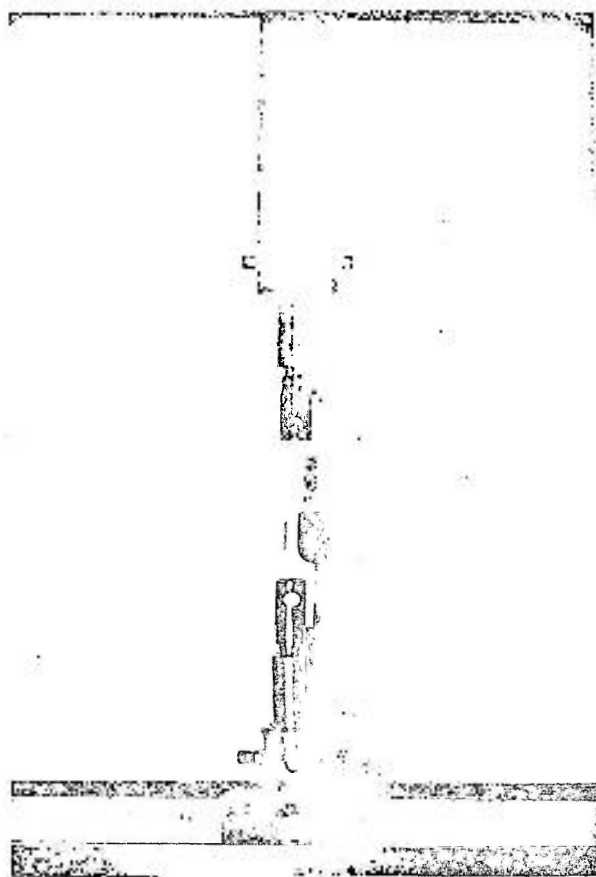
Fig. 22. Flat specimens testing with self-aligning grips.
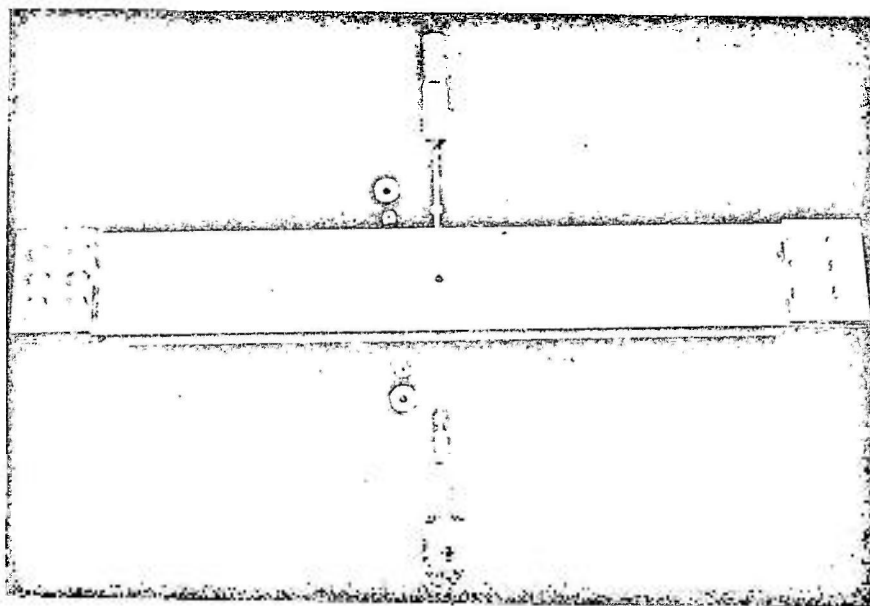
Fig. 23. Spring used to decrease the spring constant of the Instron machine.

The tests performed with a "soft" machine used a spring described in Appendix I. Figure 23 shows this spring with the fixtures used to mount it in the tensile apparatus. Note that hemispherical seats were provided for the connections of the pulling rods with the spring, so that no misalignment effects would be present. The spring constant of this piece of equipment was checked, and the result was 300 lbs/in, according to the design. Figure 24 shows the mounting used for "softening" the Instron, together with the self-aligning grips.

The tests performed at low temperatures were performed using a tube attached to the lower part of the Instron crosshead, as shown in Fig. 25. The specimen was connected on one side to the load cell through a pulling rod, and on the other side to the lower part of the tube. Alignment was assured by hemispherical seat connections. Slip in the grips was prevented by use of grooved jaws. Figure 26 shows the details of this equipment. Low temperature was obtained by mixing water and ice in the Dewar flask shown in Fig. 25, and by immersing the testing tube in it. Temperature was controlled by a low temperature thermometer.

2.3.2. Round Specimens

The equipment used in this case was similar to that used for low temperature tests, and it is shown in Figs. 27 and 28. This was done to assure good alignment in the tensile apparatus.
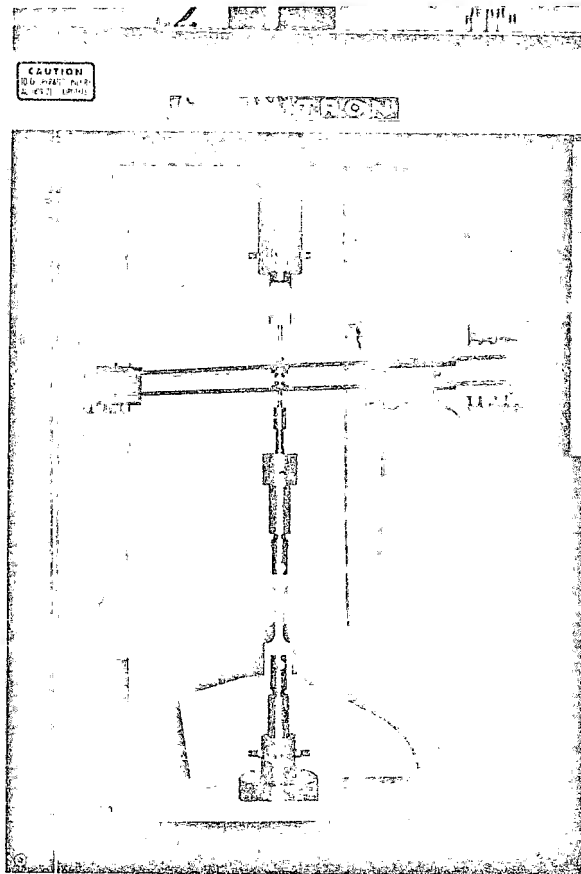
Fig. 24. Spring mounted on Instron machine.
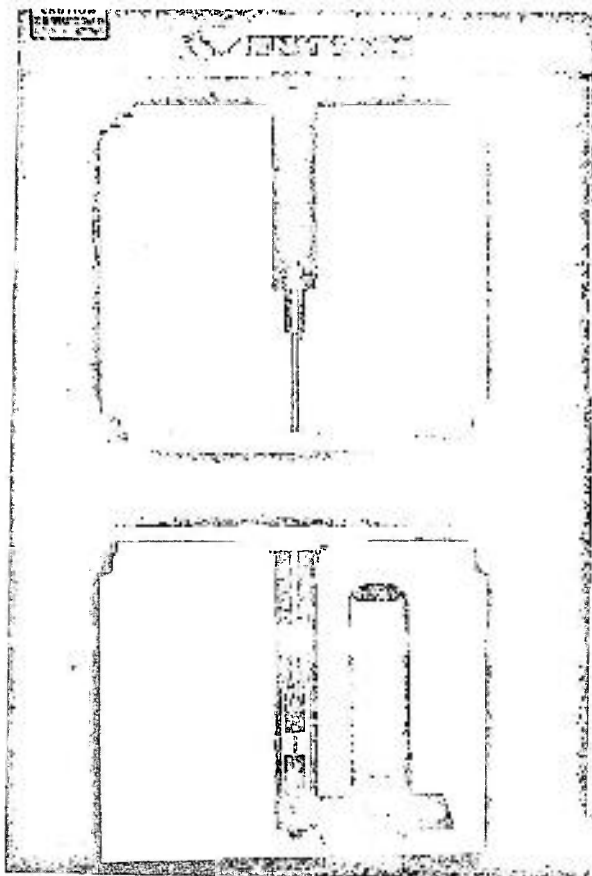
Fig. 25. Set-up used for
low temperature
testing.
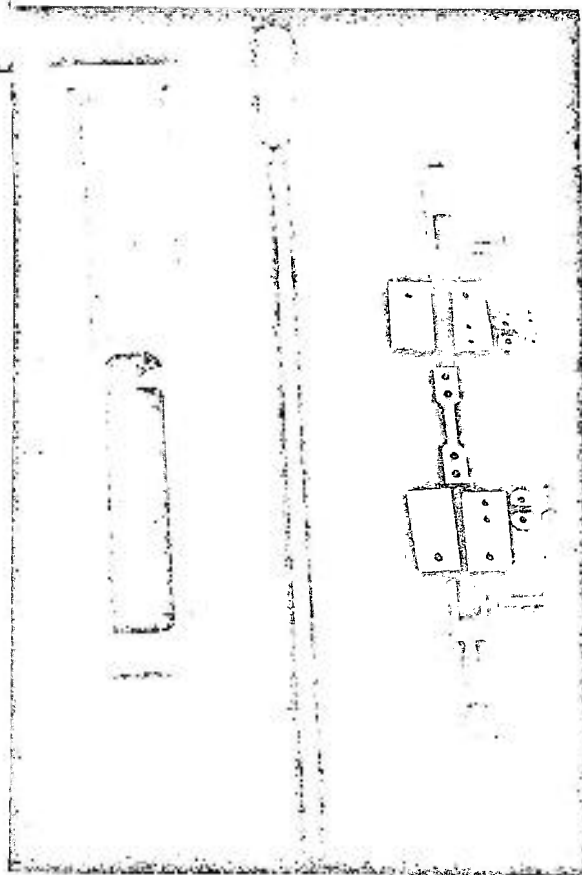
Fig. 26. Details of equip-
ment for low
temperature test-
ing.
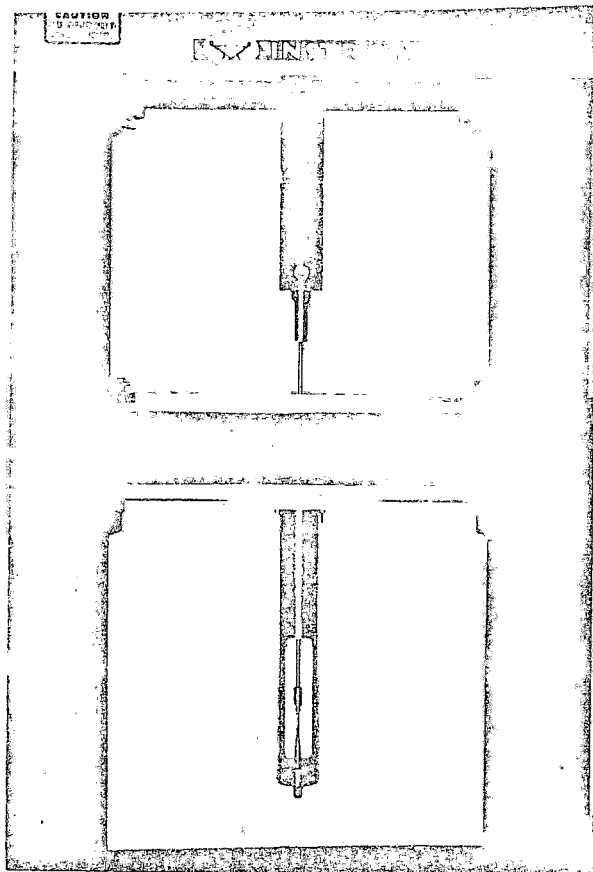
Fig. 27. Set-up for test-
ing round speci-
mens.

Fig. 28. Details of equip-
ment used for
testing round
specimens.
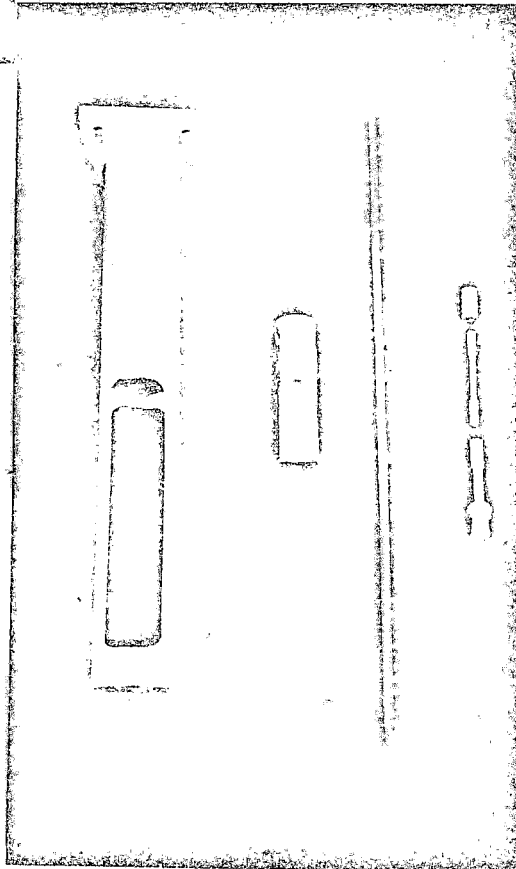
2.3.3. Specimens with Photoelastic Coatings

Photoelastic coatings may be attached to flat specimens, in order to analyze their strain behavior. These coatings, when illuminated by polarized light and viewed through a polariscope, depict local changes in strain by changes in color and the presence of fringes. Appendix II gives some insight to this method, called photoelasticity. Though one can obtain quantitative and qualitative information from photoelastic observations,we have limited ourselves to only qualitative measurements in our work.

The coating used was supplied by Photoelastic Company, and had the following characteristics: Type PS-4A, thickness 0.125±0.002 in, "f" value 18,100 µin/in/fringe, Young's modulus 1,000 psi, maximum elongation 150 percent, and maximum usable temperature 350°F. This material was selected because of ·its high sensitivity and low modulus, which minimizes reinforcement effects.

The plastic was attached to the specimen by a special epoxy resin, with modulus 1,000 psi, and that provided the reflecting backing necessary for reflection photoelasticity. Figure 29 shows a tensile specimen and the photoelastic coating, and Fig. 30 and Fig. 31 show two views of a specimen with the coating already attached to it.

A circular polariscope, model LF/M, manufactured by Budd Company, with a tungsten light bulb of 150 W, was used to illuminate the coated specimens and to view them. This
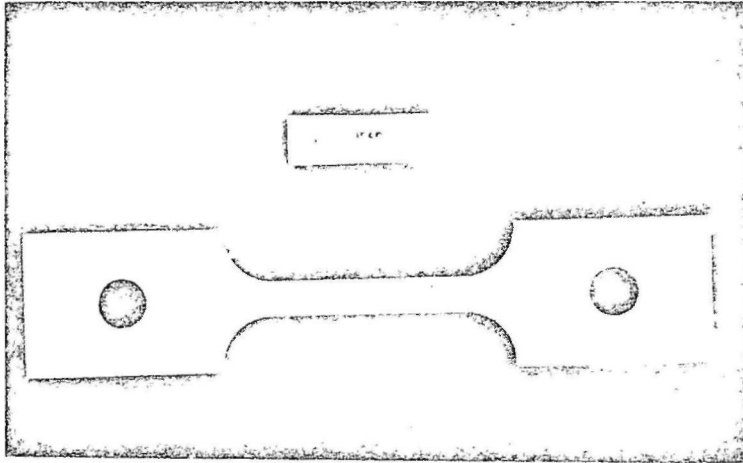
Fig. 29. Tensile·specimen and photoelastic coating.
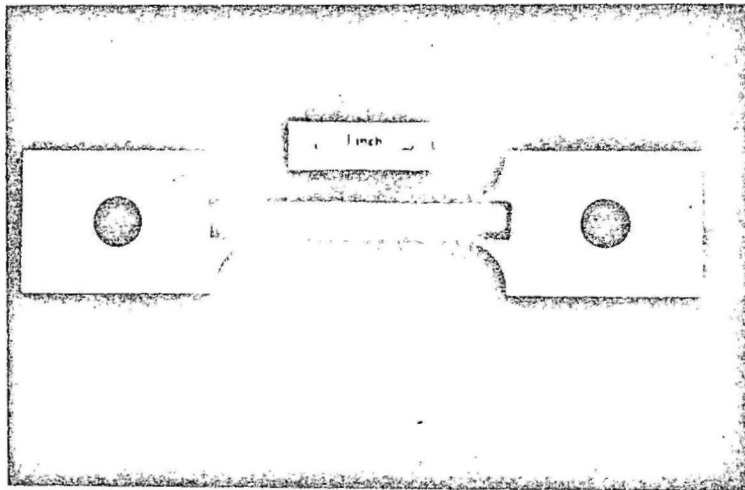
Fig. 30. Tensile specimen with photoelastic coating
          attached to it.

Fig. 31.   Lateral view of a tensile specimen with photo-
elastic coating attached to it.

instrument is shown in Fig. 32. The phenomena observed were recorded on an Ektachrome EF super 8 film, with a sensitivity of 125 ASA. The motion picture camera was regulated for 250 ASA, and the film received a special processing by Kodak, in order to increase its sensitivity to 250 ASA. This was necessary due to the low light intensity available. The camera used was a Nizo S-56, equipped with zoom and close-up lenses. It can be seen in Fig. 33. The motion pictures were taken at 18 frames per second, except in one case, where long periods of recording forced the use of a speed of 3.5 frames per second.

Figure 34 shows a typical tensile set-up for motion picture recording. The watch by the side of the specimen covers 10 seconds per revolution of the big hand and 5 minutes per revolution of the small hand, and was used to synchronize whatever was observed in the film with data obtained in the load-time diagram in the Instron chart. Finally, Fig. 35 shows a complete set-up for motion picture recording. The camera was operated by remote control, in order to allow freedom of movement to the person performing the test. Both the polariscope and the camera were mounted on tripods, and the camera was tilted horizontally (see Fig. 35), to allow better use of the frame size.

The films obtained were studied by using a Kodak Instamatic M-95 film projector, with speeds of 6, 18 and 54 frames per second.
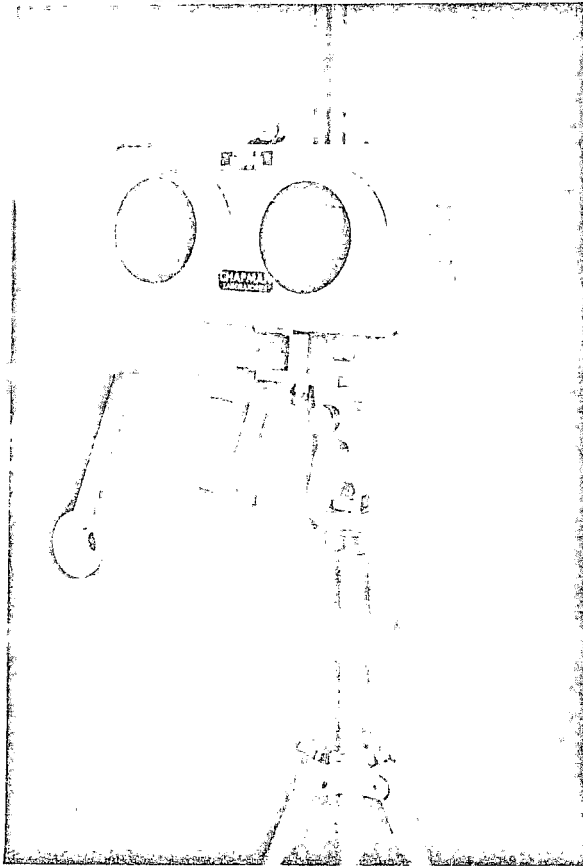
Fig. 32. Circular
polariscope.
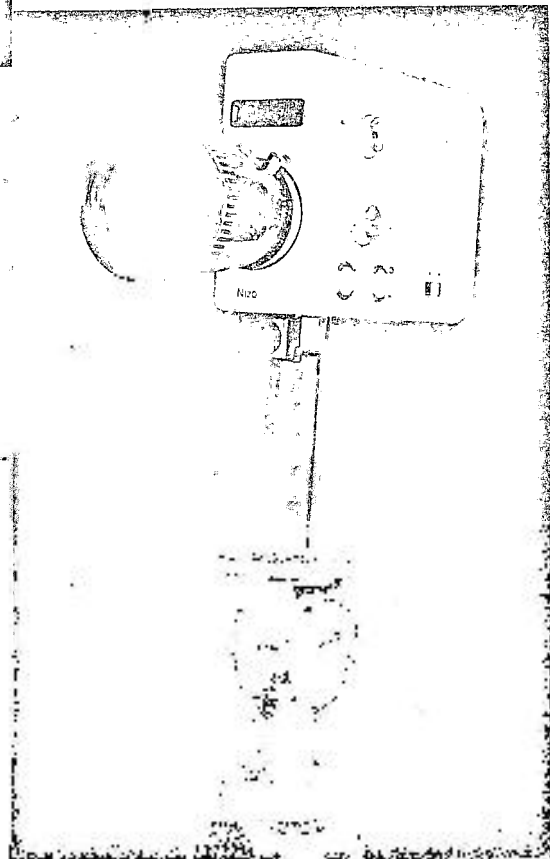
Fig. 33. Motion picture
camera.
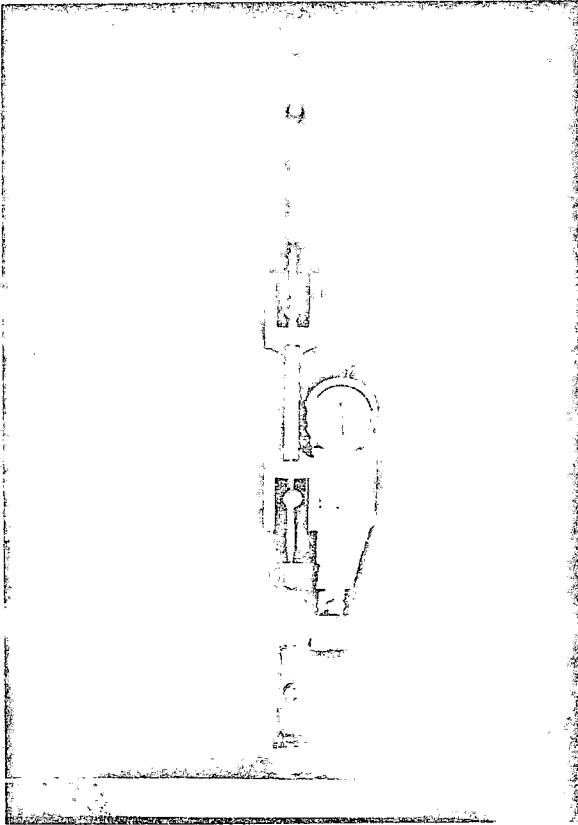
Fig. 34. Tensile set-up
for motion
picture recording.
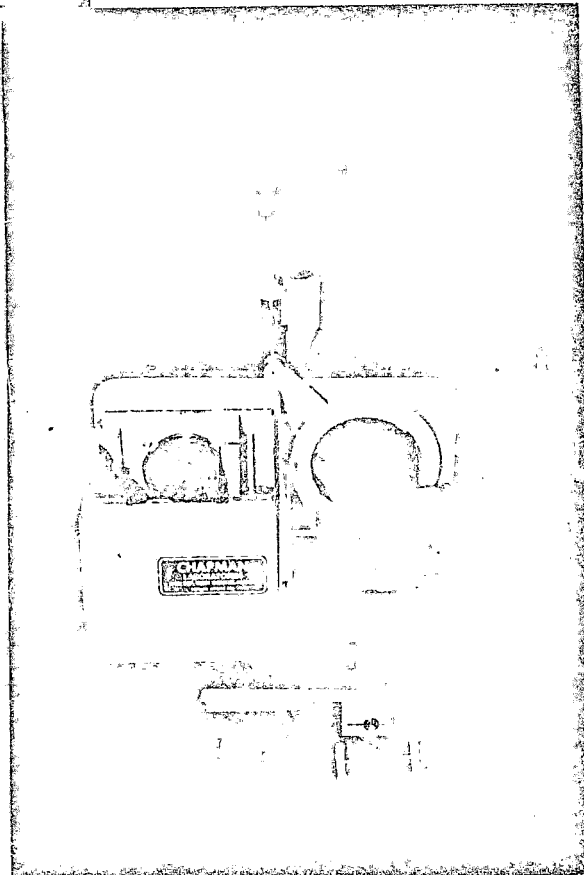
Fig. 35. Complete experi-
mental set-up
for motion pic-
ture recording.

In order to check that the serrated load-time curves
were not a result of the recording equipment in the Instron,
the load cell output was introduced in an independent, high-
speed response brush recorder. Tests were also performed
with materials that did not exhibit discontinuous flow, to
check the response of the Instron chart recorder. Finally,
a test was performed with an extensometer attached to a
smoothly deforming specimen, to recheck the overall behavior
of the tensile apparatus.

2.4. Specimen Preparation

The specimens tested without photoelastic coatings
were simply cut from the plates in a longitudinal direction
and machined to the dimensions specified.

The specimens that received the photoelastic coating
were prepared following the sequence below[31]:

1. Cut a plastic strip from the sheet of photo-
    elastic material, with length greater than
    the gage length of the specimen and width
    equal to that of the specimen. This is done
    using a sharp razor blade.

2. Wash with soap this plastic strip, rinse it
    carefully, dry and wrap it in aluminum foil.

3. Grind the surface of the specimen with 600
    grit silicon carbide grinding paper, wash it
    with water, dry under a jet of air.

4. Clean it with Trichlorethylene and dry, then
    with acetone and, finally, clean with alcohol
    and dry. Wrap the specimen in aluminum foil.

5. Weigh 0.4 g of cement resin and 0.6 g of
    hardener in small plastic cups. Wrap these
    cups with aluminum foil, leaving the upper
    side open, and immerse the hardener in water
    at 49°C and the resin in water at 43°C for
    10 minutes.

6. Mix thoroughly the cement resin and the
    hardener.

7. Mask out with adhesive tape the part of the
    specimen not to be covered by the glue, allow-
    ing a certain distance beyond the plastic
    length (see Fig. 30).

8. Spread a thin coat of glue on the part of the
    specimen to be covered by it.

9. Carefully place one end of the plastic over
    the cement, and using finger pressure, press
    the rest of it against the cement, working
    towards the opposite end. Be careful to
    avoid any air bubbles under the plastic.

10. Now built a bevel of cement at the ends of
    the plastic with a spatula. This is very
    important.

11. Let the cement stiffen approximately one
    hour, then remove the masking tape, Keep
    building the above-mentioned bevel.

12. If any cement is on top of the plastic coat-
    ing, clean top surface with a cottom swab
    immersed in alcohol.

13. Let the cement cure for 24 hours. The speci-
    men is then ready for testing.

2.5. Testing Techniques

The tests performed can be separated into six classes:

tests on solution treated and quenched specimens, tests on

annealed specimens, tests at low temperature, tests using a

spring to soften the Instron, tests on specimens with

photoelastic coatings attached to them, and finally, tests with round specimens.

The first four classes of tests were performed over a range of strain rates, in order to give a broad view of the kinds of behavior that can be obtained in Al 6061 alloy. The maximum effects were then selected to be used, with the photoelastic coating, in order to analyze their strain behavior.

The tests with the round specimens were made in order to check the establishment of strain gradients along the gage length of the specimens for Type A serrations. This phenomenon has been previously reported, as explained in the first chapter.

A few tests involving strain rate changes and constant strain relaxation were also performed.

During this investigation, very often one could observe deformation by deformation bands. When this occurs, the true strain rate may be a few orders of magnitude higher than if the specimen were deforming uniformly. This is due to the small region where the deformation is occurring during straining by bands. From now on, we shall use the term "nominal strain rate" to describe the strain rate of a test calculated just as if the material were deforming uniformly over the entire gage section.

2.5.1. Tests with Solution Treated and
Quenched Specimens

Specimens were solution treated for one hour at different temperatures, quenched in water and ice at 0°C, and tested in tension within 10 minutes after quenching. Solution treating temperatures were 535°C, 485°C, 450°C, 400°C and 350°C. Tests were performed at nominal strain rates ranging from $2x10^{-1}$ min^{-1} to $2x10^{-3}$ min^{-1}. All the specimens had a grain size of 10μ. The experimental result was simply the load-time diagram obtained from the Instron chart; in some cases the self-aligning grips mentioned before were used.

2.5.2. Tests with Annealed Specimens

Specimens were annealed three hours at 413°C and furnace cooled. Tensile tests were then performed at nominal strain rates from $2x10^{-1}$ min^{-1} to $2x10^{-3}$ min^{-1}, on specimens with grain size 10μ, 70μ and 200μ. Again the experimental result obtained was simply the above-mentioned load-time diagram. Some of these tests were performed with the previously described self-aligning grips. Whenever thicker specimens were used, a stepped zero suppression device was used. This device permits the expansion of selected parts of the load-time graph, for more detailed study.

2.5.3. Low Temperature Tests

These tests were performed using the equipment described in section 2.3.1, and covered only specimens solution treated

one hour at 485°C, quenched in a mixture of water and ice, and tested within 10 minutes. In this case, the nominal strain rates ranged from $2x10^{-1}$ min^{-1} to $2x10^{-3}$ min^{-1}. The experimental result of interest was once again the load-time Instron diagram. All specimens had a grain size of 10μ.

2.5.4. Tests with the Spring

The experimental set-up was that discussed in section 2.3.1, and the crosshead speed was 0.02 in/min, in all cases; the material had a grain size of ~10μ. All the specimens were solution treated, from 535°C and 450°C, and immediately tested. The load-time diagram supplied the desired information.

2.5.5. Tests with Photoelastic Coatings

These tests were performed on both annealed and solution treated specimens, with and without the spring. The solution treatment was performed at 535°C, on material with a 10μ grain size. The annealed specimens had a grain size of 70 and 200μ, while the tests with the spring were performed on specimens solution treated from 535°C. In the first two cases the nominal strain rate used was 10^{-2} min^{-1}, and in the last case the crosshead speed was 0.02 in/min. These conditions were chosen in order to maximize Type A and B serrations, whose strain behavior would then be observed.

Two other limitations have to be taken into consider-
ation in this case; first, the photoelastic material allowed
observations to only a limited amount of strain, namely
about 4 percent. The use of a green filter to make mono-
chromatic the light of the source increased this range
slightly but not above 7 percent. After these strains, the
colors were already very faded away, due to the superposi-
tion of the several reflected colors. Thus, whenever a
strain larger than about 4 percent had to be observed, the
specimen was first pre-strained, then it received the plas-
tic and was further deformed. Besides, an aging time of
24 hours is necessary for the curing of the adhesive cement.
In the case of solution treated specimens, this forced an
aging time of 24 hours before testing. Thus, when pre-
strain was necessary, the specimens were solution treated
and quenched, immediately pre-strained to the desired
amount, then the plastic was put on them. The specimen was
next aged for 24 hours and the test continued. Since it
was not known what would be the effect of such thermo-
mechanical treatments on the appearance of the serrations,
a simulated test without the plastic was usually run before
the final one with the plastic.

Once the specimen was in the final condition, and with
the photoelastic coating attached to it, it was mounted in
the Instron, using the screw grips, the self-aligning grips
or the spring mounting, according to the specific

circumstance. The experimental set-up shown in Fig. 20 was then arranged. At a fixed position of the big hand of the watch the test would be begun, and the motion picture camera was started some time before the yield point. Since at 18 frames per second each roll of film lasts three minutes, the test had to be stopped for changing film, and the load was allowed to relax.

Once the test was completed, the known initial time reading was located in the chart, and since the strip chart speed was known, other times could be pinpointed on it. Then, when the film was projected, any phenomenon observed in it could be easily related to the chart by simply reading times on the watch. This method proved to be highly satisfactory and accurate.

2.5.6. Tests with Round Specimens

As stated before, these were performed to verify the presence of strain gradients induced by Type A serrations. In order to do this, diameter measurements were performed before and after the tests, using a Jones and Lamson optical comparator, that allows measurements with the accuracy of 0.0001 in.

Diameters were measured at intervals of 0.1 in starting from the same end of the specimen, before and after the test, in two perpendicular directions. This led to some error, since the measurements were not performed at exactly

the same points before and after straining. However, the maximum strain used was 13.3 percent, which reduces these discrepancies. If x_o and y_o are the diameter measurements of a diameter before straining and if x and y are the same after straining, then the true strain at the point is

$$\varepsilon = \ell n \frac{x_o y_o}{xy} . \tag{2}$$

This strain was calculated along the gage length of the specimens, for several levels of total elongation. All the tests were performed at a nominal strain rate of approximately 10^{-2} min^{-1}, on annealed material, with grain size 200μ, in the set-up shown in section 2.3.2.

2.5.7. Other Tests

Tests were also performed using extensometers, introducing the load cell signal in a separate recorder and making tensile tests in steel and high purity copper, in order to obtain smooth stress-strain curves.

Besides, a few strain rate change experiments were made, in order to check the influence of the strain history of the specimens on their flow stress. The changes in nominal strain rate were made using an electronic device, and involved two orders of magnitudes from $2x10^{-1}$ min^{-1} to $2x10^{-2}$ min^{-1}, and from $2x10^{-2}$ min^{-1} to $2x10^{-3}$ min^{-1}. The chart speed was also simultaneously changed, in order to keep a constant ratio of chart speed vs crosshead speed.

Finally, some relaxation tests were performed, to check the speed of aging in our material.

CHAPTER III

EXPERIMENTAL RESULTS

3.1. Introduction

For greater clarity, the experimental results of this investigation shall be divided into four sections. First, the general load-time diagram characteristics for aluminum 6061 alloy shall be discussed, covering changes in temperature, heat treatment, grain size, etc. After that, results obtained by the use of photoelastic coatings shall be taken into consideration, followed by an analysis of strain gradients induced in round specimens. Finally, we shall point out the results obtained from tests involving strain rate changes and relaxation.

However, one should first consider the results of the experiments performed in order to check the performance of the Instron recording and pulling apparatus. A test of annealed aluminum 6061 alloy that presented Type A serrations was performed using a high response speed, independent, Brush recorder to register the signal from the Instron load cell. The result obtained was identical to that observed on the Instron chart; next tests were performed with steel and high purity copper to check if smooth load-time diagrams

could be obtained from the Instron. One was able to obtain such smooth curves consistently. Finally, tests with extensometers were performed, to make sure serrations had nothing to do with the load cell. Tests were made with copper, and smooth elongation time curves were obtained. Thus, the Instron set-up could be safely used in this investigation.

3.2. General Load-Time Diagram Characteristics

Aluminum 6061 alloy presented profuse serrations in most of the tests performed. It was observed that the parameters studied in Chapter I affected this serrated flow, and we shall now show what is their effect on the general load-time characteristics of the material studied.

3.2.1. The Effect of Strain

The variation of the serrations with strain depends very much on the heat treatment of specimens, their grain size, strain rate, mechanical characteristics of the Instron machine, and finally, temperature of tests. We shall have a quick look at this effect, since it will also be inevitably discussed in each of the following sections.

In fully solution treated and quenched, 10μ grain size material, serrated flow begins shortly after the yield point. The serrations start as irregular Type B, and as strain increases they become more and more regular. However, a perfectly regular shape, such as shown in Fig. 3, is never

attained. There always exists some variation in the average
level of the curve. This behavior can be seen in Fig. 36.
Since the Instron chart was too long to be enclosed, it was
cut into smaller pieces and mounted as shown in this figure.
Figure 36 should be read from right to left and from the
upper part to the lower. Note that the amplitude of Type B
serrations increases with strain.

When the strain rate is increased, serrations are
initially more jerky and tend to Type A, but after some
strain they turn slowly to Type B. The same is observed
when the solution treating temperature is lowered. Then, it
takes more strain to convert "jerky" Type A serrations into
Type B serrations. Figure 37 illustrates this, and it should
also be noted that the transition is slow. In both Figs. 36
and 37, and in all similar ones, the load scale applies only
to each section of the curve, and not to the full height of
the graph. In quenched specimens tested at lower temperature,
there is again a tendency for strain to cause a transition
from "jerky" flow to Type B serrations.

Thus, concerning solution treated and quenched speci-
mens, it may be stated that the effect of strain is to pro-
mote Type B serrations, and also to increase the amplitude
of these serrations. However, in the case of specimens de-
formed in a "softened" Instron, the sole effect is to in-
crease the magnitude of the load drops.
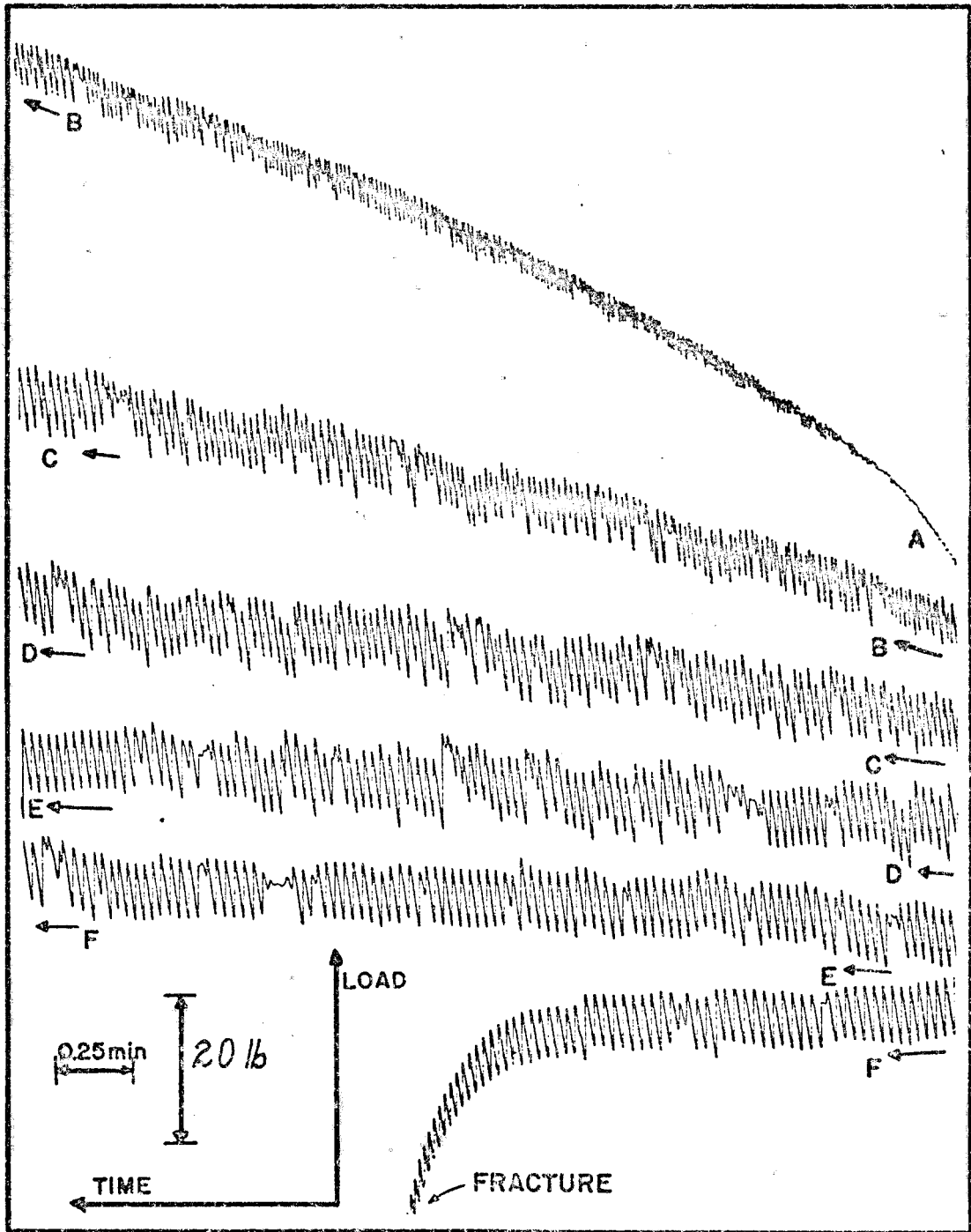
Fig. 36. The effect of strain on Type B serrations. Material solution treated one hour at 535°C, quenched in water and ice, tested at room temperature, nominal strain rate 2×10^{-3} min^{-1}, grain size 10μ.

Fig. 37. The effect of strain on Type B serrations. Material solution treated one hour at 485°C, quenched in water and ice, tested at room temperature, nominal strain rate 2×10^{-2} min^{-1}, grain size 10µ.

Annealed material usually presents Type A serrations.
Such a behavior can be seen in Fig. 38, where the load-time
diagram for a 200µ grain size, round specimen, is shown.
One should point out that not all peaks are associated with
the formation of deformation bands, as shall be discussed
in the section of results obtained from tests with photo-
elastic coatings. Thus, only the peaks with vertical arrows
over them in Fig. 38 are associated with such band formation.

The effect of strain in this case is to increase the
strain between two successive band formations ($\Delta\varepsilon$), and to
change the magnitude of the load drop associated with the
nucleation of bands ($\Delta\sigma$); $\Delta\varepsilon$ increases linearly with strain,
as shown in Fig. 39. However, $\Delta\sigma$ initially increases with
strain, then decreases and finally disappears, as high
strains promote a smoothing of the load-time diagram (see
Fig. 38). This is shown in Fig. 40, where the band drawn
shows this general tendency. As Fig. 38 and Fig. 40 show,
there is much data scatter in the values of $\Delta\sigma$, and there
is no monotonic increase or decrease in its values; regard-
ing this point, the flow is highly irregular.

3.2.2. The Effect of the Mechanical Characteristics of the Tensile Apparatus

The stiffness of the Instron machine was decreased by
the use of the set-up discussed in section 2.3.1, Chapter II.
As stated before, all tests were then performed with 10µ
grain size material, solution treated at 535°C and 450°C,
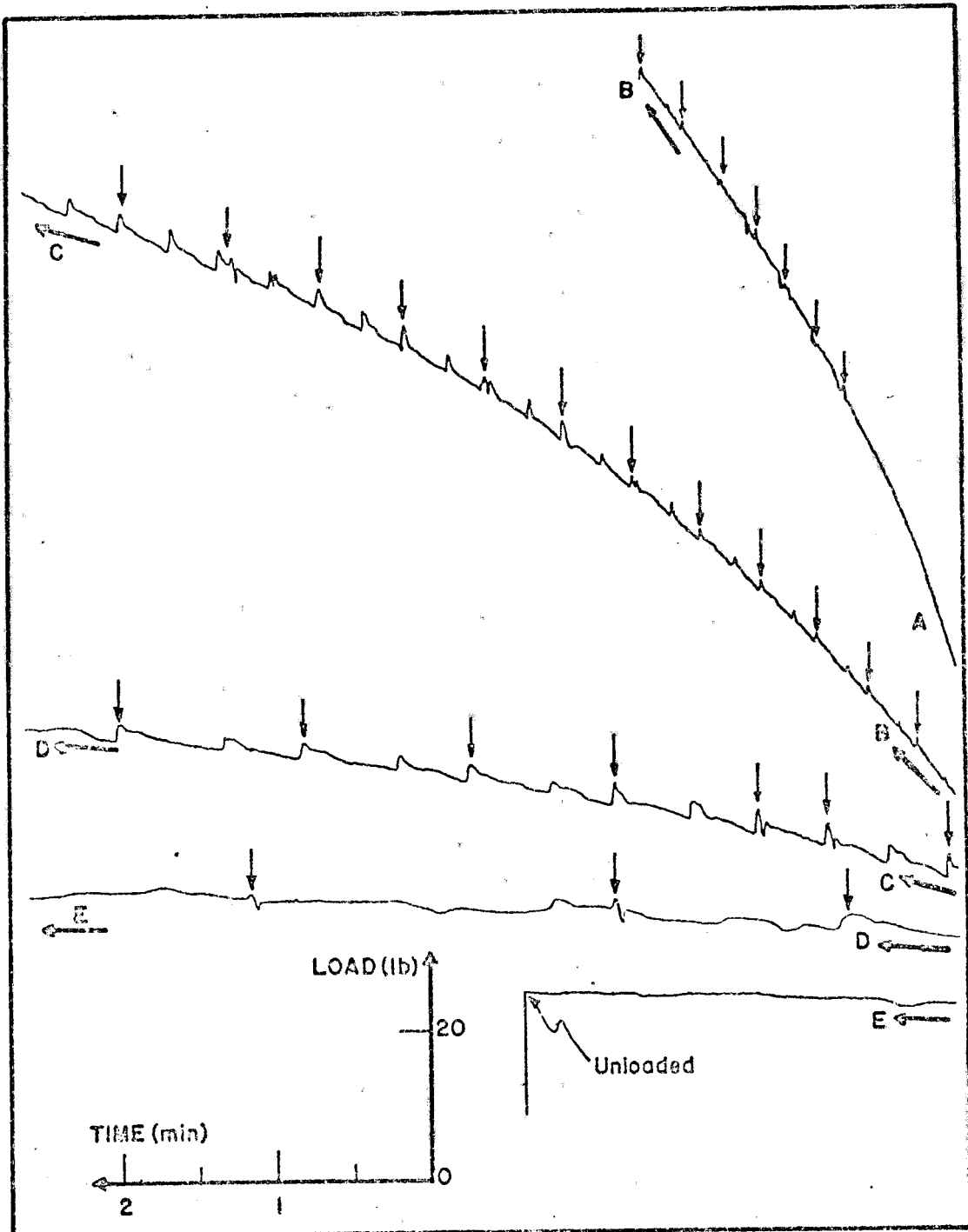
Fig. 38. The effect of strain on Type A serrations. Material annealed 3 hours at 413°C, furnace cooled, tested at room temperature, nominal strain rate 0.77×10^{-2} min^{-1}, grain size 200μ.
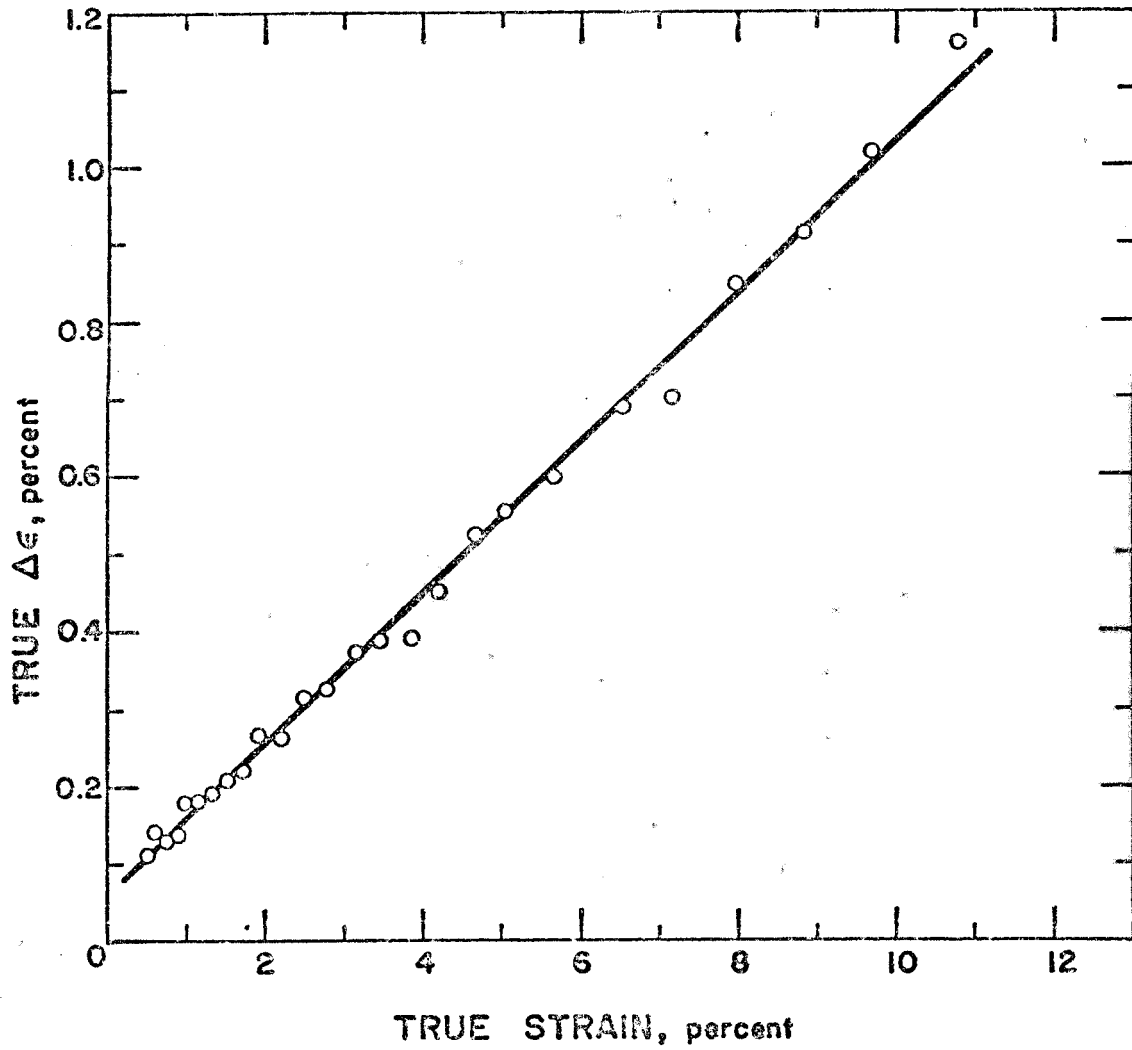
Fig. 39. The influence of total strain on the strain
between two successive Type A serrations.
Annealed material, nominal strain rate 0.77×10^{-2}
min^{-1}, grain size 200μ.
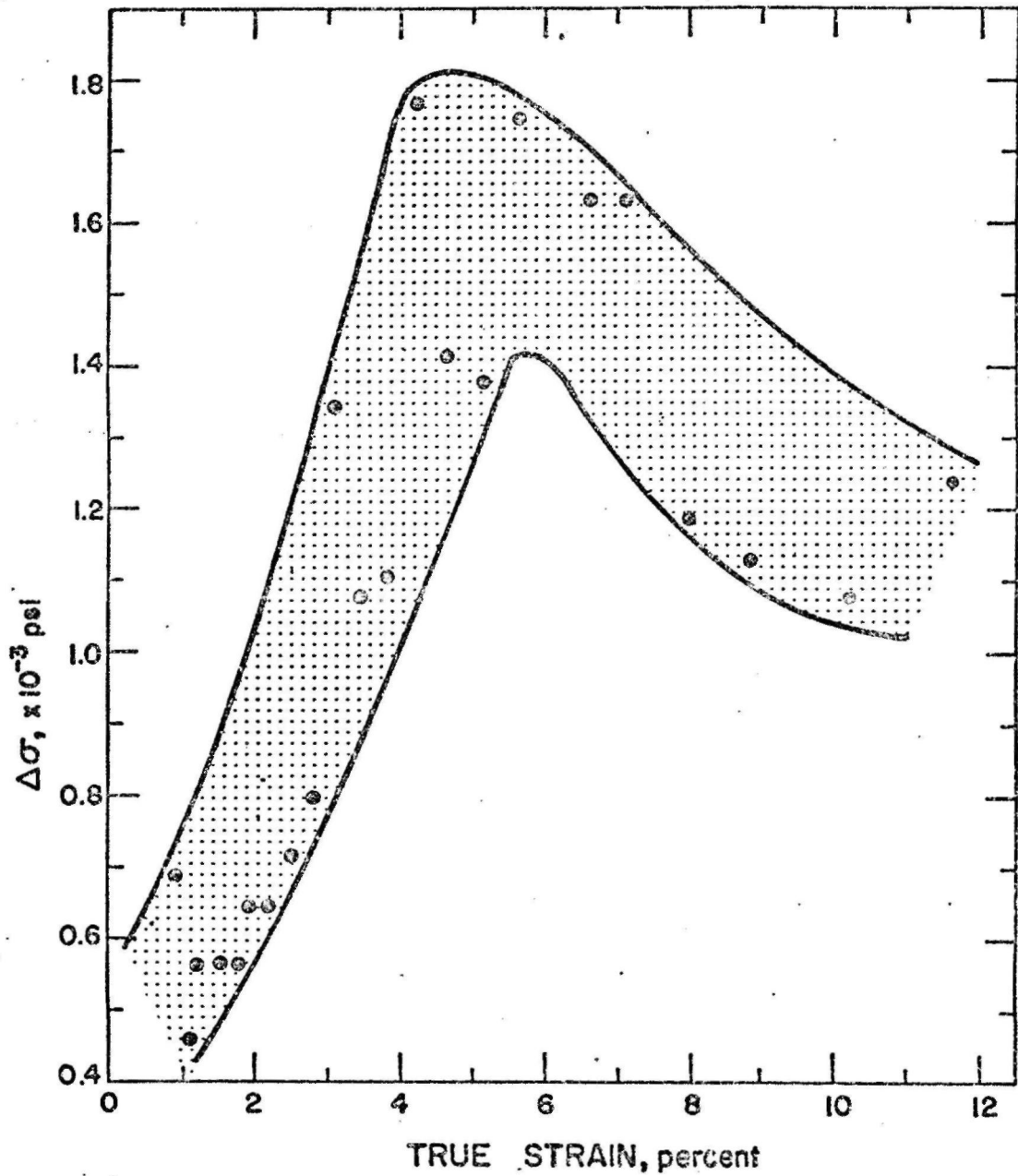
Fig. 40. The influence of total strain on the load drops in Type A serrations. Annealed material, nominal strain rate 0.77×10^{-2} min^{-1}, grain size 200μ.

and then quenched. No difference was observed in the be-
havior of the material with these two different heat treat-
ments, and thus the experimental results will be discussed
together. Type B serrations present a rise in load between
two successive load drops (see Fig. 3), that follows the
elastic characteristics of the tensile set-up. Thus, when
the Instron is softened, it should be expected that the line
between two successive load drops would be much less steep,
in the way shown in Fig. 41. This is indeed observed.
However, another important fact occurs: the number of load
drops decreases very much; in a regular test, as shown in
Fig. 36, one gets about 1,000 peaks in the curve. A similar
test with the spring exhibits about 40 peaks. This implies
that the deformation associated with each peak is higher in
this case than when one is dealing with a stiff machine.
This can also be seen in the following argument: the load
drops increase with strain in tests with a soft machine
until they reach a value comparable to those obtained in a
stiff machine. This implies that in the soft machine the
deformation associated with a load drop is much higher.
This is confirmed by the fact that the specimens always fail
suddenly, in one of the load drops.

As it has been stated before, when a specimen is
quenched from 450°C and then tested, the flow is initially
"jerky" Type A and then goes slowly to Type B. However,
when the spring is introduced, all this initial part is
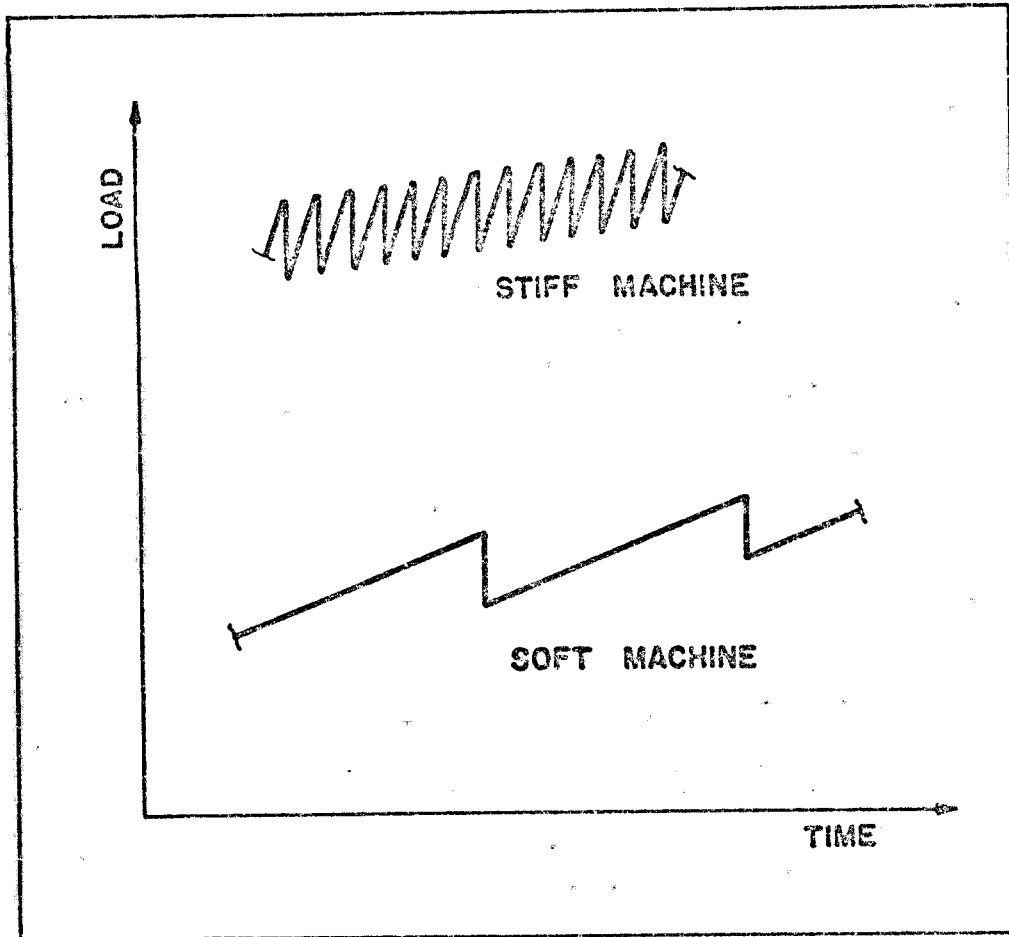
Fig. 41.   The influence of the mechanical characteristics
of the tensile apparatus on the load-time curve.

wiped out. All that is observed is the presence of small plateaus in the initial part of the curve.

Here, the strain rate is obviously not determined by the crosshead speed. However, in all tests the crosshead speed used was 0.02 in/min.

3.2.3. The Effect of Temperature

A few tests were performed at the temperature of water and ice, using the set-up discussed in section 2.3.1.

Figure 37 shows the appearance of the load-time diagram for a 10μ grain size material, solution treated one hour at 485°C, quenched in water and ice, and deformed at a nominal strain rate of 2×10^{-2} min^{-1}, at room temperature. The same test performed at ≈ 1.5°C has quite a different aspect: first of all, no Type B serrations are present, and there is a much greater tendency for the presence of Type A serrations, that persist up to the point of failure. However, no regularity in their appearance, such as shown in Fig. 38, is observed. Finally, the critical stress for the beginning of serrations is increased as we go down in temperature, as shown in Fig. 42. The dashed line just shows the overall tendency, since two experimental points are obviously not enough to determine the curve. The critical strain (ε_0) vs temperature curve for 6063 aluminum alloy is also shown, for comparison. This curve was taken from McCormick's work.[3]
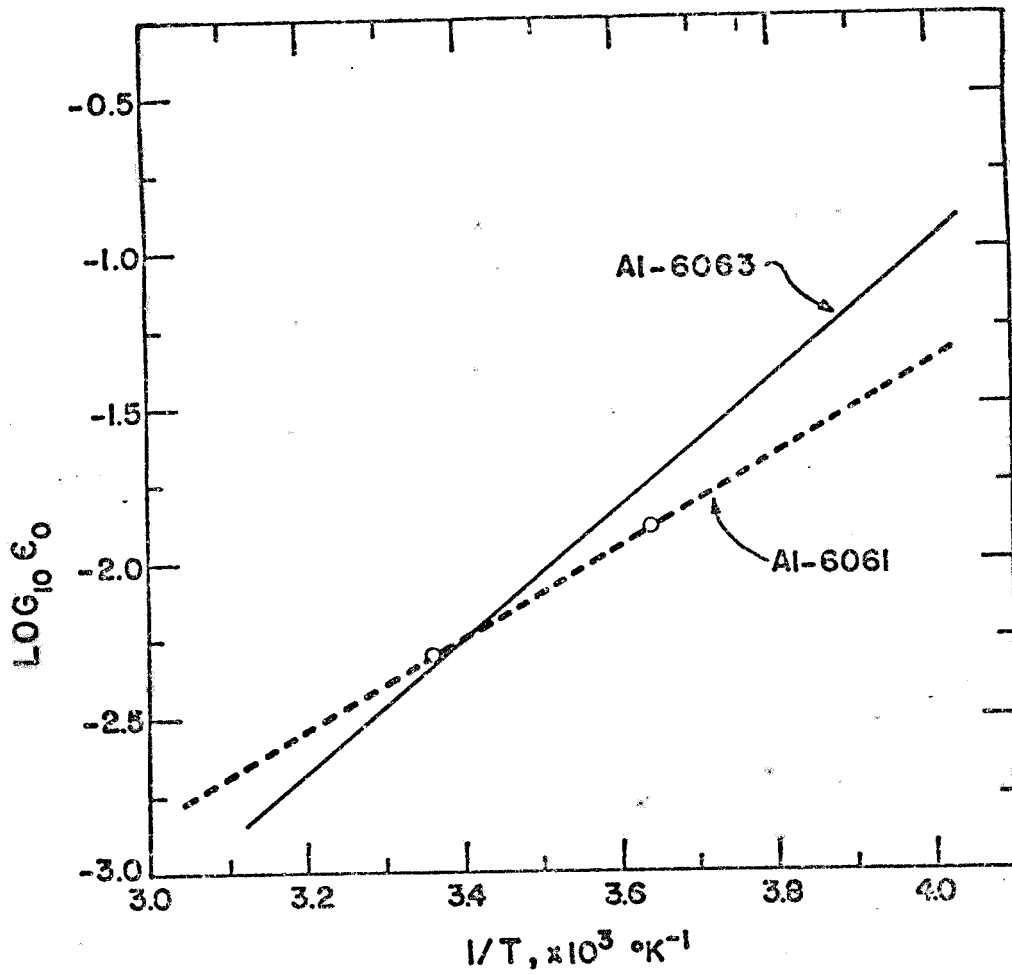
Fig. 42. The influence of temperature on the critical
strain ε_o for the onset of serrations. Material
solution treated one hour at 485°C, quenched in
water and ice, nominal strain rate 2×10^{-2} min^{-1},
grain size 10μ.

If one draws an approximate average load-time diagram

for serrated curves such as shown in Figs. 37 and 38, it

is possible to have an idea of their stress-crosshead dis-

placement behavior. Figure 43 shows two such curves, com-

paring two stress-crosshead displacement curves at differ-

ent temperatures.

3.2.4. The Effect of Strain Rate

The range of nominal strain rates used in this investi-

gation was $2x10^{-1}$ min^{-1} to $2x10^{-3}$ min^{-1}. Although the ef-

fect of strain rate depends on heat treatment, grain size

and other factors, a general trend may be identified: high

nominal strain rates usually promote smoother curves. As

the nominal strain rate is lowered, first one goes through

a region where Type A serrations are favored, and later, at

still lower strain rates, profuse Type B serrations are

present. Concerning this type of serrations, a decrease in

nominal strain rate also increases their amplitude. Now we

shall divide the specimens by heat treatment and analyze

their behavior in more detail.

Specimens with grain size 10μ, solution treated for one

hour at 535°C and quenched, present very profuse Type B ser-

rations at low nominal strain rates $(2x10^{-3}$ $min^{-1})$. As the

strain rate is raised, jerky or irregular Type A flow ap-

pears in the beginning of the deformation; Type B serrations

appear at higher strains, and their amplitude decreases with

increasing nominal strain rate. This behavior is similar
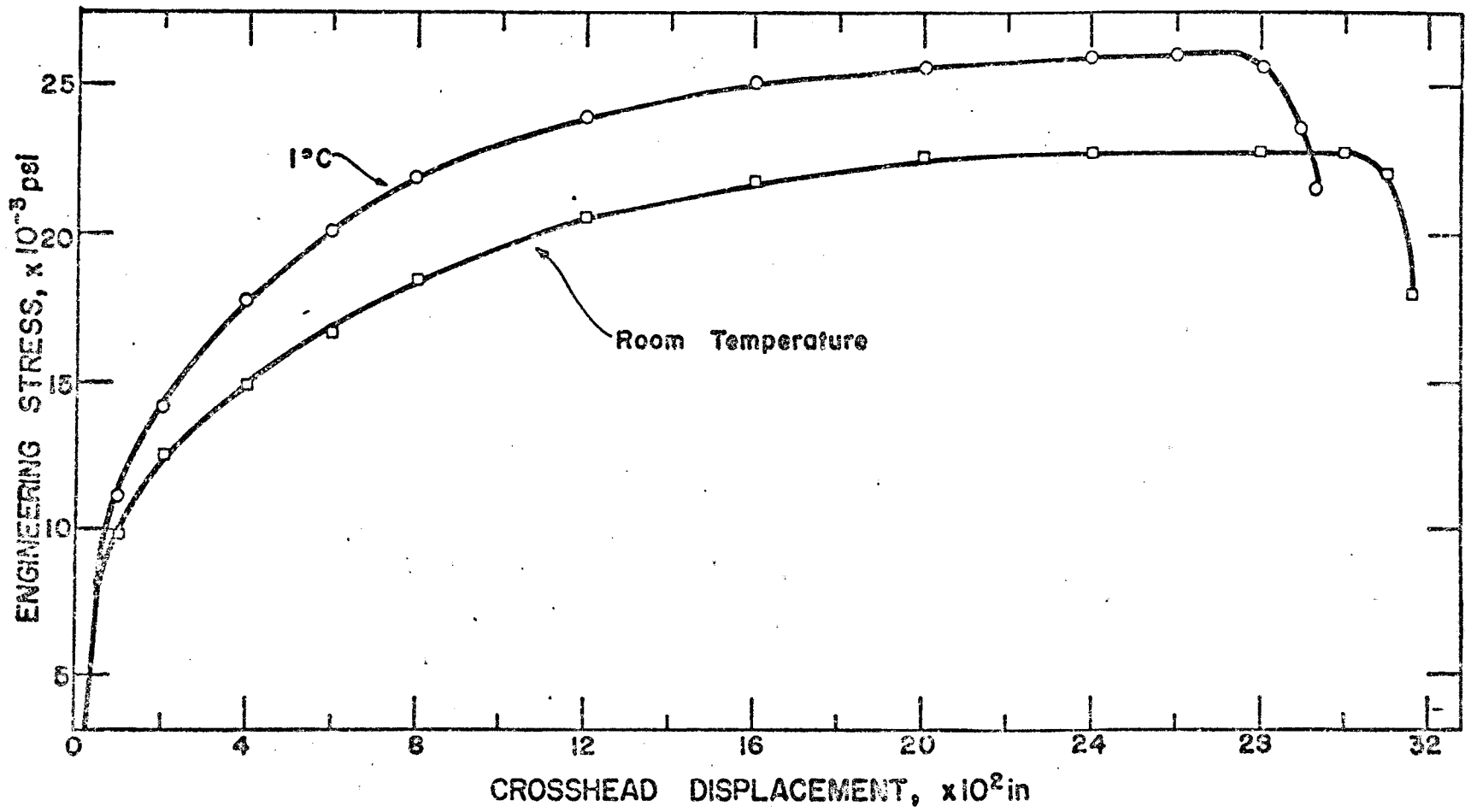
Fig. 43. Temperature dependence of the stress-elongation curves for specimens
solution treated one hour at 485°C and quenched in water and ice,
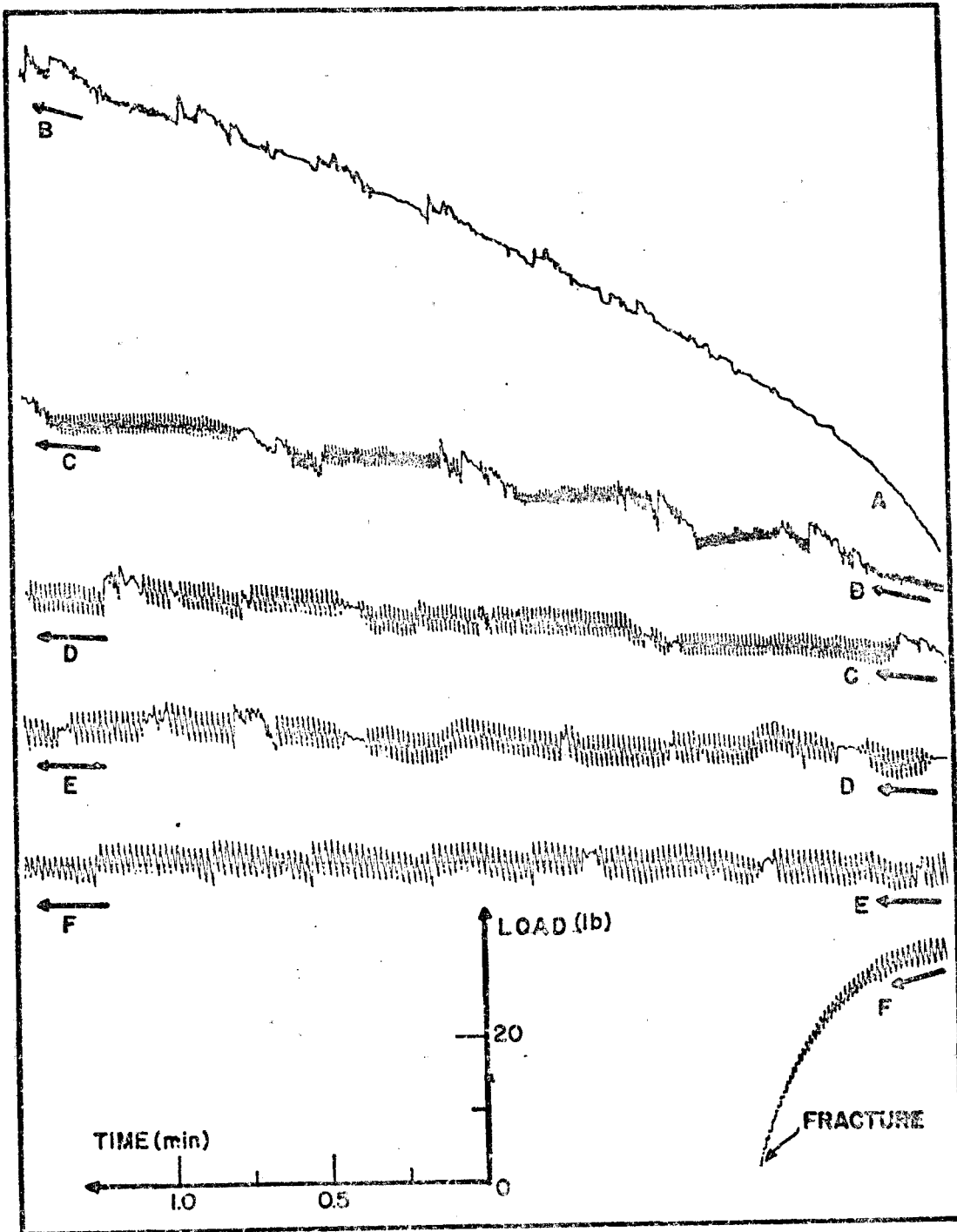tested at a nominal strain rate 2×10^{-2} min^{-1}, grain size 10μ.

to that shown in Fig. 37, and can also be observed in Fig. 44, which should be compared with Fig. 36. This material also presents an inverse stress-nominal strain rate relationship, as seen in Fig. 45. The curves in this diagram were obtained in the same way described in section 3.2.3.

For specimens with grain size 10μ, solution treated at temperatures below 535°C, no full tests at different strain rates were performed, but only nominal strain rate changes during the test. This will be considered in a later section. However, the specimens solution treated at 485°C and tested in water and ice covered three nominal strain rates: 2×10^{-1}, 2×10^{-2} and 2×10^{-3} min^{-1}. At the high strain rate, the curve was almost smooth, with occasional "bumps" and plateaus. At the intermediate curve, relatively irregular Type A serrations are present, and profuse Type B serrations occur at the lowest strain rate. Figure 46 shows the effect of strain rate on the averaged stress-crosshead displacement curves for these specimens.

High nominal strain rate (2×10^{-1} min^{-1}) tests produced smooth curves in annealed, 10μ grain size material. As this strain rate was lowered, Type A serrations started appearing, and at very low nominal strain rates (2×10^{-3}), the load-time diagram had the appearance shown in Fig. 47. Annealed material had a flow stress relatively independent of nominal strain rate, as shown in Fig. 48. These curves were obtained in the way already described.
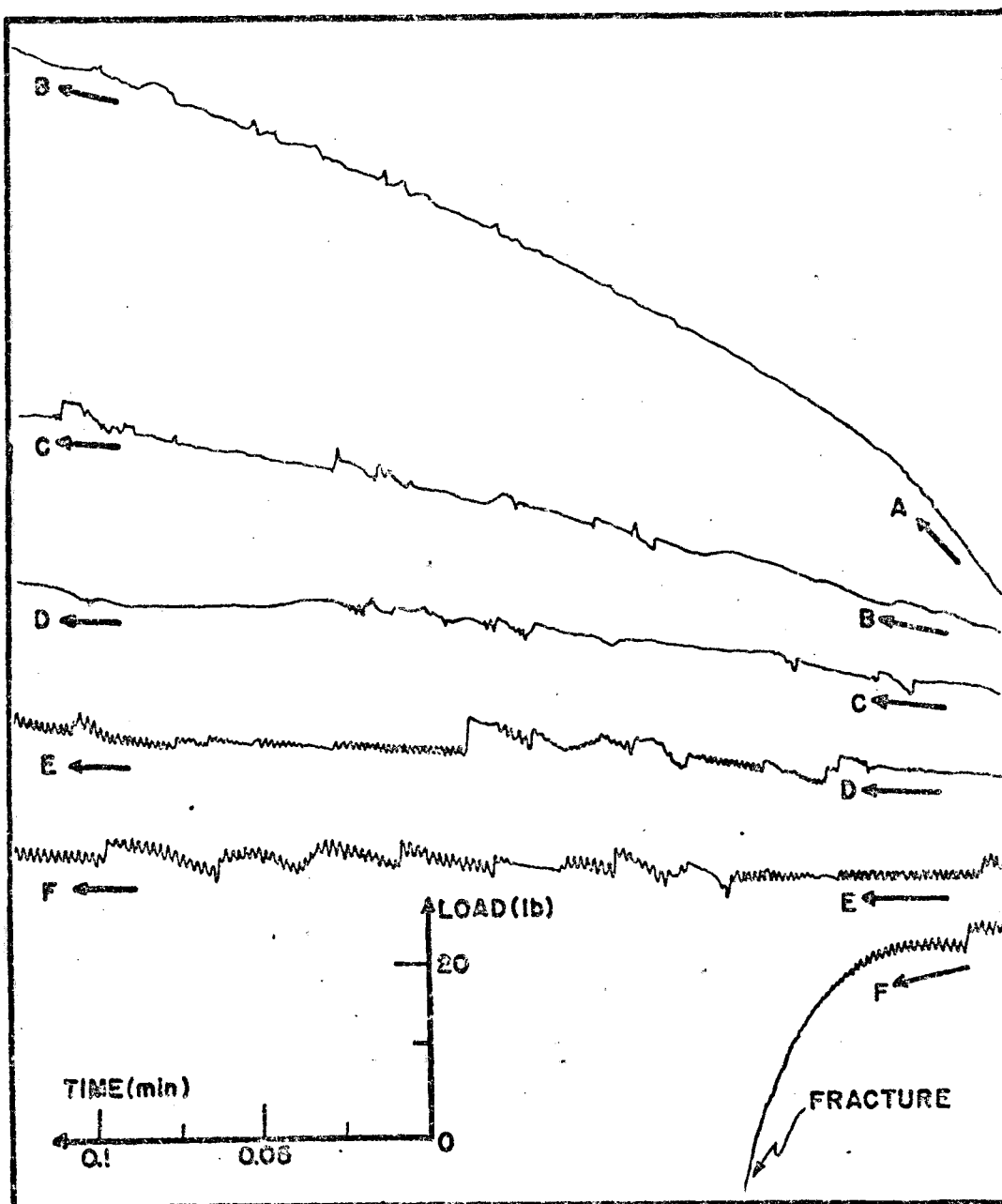
Fig. 44. Effect of high nominal strain rate on the load-
time diagram for a 10μ grain size specimen,
solution treated one hour at 535°C and quenched
in water and ice, tested at a nominal strain
rate of 2x10^{-1} min^{-1}.
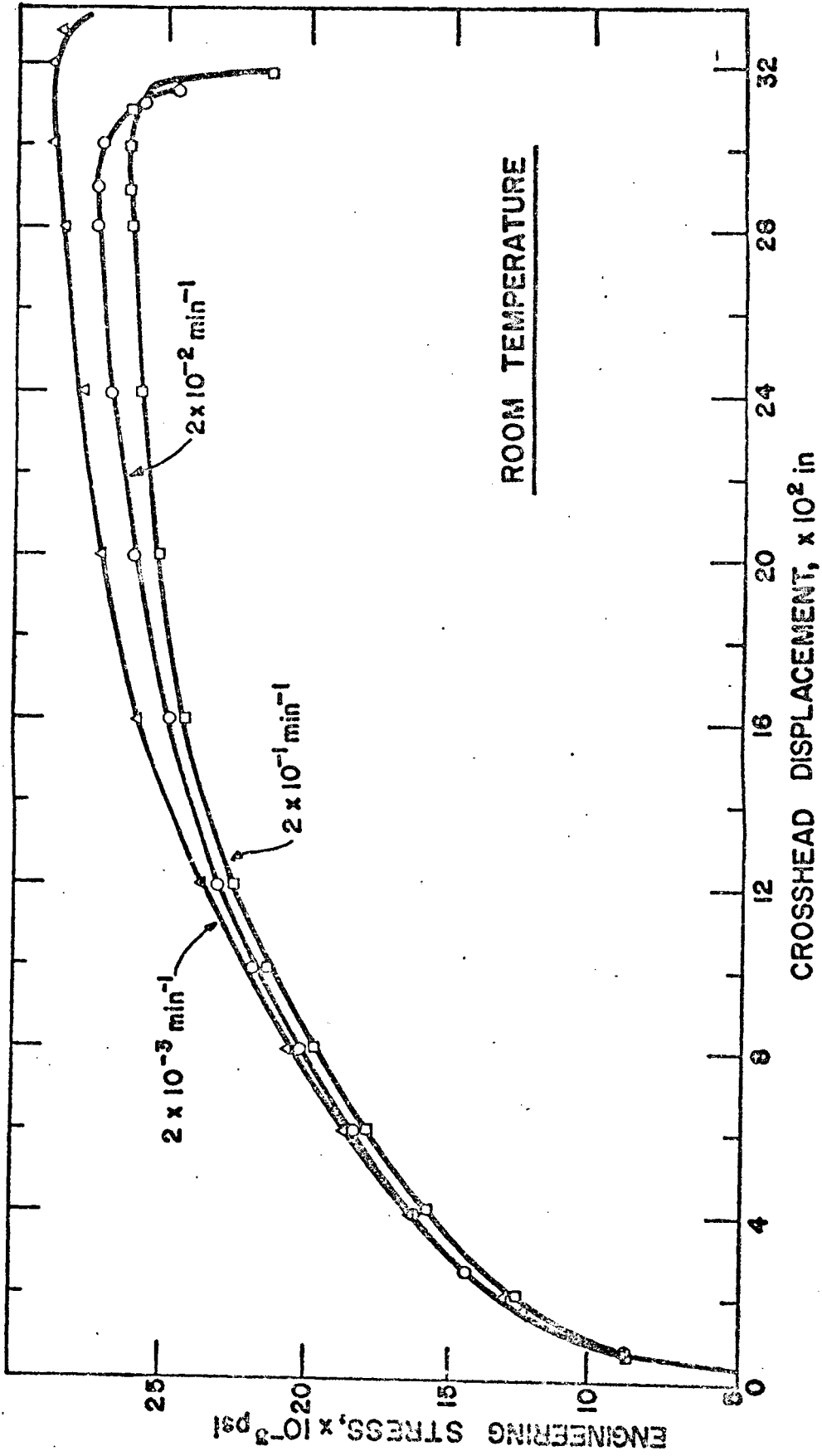
Fig. 45. The effect of nominal strain rate on the stress-elongation curves for material with 10μ grain size, solution treated one hour at $535°C$, quenched, and tested at room temperature.
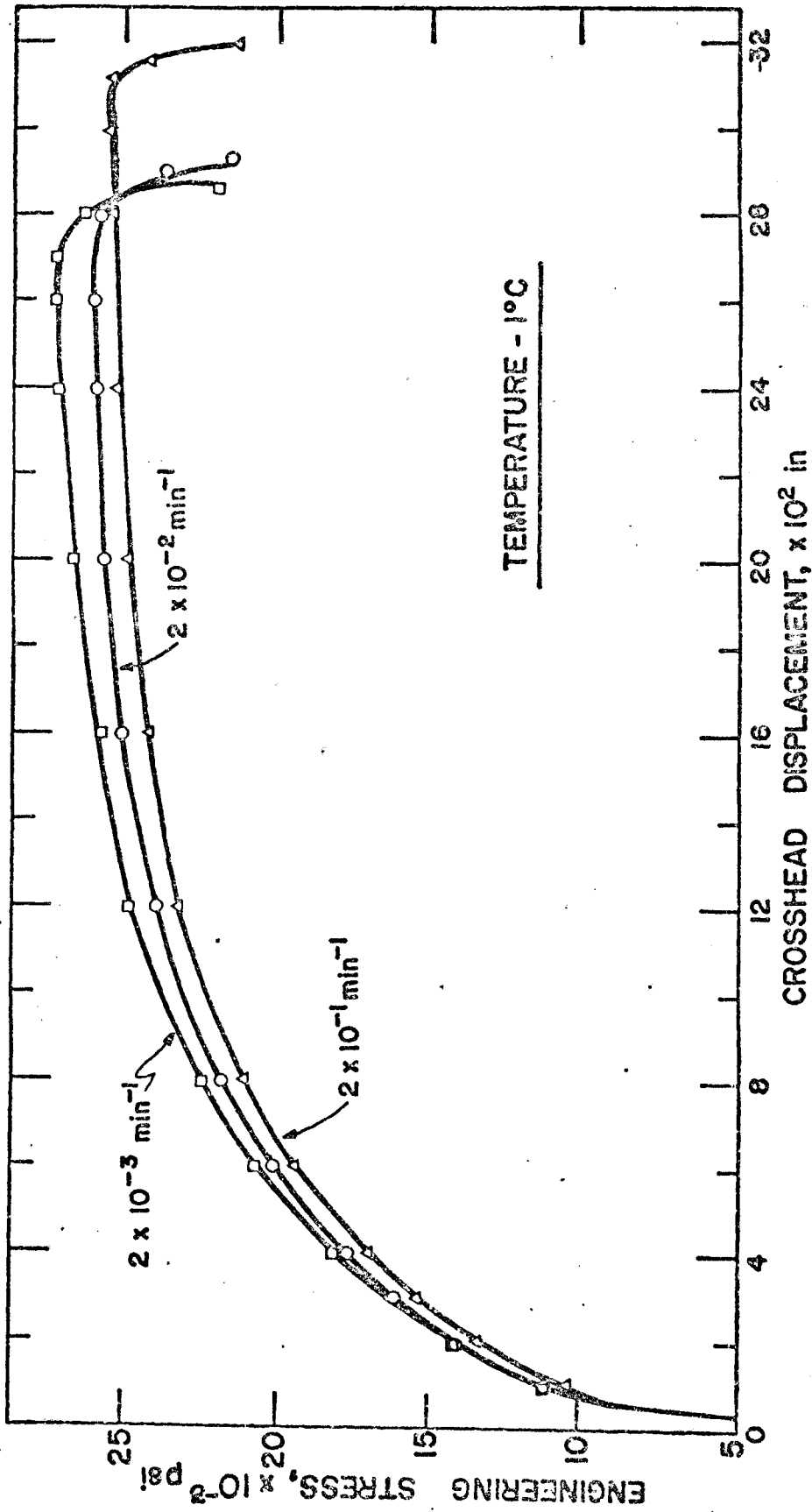
Fig. 46. The influence of nominal strain rate on the stress-elongation curves for 10μ grain size material, solution treated one hour at 485°C, quenched and tested in water and ice.
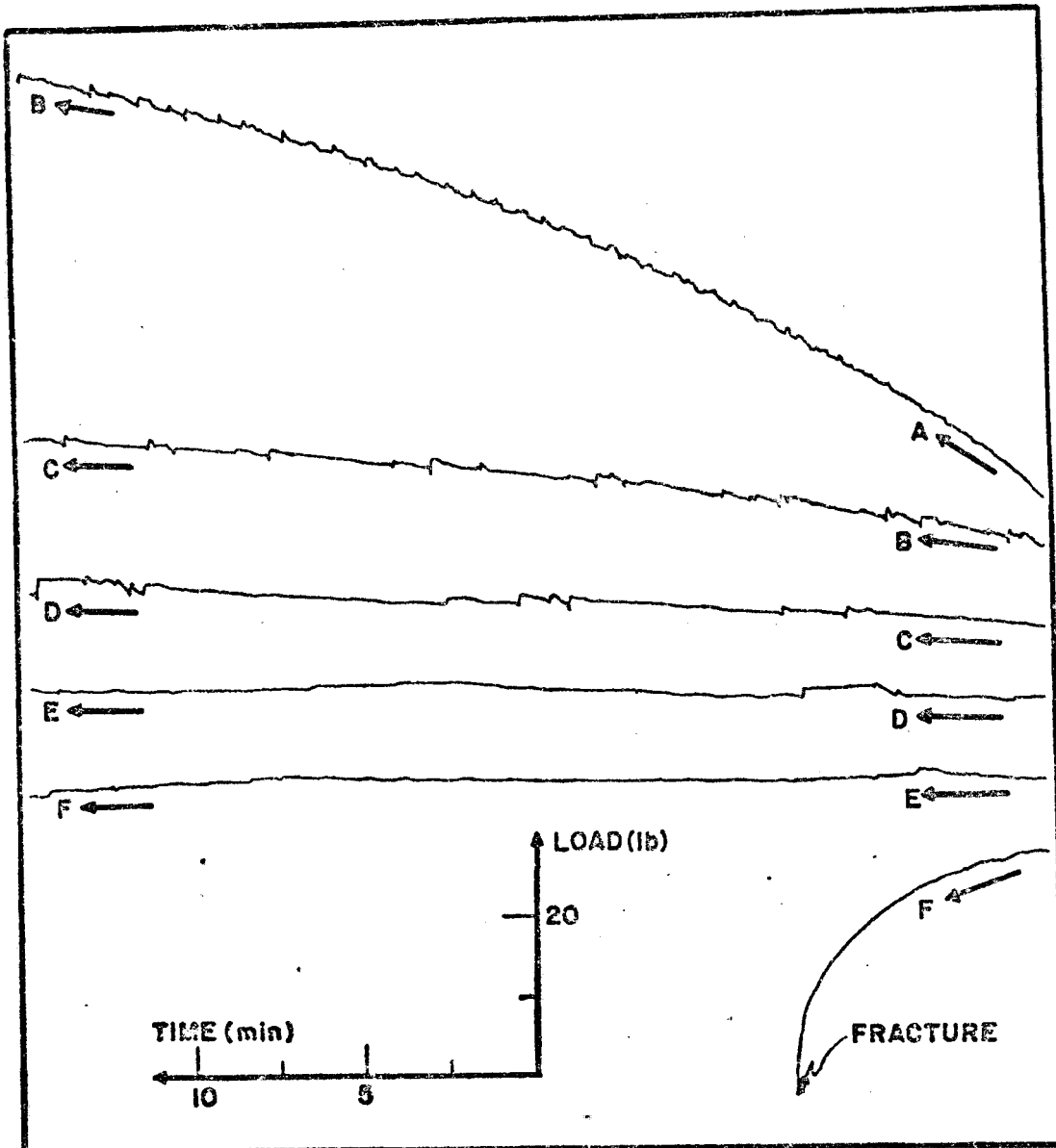
Fig. 47. The influence of low nominal strain rate on the load-time curve for an annealed, 10μ grain size specimen. Nominal strain rate 2×10^{-3} min-1.
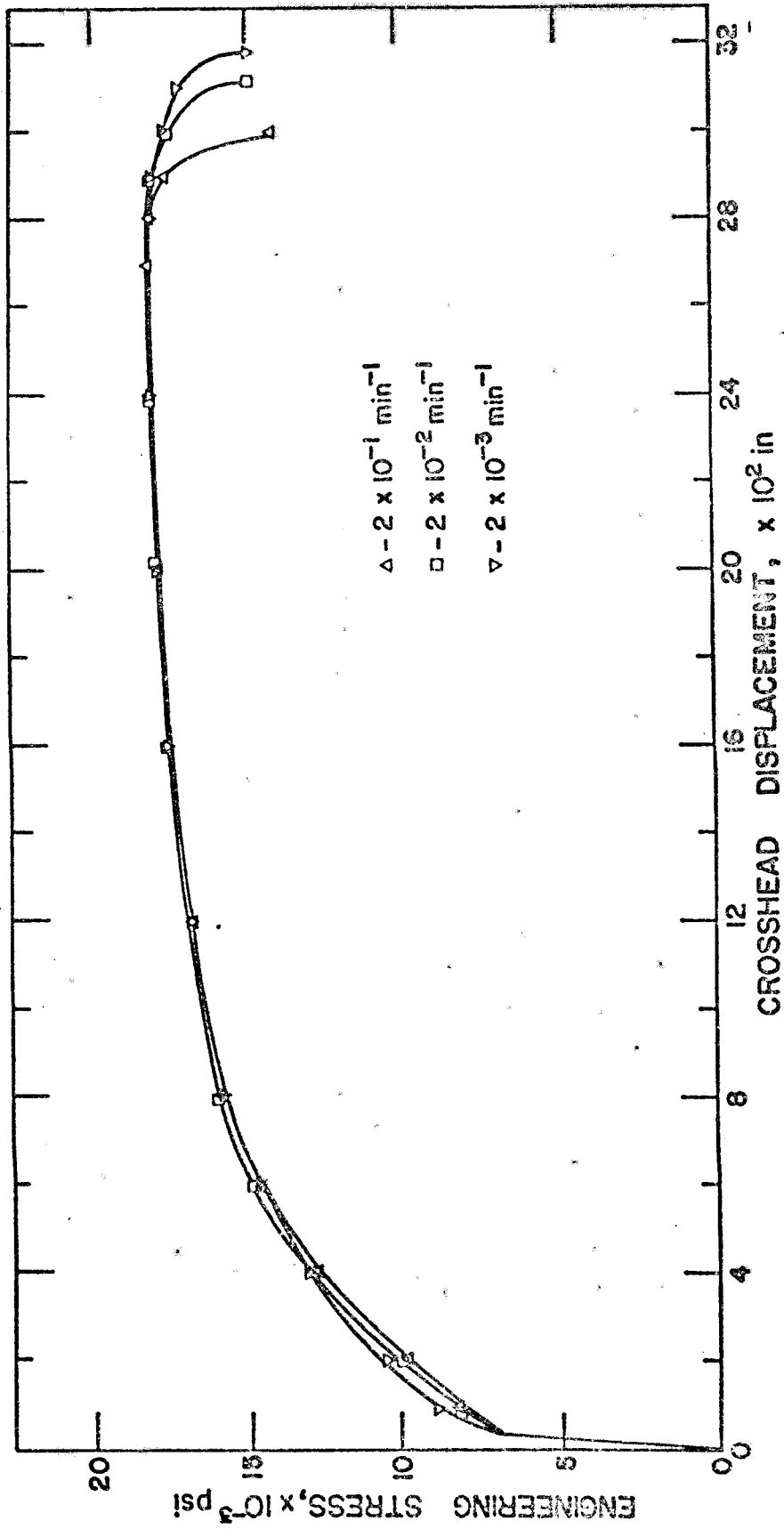
Fig. 48. The influence of nominal strain rate on the stress-elongation curves of annealed, 10μ grain size material.

Another fact that should be taken into consideration
is the influence of nominal strain rate on the critical
strain to start serrations, ε_o. In all cases, it increased
with increasing strain rate. This behavior is shown in Fig.
49. It should be pointed out that ε_o is frequently of dif-
ficult determination, and the straight lines in Fig. 49
should be considered more as a general trend than accurate
curves.

3.2.5. The Effect of Heat Treatment

The heat treatments involved in this work included
annealing and solution treating at several temperatures, fol-
lowed by quenching. Solution treated specimens were usually
tested immediately after quenching. However, whenever a
photoelastic coating was to be used, they had to be aged 24
hours at room temperature to be tested. Thus, some tests
were performed to analyze this effect.

The influence of annealing the material has already
been described in the previous sections; concerning solution
treating, quenching and immediately testing, it was observed
that the temperature of solution treatment was important.
The main effect of lowering this temperature below 535°C
was to increase the region of Type A or jerky flow, before
the appearance of Type B serrations. The strain before the
onset of serrations (ε_o) wasn't changed, for the same strain
rate. For example, for a quenching temperature of 400°C, at
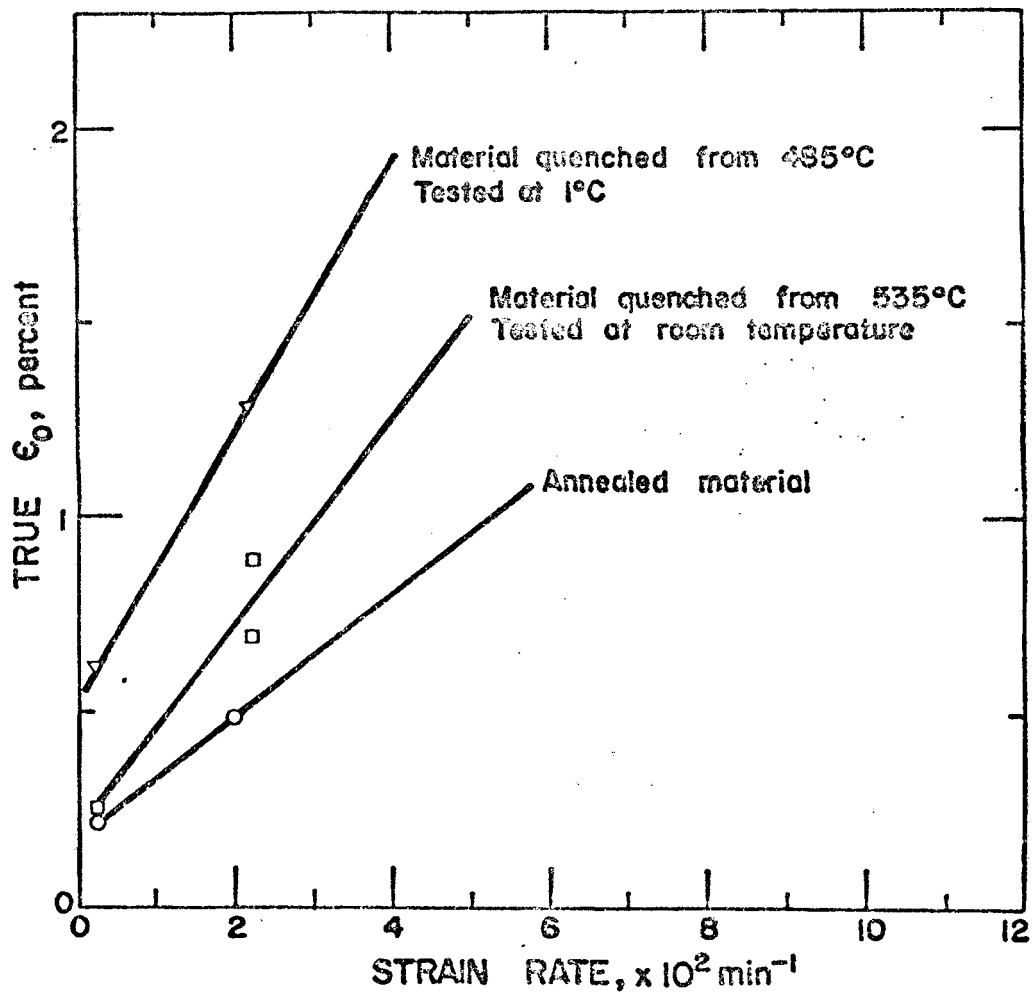
Fig. 49. General trend of the critical strain for the
onset of serrations, ε_0, as a function of
nominal strain rate.

a nominal strain rate of $2x10^{-2}$ min^{-1}, one already gets only
irregular Type A serrations on all the curves.

The effect of aging the material for 24 hours before
testing depends on the solution treatment temperature.
Material solution treated from 535°C, for example, has its
critical strain greatly increased, and presents only irregu-
lar Type B serrations.[32] On the other hand, material solu-
tion treated at 450°C presented no such phenomenon: the
critical strain was unchanged by the aging. However, the
initial serrated flow, that in the freshly quenched material
is irregular Type A, is completely irregular and jerky in
the aged material.

Concerning the stress-crosshead displacement curves
for these materials, Figs. 50 and 51 show that the material
quenched and immediately tested has higher flow stress than
the one aged 24 hours at room temperature, and that the
solution treatment temperature is very important in deter-
mining the stress of the materials in question. Note that
at T = 350°, there is a reversal in the trend of lower
stresses for lower solution treating temperatures. The
curves for 350°C and 400°C were run only to a limited strain.

Figure 49 also shows that at room temperature, the
critical stress for the onset of serrations (ε_o) depends on
the heat treatment of the specimens. The impossibility of
better accuracy in the measurement of ε_o for the 10μ speci-
mens, however, prevents any definite observation regarding
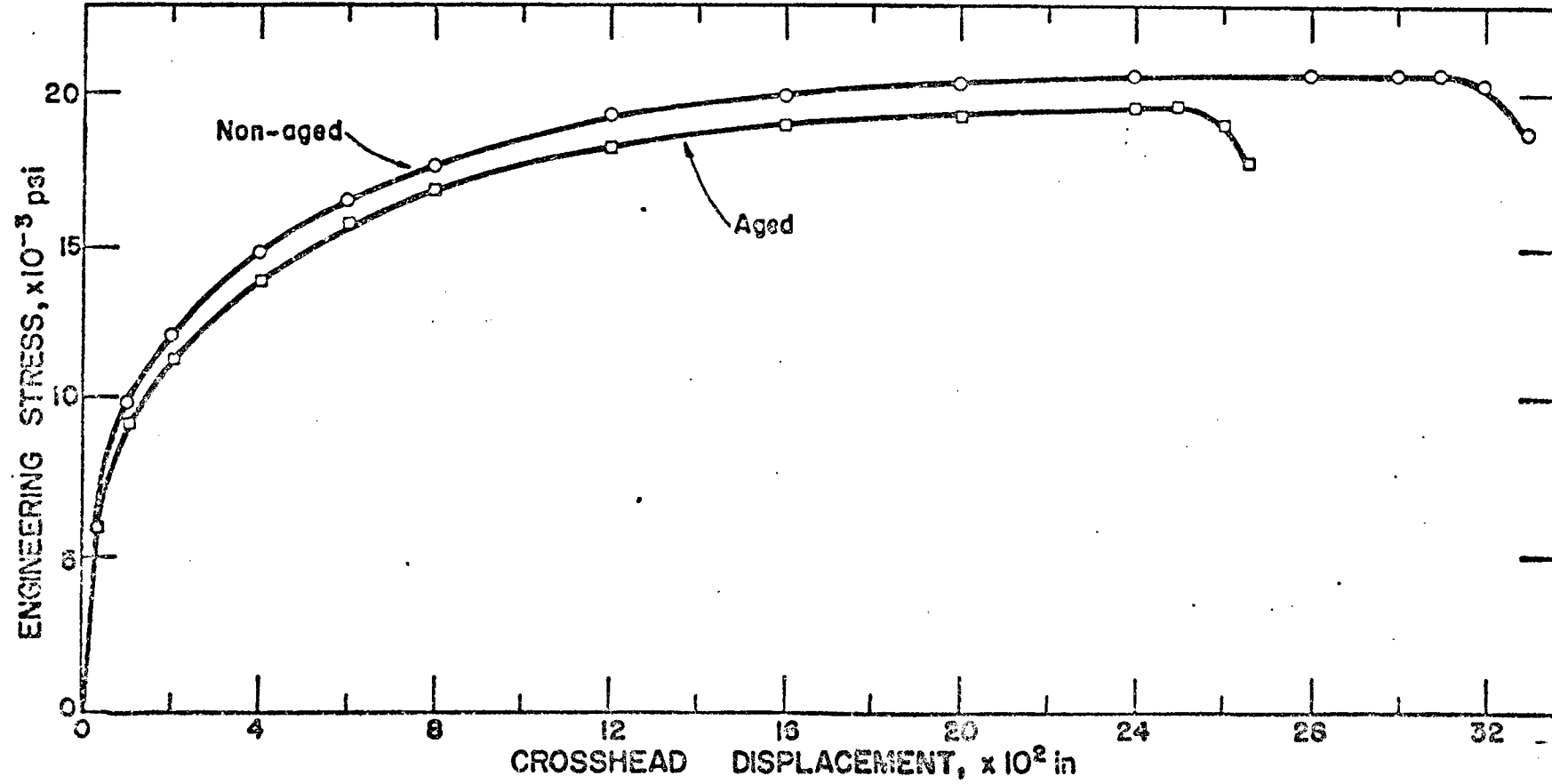
Fig. 50. The influence of 24 hours aging at room temperature before testing on the stress-elongation curves for 10μ grain size specimens, solution treated one hour at 450°C and quenched in water and ice, nominal strain rate 2×10^{-2} min^{-1}.
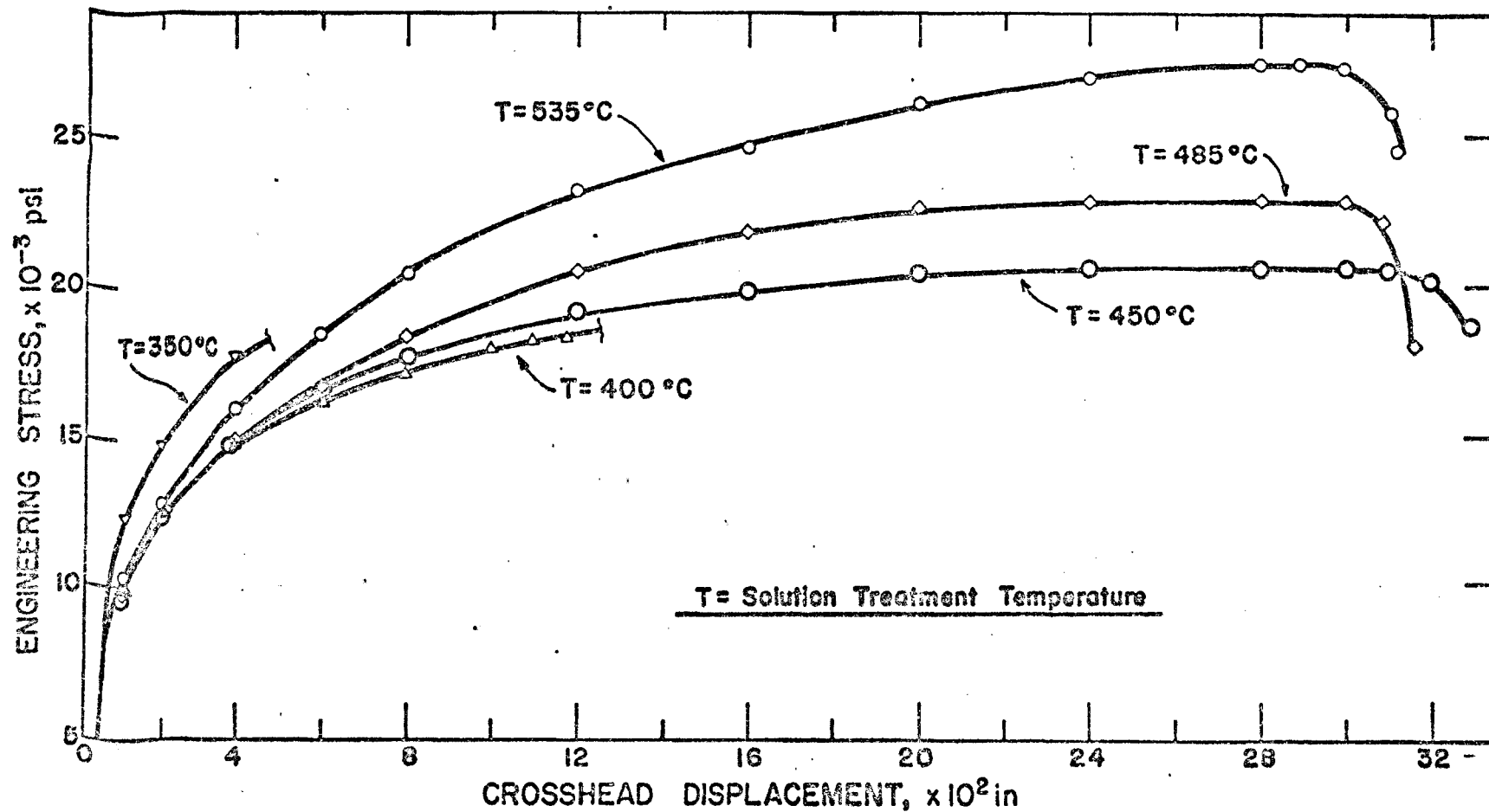
Fig. 51. The influence of solution treating temperature on the stress-elongation
curves for 10μ grain size material, deformed at room temperature at
nominal strain rate 2×10^{-2} min^{-1}. All specimens quenched in water and
ice.

the effect of heat treatment. As stated before, Fig. 49
merely shows the trend of ε_o with strain rate.

3.2.6. The Effect of Grain Size

The influence of grain size can be assessed only for
annealed specimens, since all solution treated specimens
had a constant grain size of 10μ.

First of all, increasing grain size invariably tended
to promote Type A serrations. Actually, at the higher grain
size used (200μ) not even a tendency for irregular jerky
flow was ever observed at the nominal strain rates used
(10^{-2} and 10^{-3} min^{-1}).

Table 2 summarizes the effect of grain size on the
critical stress for the onset of serrated flow (ε_o), and
the corresponding stress (σ_o) for two nominal strain rates.
As one can see, there is a general tendency for ε_o to in-
crease with grain size; however, σ_o is practically inde-
pendent of this parameter.

3.2.7. The Effect of Composition

This variable wasn't monitored at all in this work.
It should be pointed out that the three plates used (with
three different grain sizes) came from different heats.
However, they are bounded by the limits of alloying elements
specified in Table 1.

Table 2

The Influence of Grain Size on
ε_o and σ_o for Annealed Material

A - nominal strain rate 2×10^{-2} min^{-1}

Grain Size (μ)	ε_o (percent)	σ_o (psi)
10	~0.50	10.000
70	~0.85	9.850

B - nominal strain rate 2×10^{-2} min^{-1}

Grain Size (μ)	ε_o (percent)	σ_o (psi)
70	~0.40	9.450
200	~0.63	9.450

3.3. Experimental Results Obtained Through the Use of Photoelastic Coatings

The technique used in these tests and the principles involved in them have already been explained in section 2.3.3 and Appendix I, respectively. This method was used to study the strain behavior associated with Type A serrations, Type B serrations, and in deformation in a "softened" Instron machine.

Thus, the photoelastic material was applied to specimens in conditions such that the desired effects would be maximized. For Type A serrations, this corresponded to annealed material with grain size 70 and 200μ, for Type B serrations and for tests with the spring, this corresponded to 10μ grain size material, solution treated at 535°C and quenched. We shall divide this presentation in three parts, dealing with each topic. Since the reproduction of movies is impossible here, these shall be kept in the files of the Department of Metallurgical and Materials Engineering, University of Florida, Gainesville, Florida.

3.3.1. Type A Serrations

Type A serrations data were obtained for two kinds of specimens: specimens of Type 2 and of Type 6 in Fig. 19. Type 2 was substituted because its use with screw grips could easily lead to misalignment effects, as we shall see. However, we shall first analyze the results obtained from a specimen of this type. As already described, a movie was

made of the phenomena observed, and then it was related to whatever was registered in the Instron chart. First, the specimen, which had grain size 70μ, was annealed and pre-strained 1.6 percent, so that one would be well within the range of serrations. The plastic was put on it, and it was further deformed 2.8 percent. Then, the first roll of film was over, the test was stopped, the load allowed to relax, and later the test was resumed, for about 2.5 percent strain more.

After that, the photoelastic coating didn't work any more, so that it was taken out of the specimen, a new one was put on, and the process repeated. We shall analyze in detail the behavior in the first 2.8 percent of deformation, and in the beginning of the 2.5 percent deformation. This will clarify the possibilities of this method, and allow us to just refer to other results obtained. Figure 52 shows the load-time diagram for this region. Up to point A, the smooth deformation seen in the graph was used to align the specimen with respect to the tensile apparatus. This was done by localized deformation in its upper left part and lower right part in Fig. 53-A. Figure 53 shows enlargements of frames of the motion picture. As we shall see, this initial deformation determines all the secondary aspects of the curve in Fig. 52. This localized deformation starts spreading to the center of the specimen following its borders, and finally nucleates a deformation band, or a Lüders
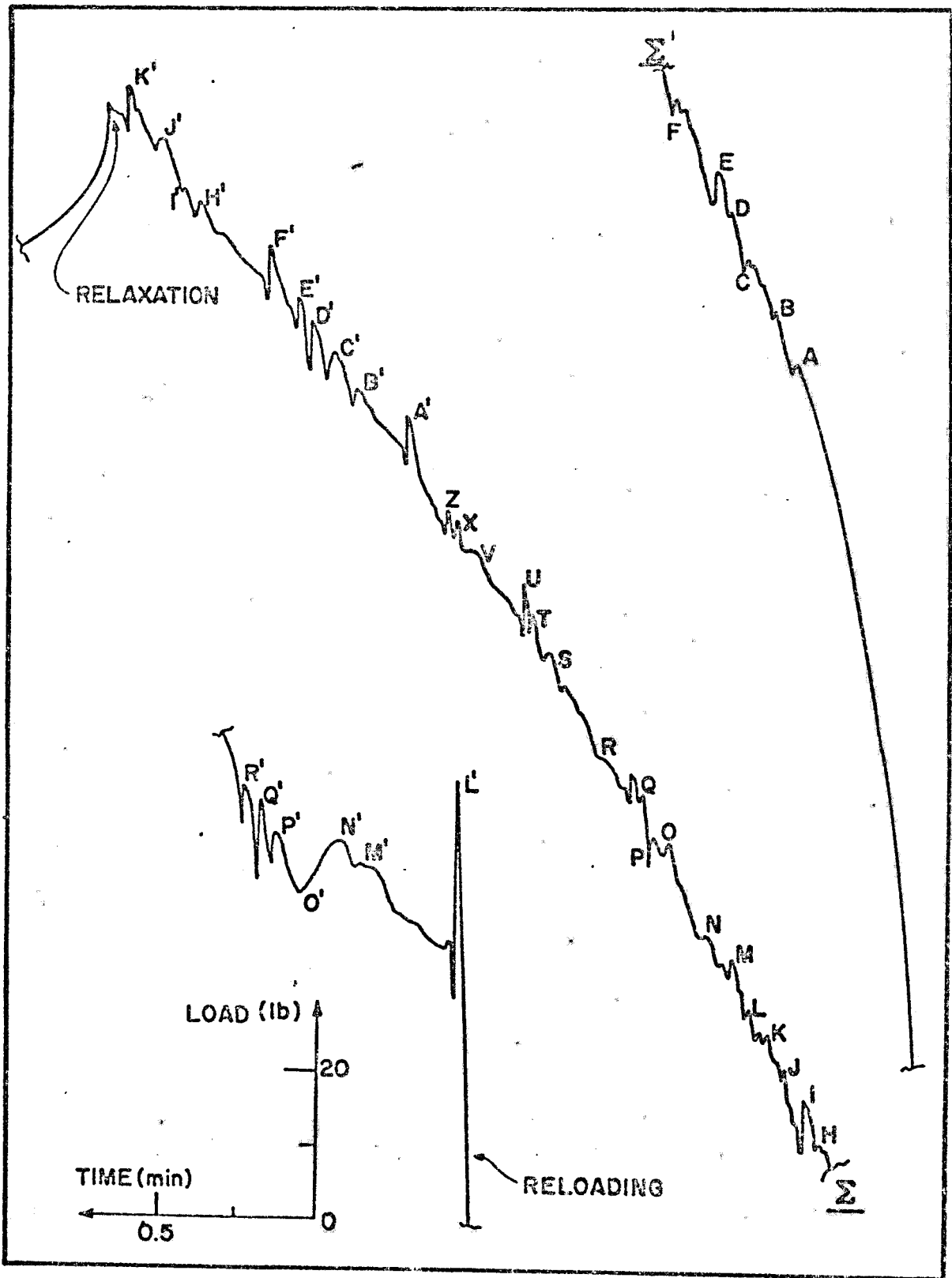
Fig. 52. Load-time curve used to analyze the strain behavior associated with Type A serrations. Annealed material, grain size 70μ, nominal strain rate 2×10^{-2} min^{-1}.
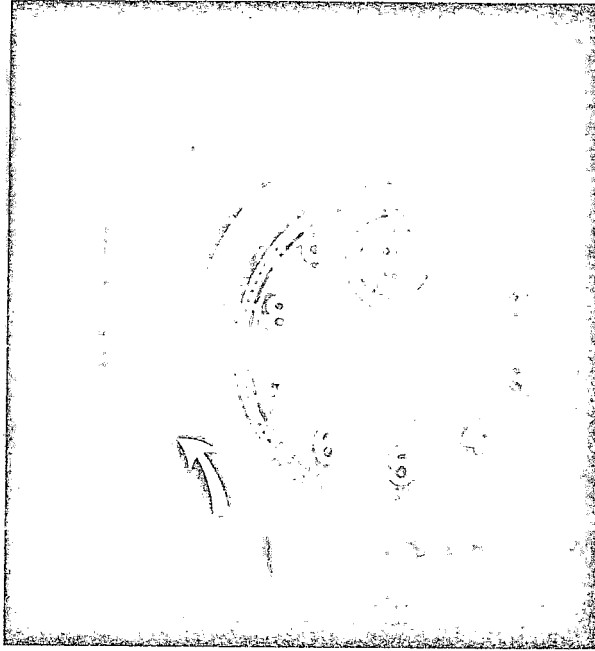
Fig. 53-A. Band starts propagating in the lower end of the specimen (red area pointed by white arrow).
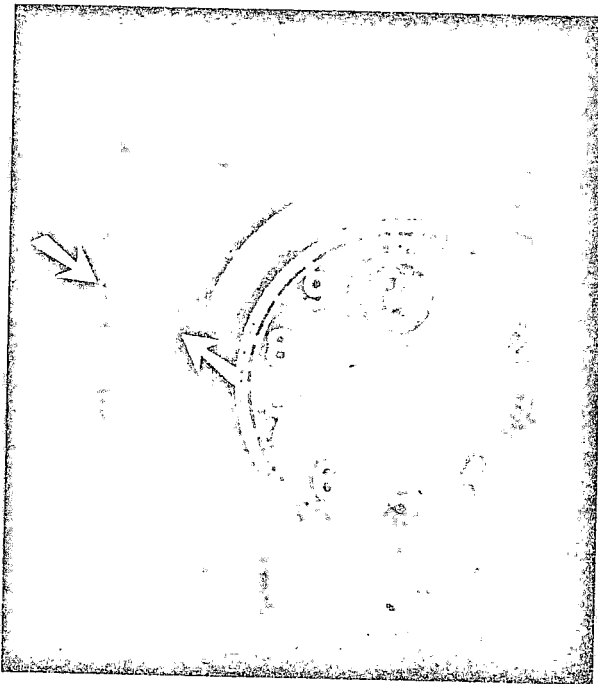
Fig. 53-B. Band is midway in its propagation to the upper part (see white arrows).
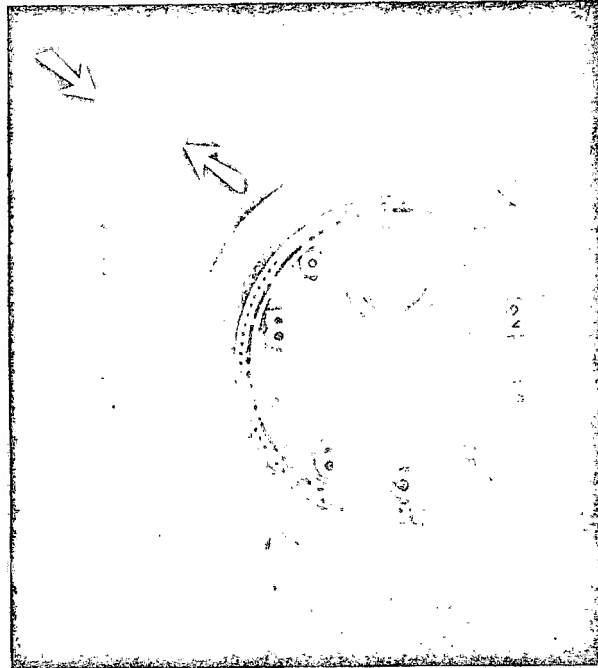
Fig. 53-C. Band completes its propagation over the gage length (see white arrows).
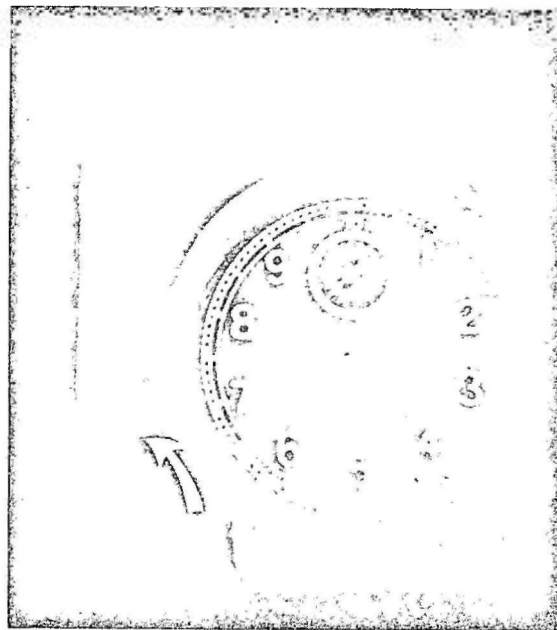
Fig. 53-D. New band is nucleated in the lower part of the specimen (green region, pointed by white arrow).

band in a general sense, in the middle of'the specimen.
This happens at point A. This band spreads then to both
sides of the gage length, and points B, C and D correspond
to sudden bursts in this propagation. At point E, another
band nucleates in the middle of the specimen, in the same
way described before, and propagates in both directions
with bursts forward at points F and H. At point I another
band is nucleated in the middle of the specimen, and propa-
gates with bursts at points J, K and L. The bands formed
in the middle of the gage length nucleated approximately in
the same point, and it seems that the bursts are associated
with localized strain gradients due to the above-mentioned
localized strain. When the band meets a more work hardened
region, it slows down, the load goes up, and the band bursts
forward through this region, with a load drop.

At point M, the new band formed is nucleated at the
lower end of the specimen, where one had localized strain.
From now on successive bands nucleate in this region, sweep-
ing the gage section upwards. When the gage length is com-
pletely covered, another band is formed at the lower end,
and so on. Figure 53 describes this behavior. Picture A
shows the formation of a new band (red region pointed out
by white arrow). In picture B it is midway through the gage
length. In picture C it has completely covered the gage
length, and in picture D a new band (green, pointed by arrow)
is already nucleated.

However, this propagation is not smooth, as can be
seen by the load drops between the nucleation of bands at
points Q, U, A', F' and K'. As Fig. 52 shows, the appear-
ance of the curve is regularly repeated, though the magni-
tude of the intermediate load drops may change. It was ob-
served that this similarity corresponded to the same propa-
gation behavior of the band over and over again. Let's
analyze, for example, the behavior between points U and A'.
At point U, a band is nucleated at the lower end of the
specimen, and starts propagating upwards until it meets the
region in the upper part that was locally deformed by mis-
alignment effects. Then, it decelerates, the load increases,
and there is a small burst forward corresponding to the
load drop V. Then, the band is definitely stopped, the
load goes up elastically, and one has a load drop at point
X. This corresponds to the propagation of the lower front
of the band downwards, covering that part of the gage length.
Then, the load goes up again, a new load drop occurs at
point Z, and the band resumes its upward propagation, cover-
ing the remainder of the gage section. Note that before the
load drop and new band formation at point A', the load goes
up, following the elastic slope in the upper part of the
peak. However, its initial rise is not that steep, imply-
ing that the band is driven upwards in the gage section
until it cannot move anymore, by sheer lack of stress. The
behavior described is shown schematically in Fig. 54;
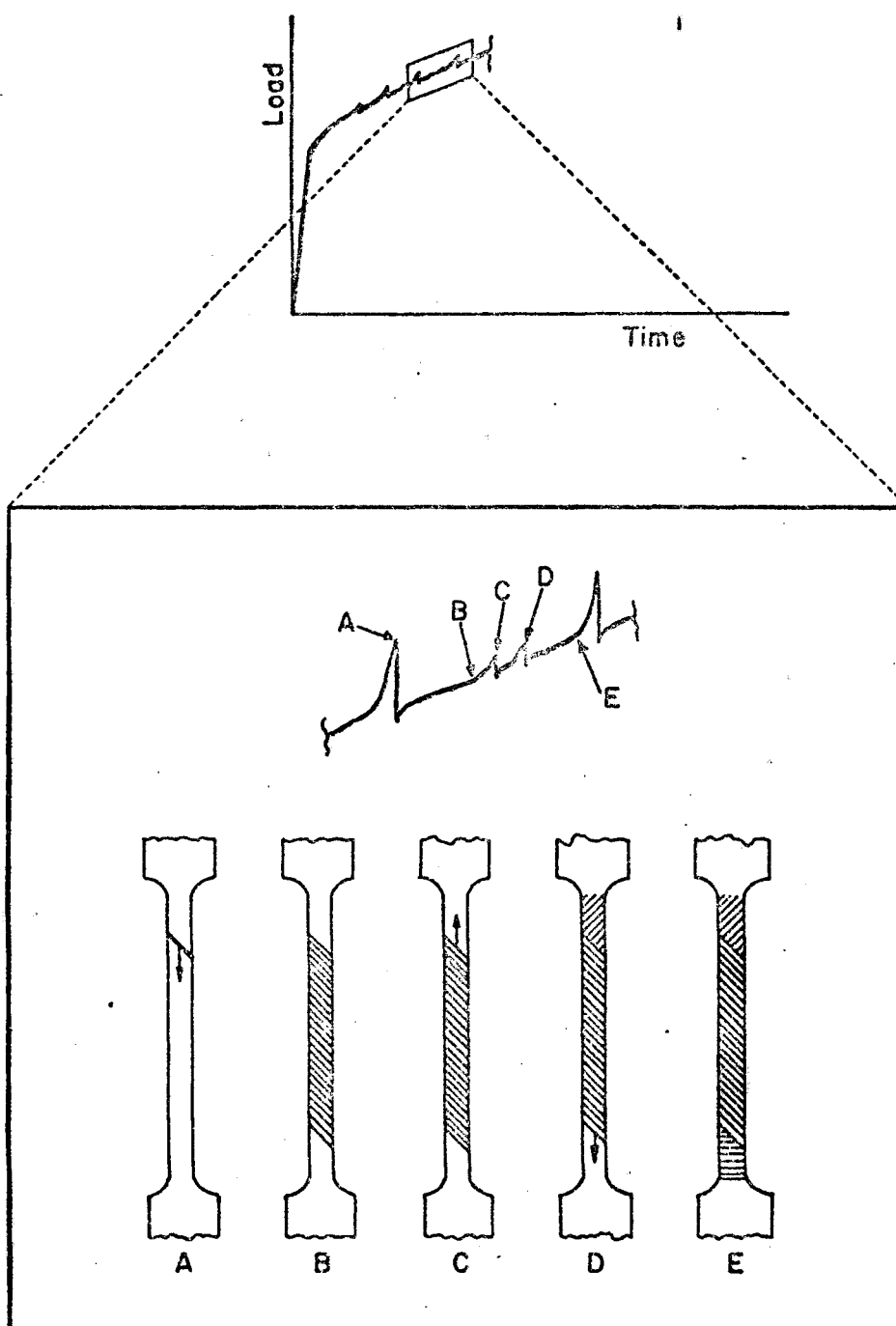
Fig. 54.   Schematic band propagation behavior during
Type A serrations. The behavior described
in the text starts with a band nucleating
at the lower part of the specimen, at point A.

however, this schematic drawing shows the' band initially nucleating in the upper part. In our curve, changes in direction of propagation of bands are associated with points O, P, S, T, X, Z, D', E', I' and J'. The other load drops are associated with deceleration of bands (rising load) followed by sudden bursts (load drops) in their propagation. From now on, we shall call any intermediate irregularities secondary serrations.

A Type A load-time diagram behavior similar to that discussed above has already been observed, for example, in α-brass.[5] This is particularly true regarding the similar appearance of load-time diagrams between successive Type A serrations. However, the methods used previously in this kind of investigation did not allow a better understanding of the phenomena presented. These methods included the use of extensometers, strain gages attached to the gage length of the specimen, and visual observation of the localized deformation associated with each load drop, whenever this was possible. The use of the method already described in previous sections, however, allowed us a very clear insight into these load-time diagram details.

As Fig. 52 shows, the test was stopped after point K', and the load was allowed to relax. Upon reloading the specimen, a big peak was observed, at point L', where a Lüders band was nucleated in the center of the specimen, and which propagated upwards until point M'. Then, one has a

load drop just after point M', and the lower band front

starts moving downward, the load goes up to point N', and

then the band sweeps downwards under a decreasing load!

This phenomenon was commonly observed whenever relaxation

and reloading tests were performed. Finally, points P',

Q', R' are associated with bursts forward in the propaga-

tion of the band, or with its change in direction of propa-

gation. After point R', however, when a regular deforma-

tion behavior set in, the bands were nucleated at the top

of the specimen and propagated downwards, with secondary

serrations between the Type A ones. However, it should be

expected that if no relaxation occurred, bands would keep

nucleating at the lower end. Thus, not all load drops cor-

respond to the nucleation of serrations, even though secon-

dary serrations can be as big as Type A ones. This is the

reason why in Fig. 38 we carefully stated that bands nucle-

ated only at the points shown with vertical arrows. As we

can see in this figure, the behavior is very regular, and

one can easily discover which points are associated with

band nucleation in the following way: first, the strain

between two successive serrations increases monotonically

(see Fig. 39), a fact that has been verified for other mate-

rials and for other specimens. Thus, some of the peaks can-

not be associated with nucleation, by sheer comparison of

the strain between peaks. Secondary serrations can then

be identified by the fact that they increase faster with

strain (see Fig. 52) than Type A serrations, and then fade away with strain faster than Type A serrations. This can be seen in Fig. 38, and has been observed also in many other cases.

Another fact that should be clear by now is that by no means should tests performed with different specimens present the same secondary serrations. As we have seen, these depend very much on the initial part of the test, where effects like small misalignments in the tensile apparatus can be very important. It seems that any initial localized deformation in the specimen will cause secondary serrations also. Thus, another factor to be taken into consideration is the perfection and homogeneity of the material. However, during one given test, secondary serrations should be quite repetitive and regular. This has been regularly observed in our work (see Fig. 38).

It should be pointed out that round specimens, pulled in the way already described, exhibited behavior far simpler than the behavior observed with specimens where misalignment problems were present. At times, some tests actually presented no secondary serrations at all, probably due to homogeneity in the initial deformation along the gage length. Thus, a special self-aligning grip for flat specimens was built, as shown in section 2.3.1. Tests performed with these grips and with photoelastic coatings showed that indeed, in this case, the deformation behavior was much

simpler. In one case, there was some localized deformation in the center of the specimen in the beginning of the tests. After the initial discontinuous flow, that shall be shortly discussed, all bands started nucleating in one end of the specimen and sweeping the gage length to the other end. The only irregularity observed was a secondary serration when the band swept through the center region where one had some deformation in the beginning. When the band went through this region, it was slowed down, the load went up, and then it overcame the region and the load dropped, as seen in Fig. 55. This secondary serration increased in the initial bands, then started decreasing and was finally flattened out at higher strains, as seen in the lower curve in Fig. 55, that also shows a case where a band nucleated without any peak. Anyway, no behavior such as shown in Fig. 54 was observed.

It has. also been observed that the initial discontinuous flow is usually complex, with bands forming after some smooth deformation, that may be localized and usually determines the region of nucleation of these first bands. Only after some strain a regular behavior starts, with bands always nucleating in one end of the specimen and sweeping the gage length to the other end.

Finally, as the strain increases, the velocity with which the bands propagate decreases, and at large deformations, where serrated flow fades away in this case, bands nucleate without any pronounced load peaks, and sweep the
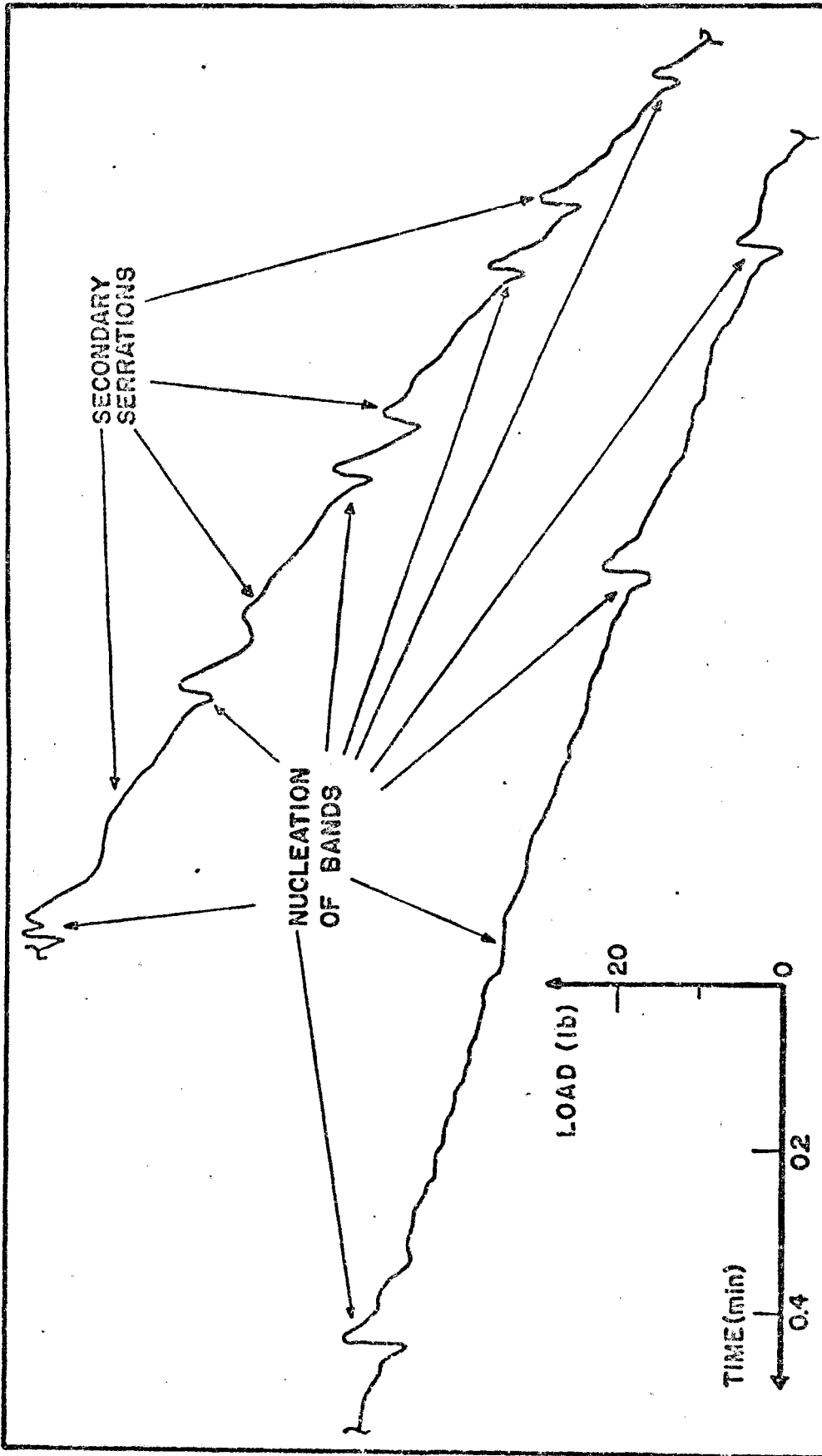
Fig. 55. Load-time curve used in the analysis of the strain behavior associated with Type A serrations, with the use of self-aligning grips. The lower curve is the continuation of the higher one, at higher levels of strain. Annealed material, grain size 200μ, nominal strain rate 10⁻² min⁻¹.

gage very slowly. No deformation was observed either behind or ahead of a band during its movement.

3.3.2. Type B Serrations

A 10µ grain size, Type 5 specimen (see Fig. 19) was solution treated one hour at 535°C, quenched, and immediately strained about 10 percent. It was then unloaded and aged 24 hours at room temperature, during which time a photoelastic coating was applied to the specimen. The result of this aging was a decrease in the amplitude of the serrations. Besides, actual Type B serrations observed in experimental tests are not as regular as the ideal case, shown in Fig. 3. Figure 56 shows a part of a load-time diagram that was analyzed using photoelastic coatings.

The observations made confirmed the current concept that in this case deformation bands nucleate and stop at each load drop in the load-time diagram. Figure 57-A shows the strain pattern in the specimen after the two first successive load drops seen in Fig. 56; Fig. 57-B shows the same after the first nine load drops, and Fig. 57-C shows the strain pattern after a large number of load drops.

It was observed that the deformation bands could form in three different ways: at random along the gage length of the specimen, repeatedly in the same region of the specimen, and successively ahead of each other, constituting what has been called discontinuous propagation. Furthermore, these three modes occur in the same test, and it

118
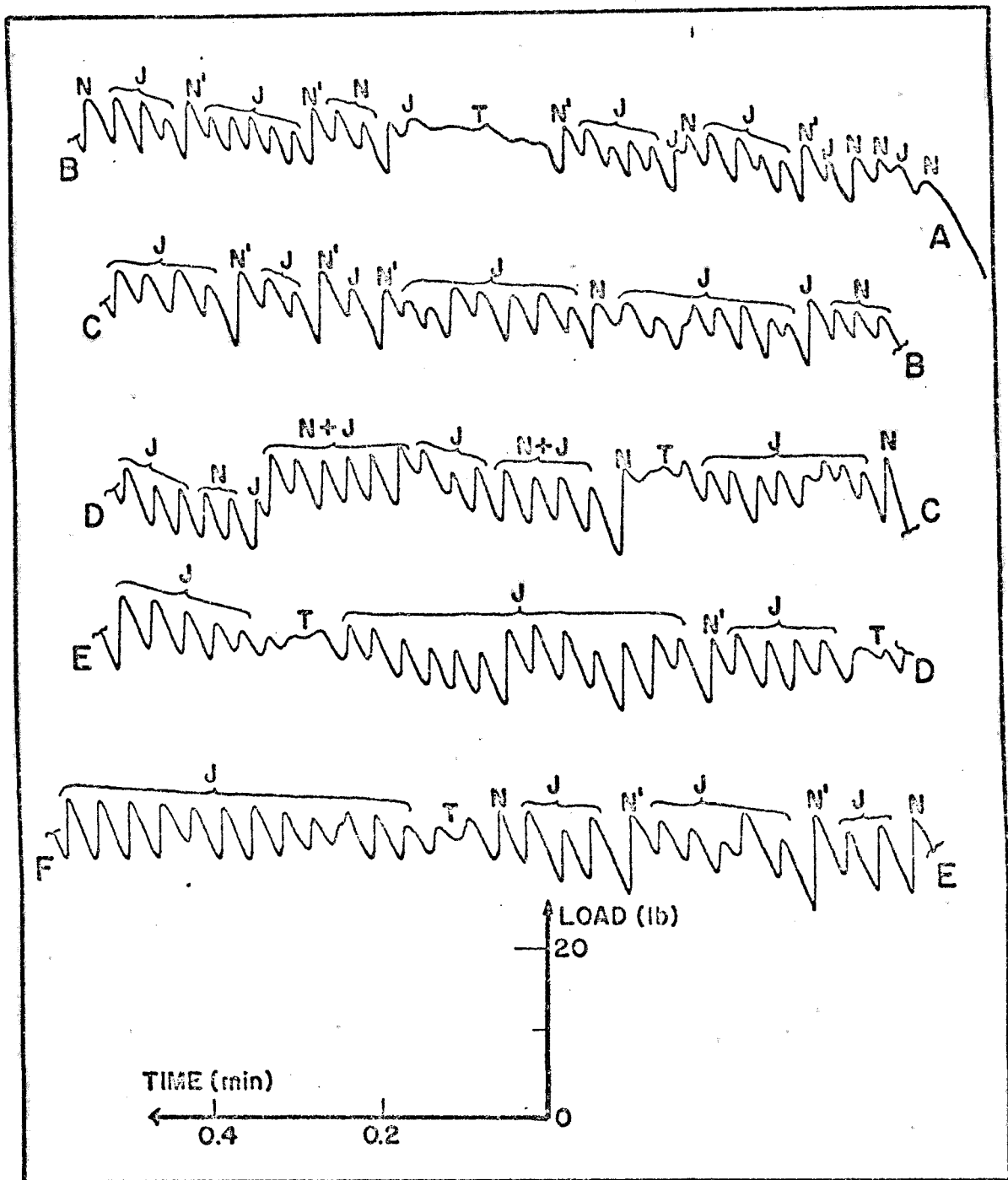
Fig. 56. Load-time curve used in the analysis of the strain behavior associated with Type B serrations. Material solution treated from 535°C and quenched, grain size 10μ, nominal strain rate 10^{-2} min^{-1}. N = nucleation, J = discontinuous propagation, T = smooth propagation.
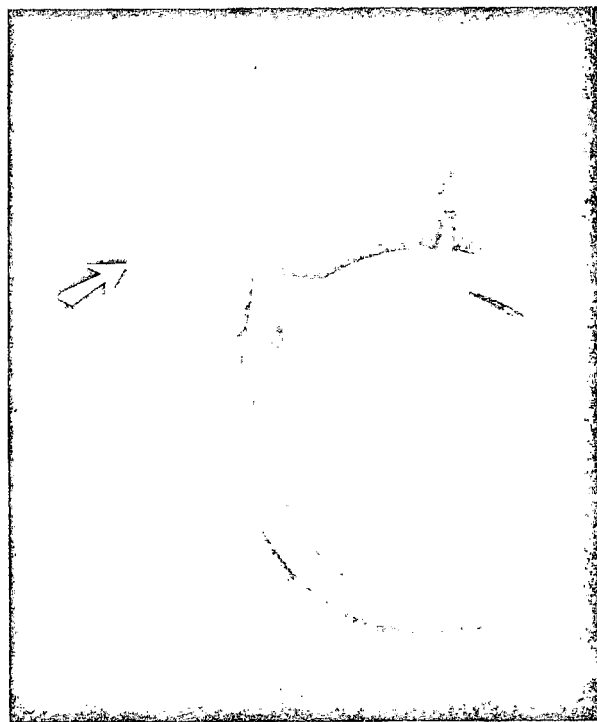
Fig. 57-A.　Strain pattern after the first two load drops in Fig. 56. These correspond to the nucleation of a band and its "jump" in discontinuous propagation.
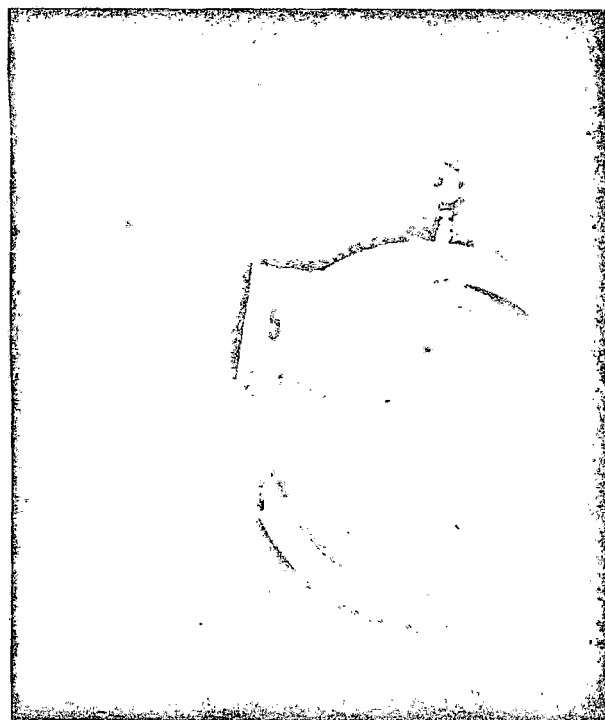
Fig. 57-B.　Strain pattern after the first 9 load drops in Fig. 56. Since one has only four regions of localized strain, discontinuous propagation, or nucleation of bands in the same region, must have occurred.
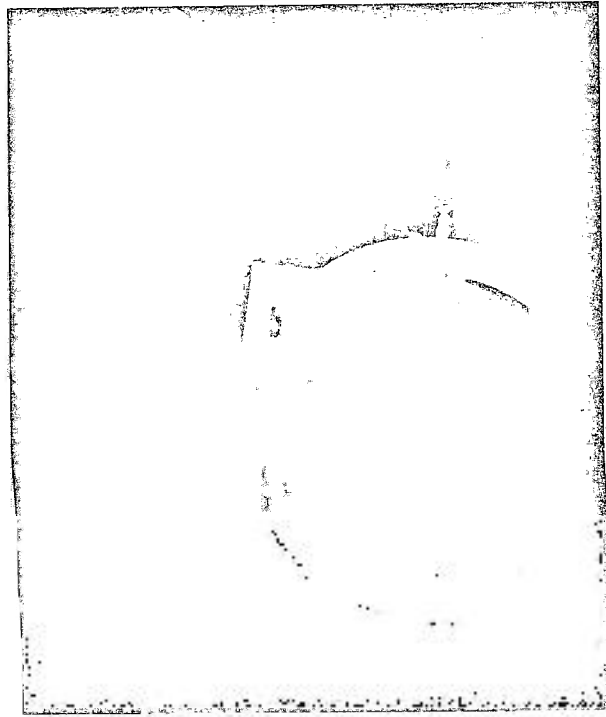
Fig. 57-C. Strain pattern after a large number of load drops.

seems that there is no pattern for their occurrence. The only tendency that was observed is that at large strains, there seems to occur more discontinuous propagation (one band next to the other in succession) than the other two modes of deformation. There seems to be no way of recognizing directly from the load-time diagram what kind of nucleation of bands we have at each load drop. Only the photoelastic coating affords this information, and we have identified in Fig. 56 two kinds of nucleation: "J" indicates a discontinuous propagation, and "N" just the formation of bands, both at random and in the same point in the specimen. However, larger load drops, such as those indicated by the letter "N'" in Fig. 56, have some tendency to be associated with the random nucleation of bands, but this is not always observed. Figure 56 also shows that there are some regions, marked "T," where the flow is relatively smooth. This can also be observed in Figs. 36 and 37. It was observed that these regions correspond to the "smooth" propagation of a band, either transversely across the width of the gage length, or longitudinally over very small distances.

Let us consider the first region marked T. Figure 58 reproduces this region and shows schematically what is observed. At the load drop marked "N" a wedge-shaped band is nucleated, and then starts propagating transversely. Finally, when it reaches the other side, a band is nucleated at its
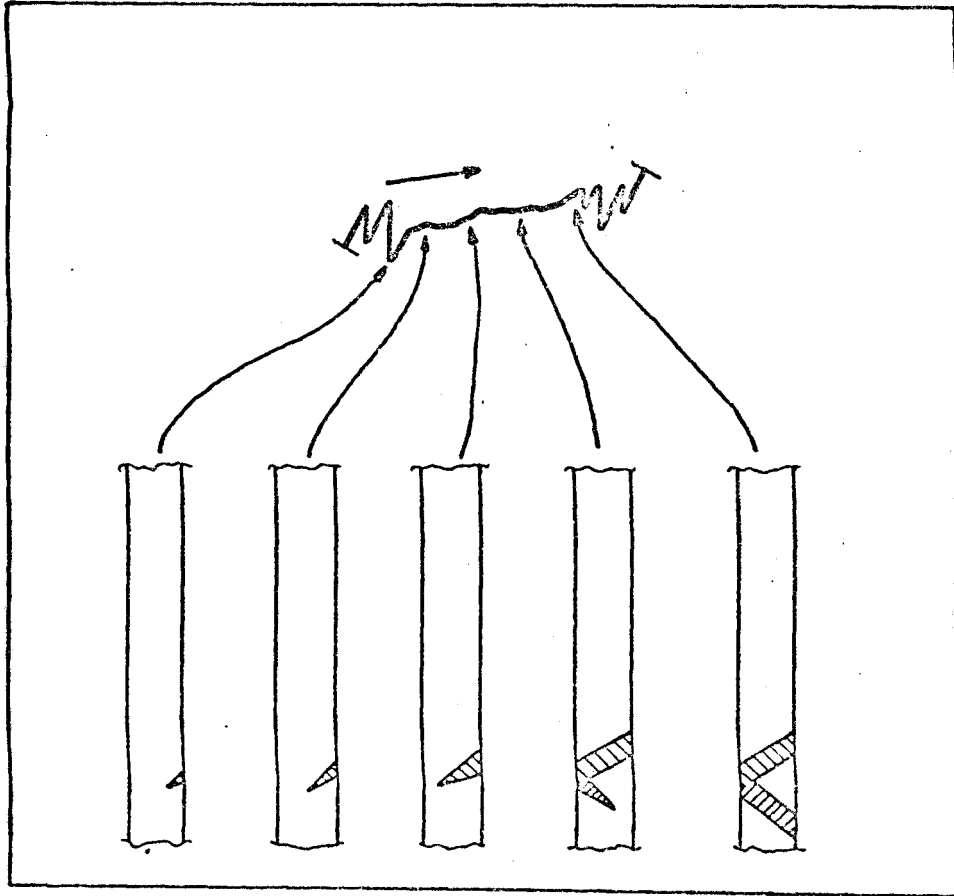
Fig. 58.   Strain behavior associated with the first two
            "smooth" regions marked "T" in Fig. 56.

top and making an angle of approximately 60° with it, and
that also crosses smoothly the gage section in a transversal
sense. The resulting pattern can actually be seen in the
lower end of the specimen in Fig. 57-C, where it appears as
a "less than" (<) sign.

The second region marked "T" corresponds to a similar
behavior at the upper end of the specimen. However, the two
last actually correspond to a longitudinal smooth propaga-
tion of a band over very small distances.

Finally, it was observed that while bands were nucleat-
ing and propagating discontinuously in one region of the
gage length, other already nucleated bands in other regions
could move slowly over very small distances, or even small
wedge-shaped bands could nucleate very slowly in other re-
gions. Besides, when a band was propagating discontinuously
in one direction, at times some deformation also occurred
behind it.

3.3.3. Tests in a Softened Machine·

A specimen of Type 5 (Fig. 19), grain size 10μ, was
solution treated one hour at 535°C and quenched, and immedi-
ately strained about 10 percent in a stiff Instron machine.
After that, it was unloaded and aged 24 hours at room tem-
perature, during which time a photoelastic coating was
attached to it. It was then strained in a softened machine,
using a set-up already described. The load-time curve had
the appearance shown in Fig. 41, for soft machines.

No deformation whatsoever was observed during the period the load was increasing elastically between two successive load drops. However, these load drops are associated with the formation of a deformation band in the gage length of the specimen, and with its propagation over a certain distance at extremely fast speeds, during the time the load drops last.

In the beginning of the strain the load falls are small, and the bands formed cover a relatively small fraction of the gage length. However, as the strain increases, the load drops increase, the strain associated with each load drop increases very much, and the distances over which the bands propagate go up to about half the gage length. The propagation velocity is very fast indeed.

It has also been observed that during the propagation of the band, the strain distribution may be very complex, with band fronts assuming momentarily shapes other than straight lines. This is shown schematically in Fig. 59, where faster propagation of the band in the lower part of the specimen caused a front shape as shown during its propagation.

3.4. Strain Gradients Along the Gage Length of Specimens

This part of the investigation was performed on annealed, 200μ grain size, round specimens of Type 7 (Fig. 19).

Previously nucleated
band

New band nucleates
and propagates

New band meets the
first one and complex
strain pattern is
formed

The first band
also propagates

Both bands
come to a
stop
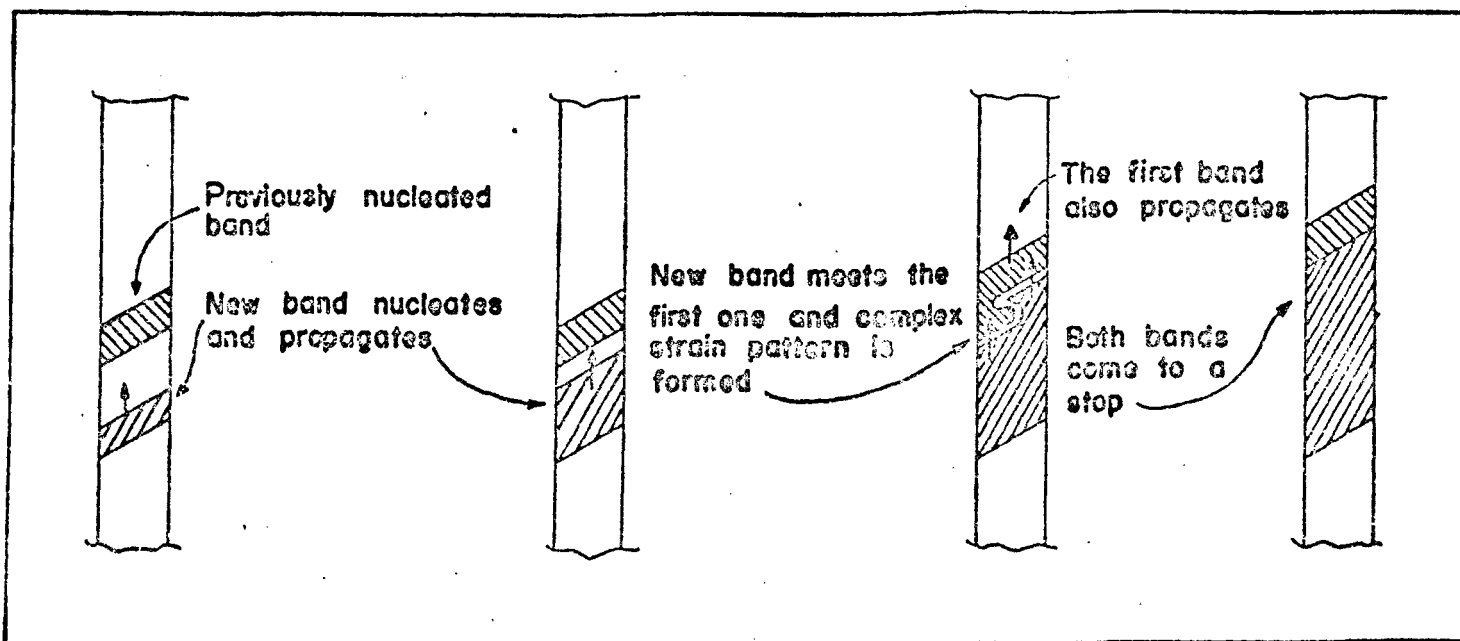
Fig. 59.   Complex deformation band front shape during the propagation of
a band.   Deformation performed in a "softer" machine.

Several specimens were deformed to different total
elongations and the strain was calculated at different
points along the gage length of each, following the pro-
cedure explained in section 2.5.6. The results are shown
in Fig. 60. It was observed that the profile of the speci-
men after deformation tended to resemble the shape of the
original profile of the specimens. This is shown in Fig.
61-A and B.

The aluminum specimens in question exhibited profuse
Type A serrations, and it would be interesting to analyze
what would be the results for a material that deforms
smoothly. Thus, tests were run with commercial purity
nickel specimens, of diameter 0.250 in and gage length
1.300 in. Different specimens were deformed to various
levels of strain, and their strain profiles can be seen in
Fig. 62. The same tendency of similarity between the origi-
nal diameter profile and the final one, after deformation,
was again observed. This is shown in Fig. 63-A and B.

It should be pointed out that the profiles shown in
Fig. 60 present pronounced peaks, which are not observed in
Fig. 62. Thus, the sweeping of deformation bands down the
gage length of the aluminum specimens may be responsible
for the heightening of the peaks in Fig. 60; Fig. 62 also
shows these irregularities, but much less pronounced than
in the former case.
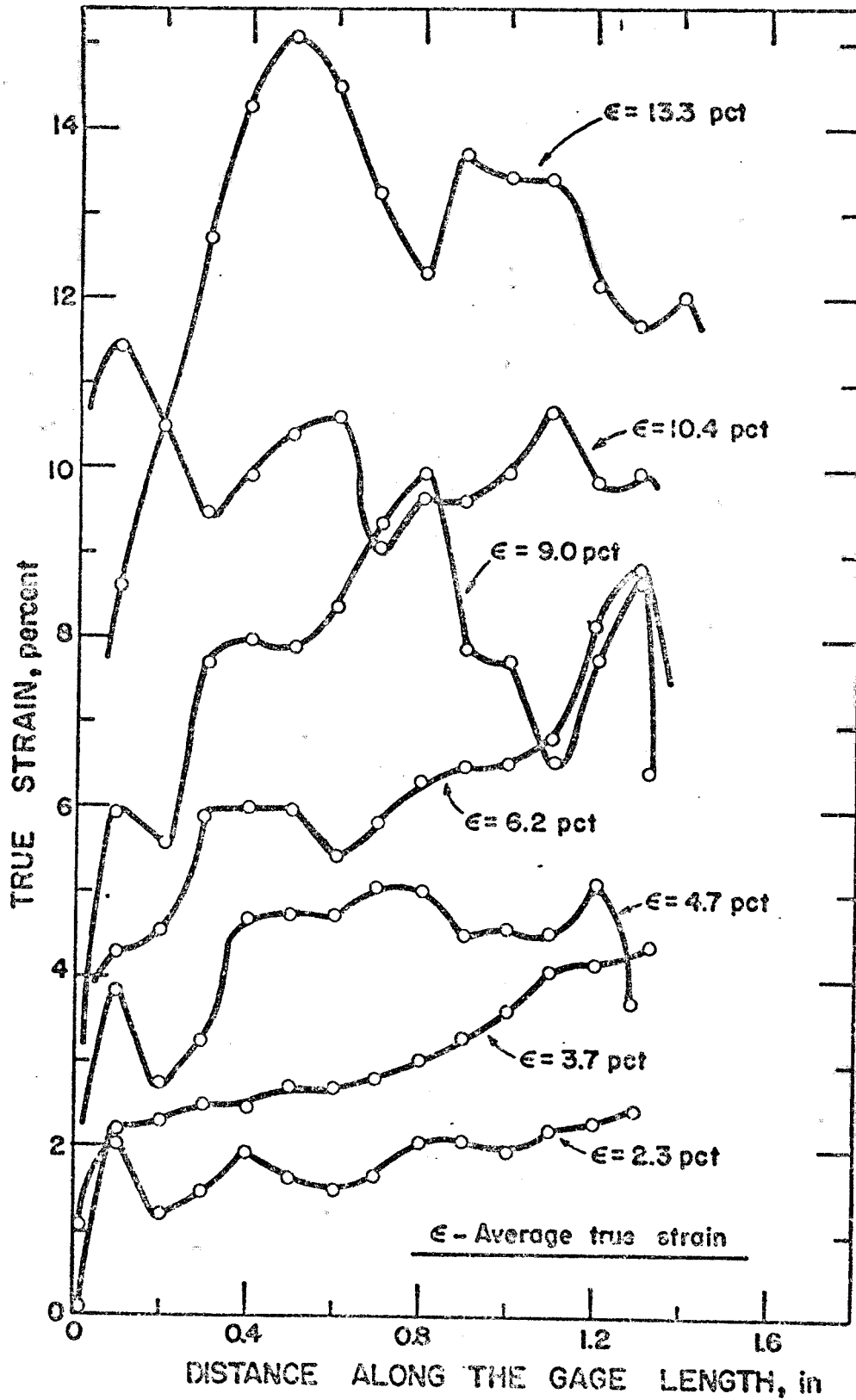
Fig. 60. Strain profiles along the gage length of
annealed specimens, grain size 200μ, nominal
strain rate 0.77x10⁻² min⁻¹.
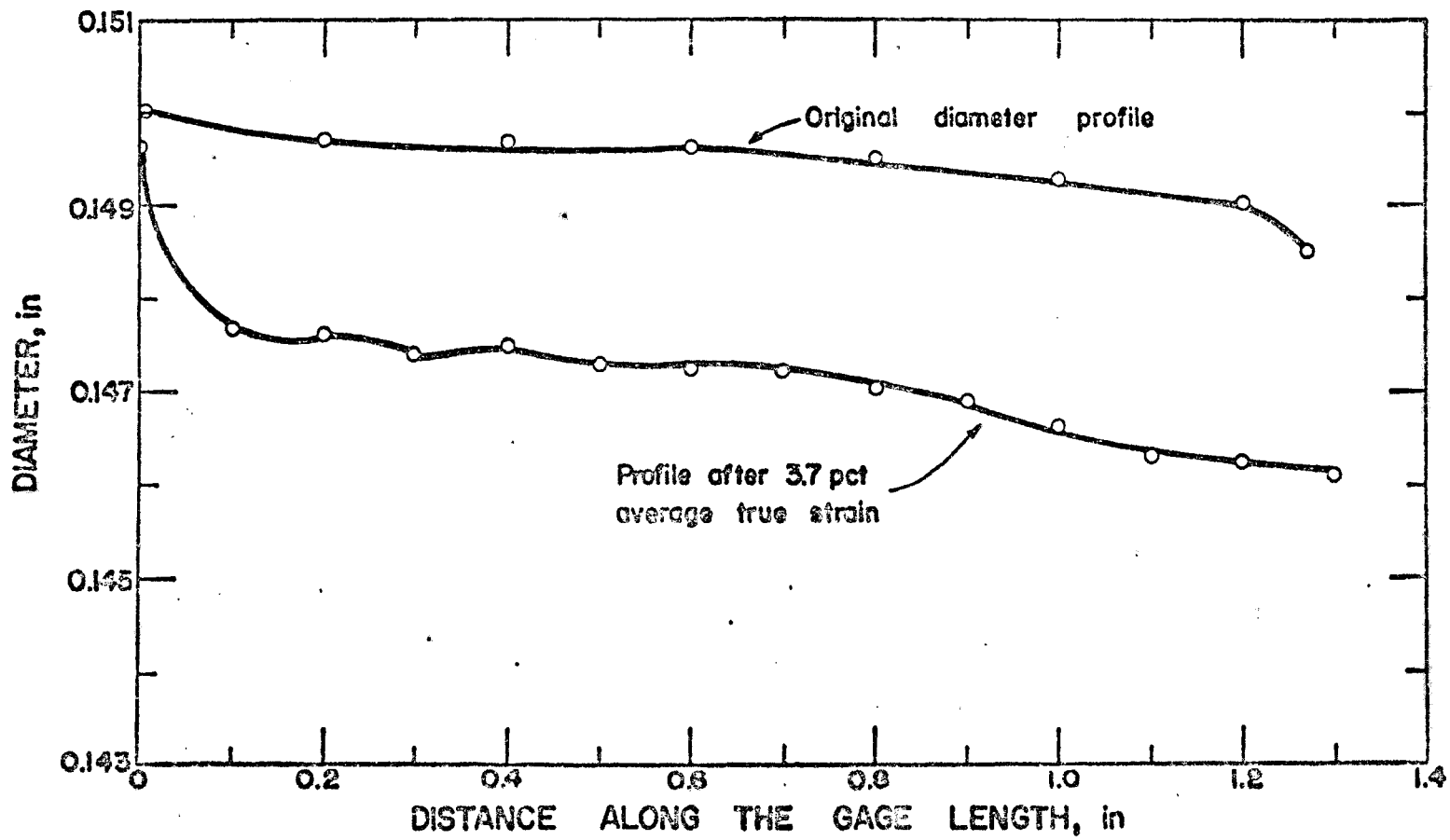
Fig. 61-A. Diameter profiles of an aluminum specimen before and after strain.
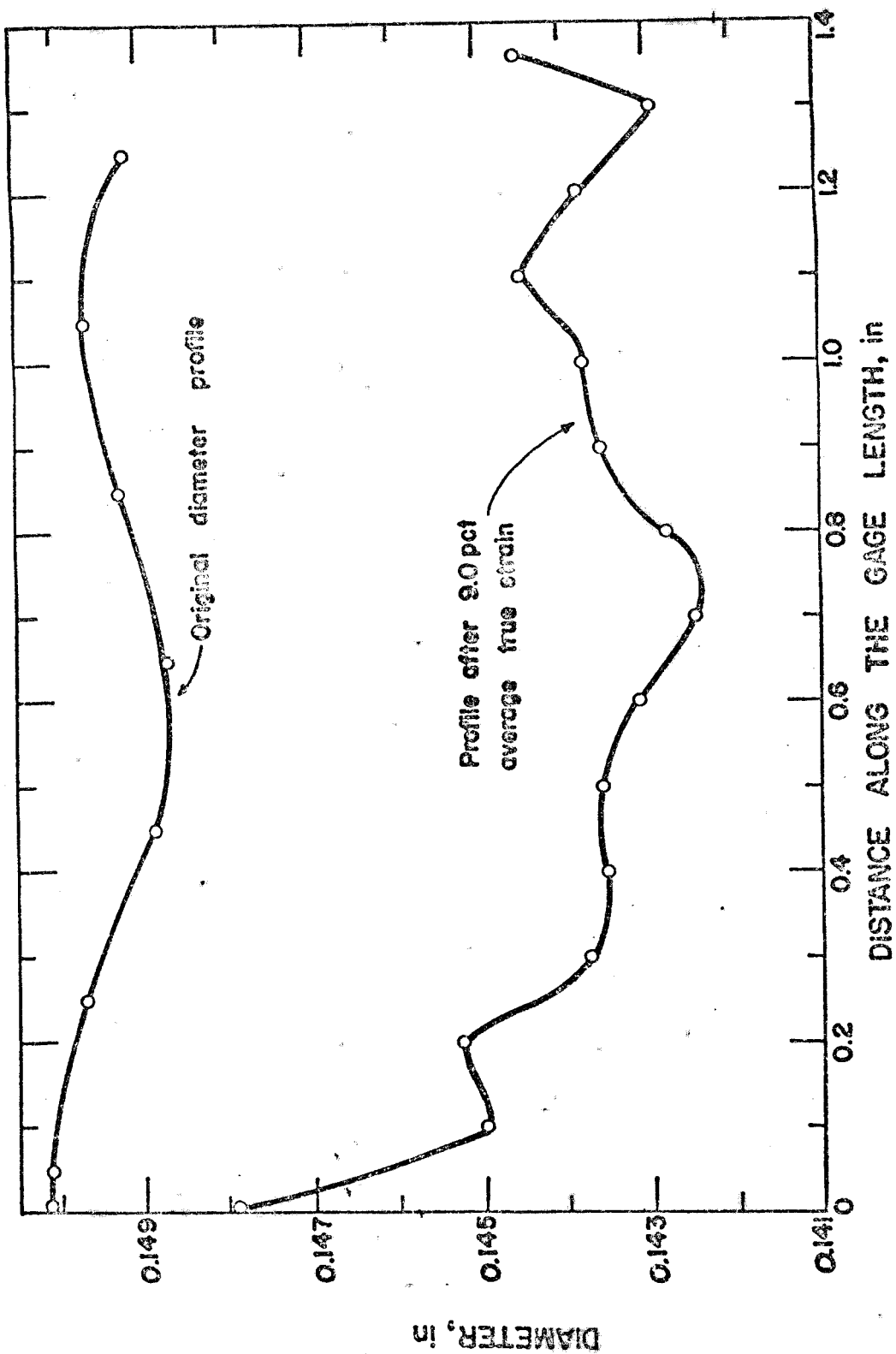
Fig. 61-B. Diameter profiles of another aluminum specimen before and after strain.
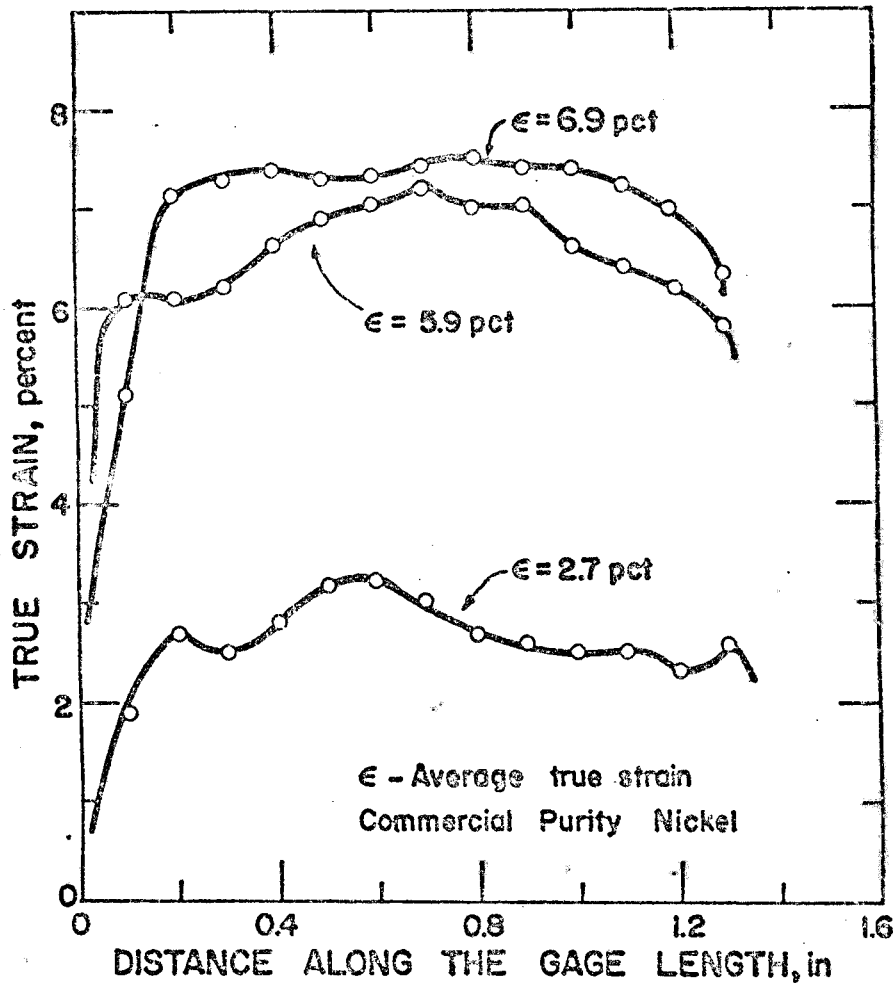
Fig. 62. Strain profiles along the gage length of commercial purity nickel specimens; strain rate 1.54×10^{-2} min^{-1}.
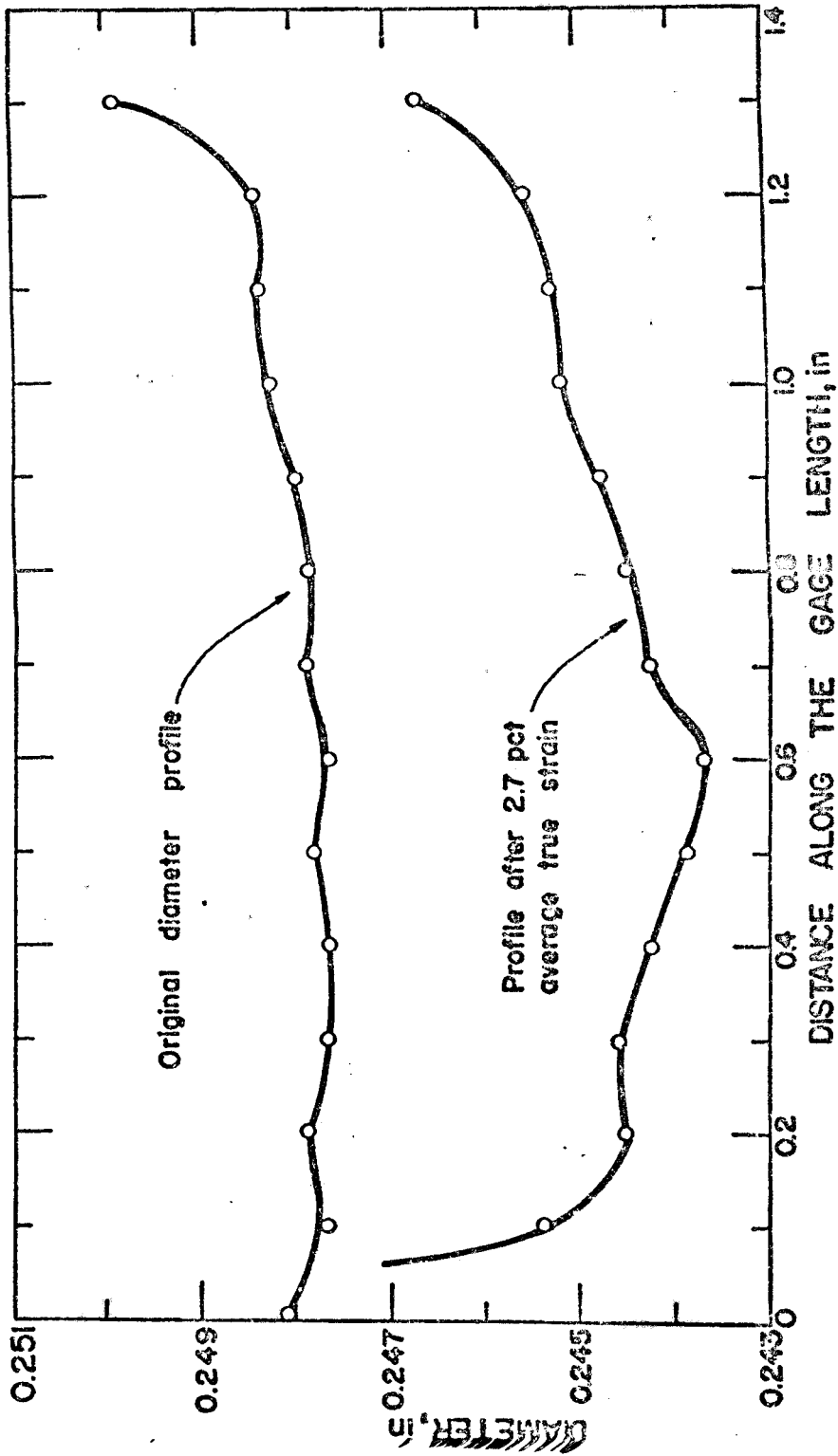
Fig. 63-A. Diameter profiles of a commercial purity nickel specimen, before and after straining.
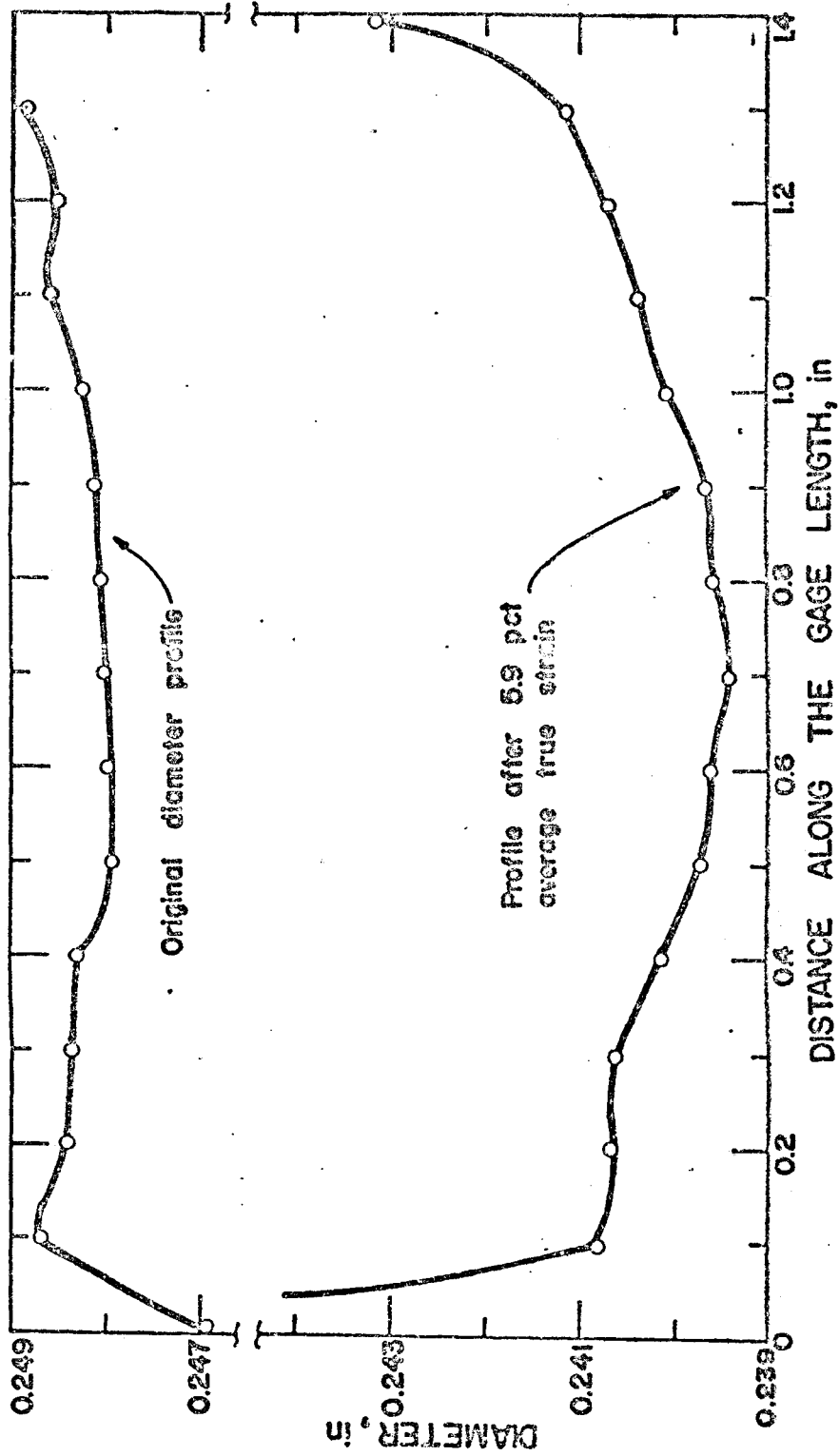
Fig. 63-B. Diameter profiles of another nickel specimen, before and after straining.

3.5. Tests Involving Changes in Nominal Strain Rate and Relaxation

Changes of nominal strain rate were made on annealed and 535°C solution treated specimens. The changes involved a factor of 10, and the curves obtained were averaged as explained before, and are shown in Figs. 64, 65 and 66. Figure 64 shows the influence of strain rate change from 10^{-2} min^{-1} to 10^{-3} min^{-1} and vice-versa in an annealed, 70μ grain size specimen, Figure 65 shows the effect of a strain rate change from 2×10^{-1} min^{-1} to 2×10^{-2} min^{-1} and vice-versa, in a solution treated, 10μ grain size specimen, while Fig. 66 shows the effect of changes from 2×10^{-2} min^{-1} to 2×10^{-3} min^{-1} in the same material.

As one can see in Figs. 64, 65 and 66, there is a general tendency of the curves for a decrease in the slope with increasing nominal strain rate, and vice-versa.

Figure 67 shows two of the changes in nominal strain rate, for an annealed specimen (A) and for a solution treated specimen (B). The solution treated material presented some negative strain rate sensitivity for very low strains. However, very soon this parameter was practically zero, as seen in Fig. 67-B. The same is true for annealed specimens. However, if the peak just after the strain rate change is disregarded, then the strain rate sensitivity even at high strains would be a little bit negative, as seen in Fig. 67-A.
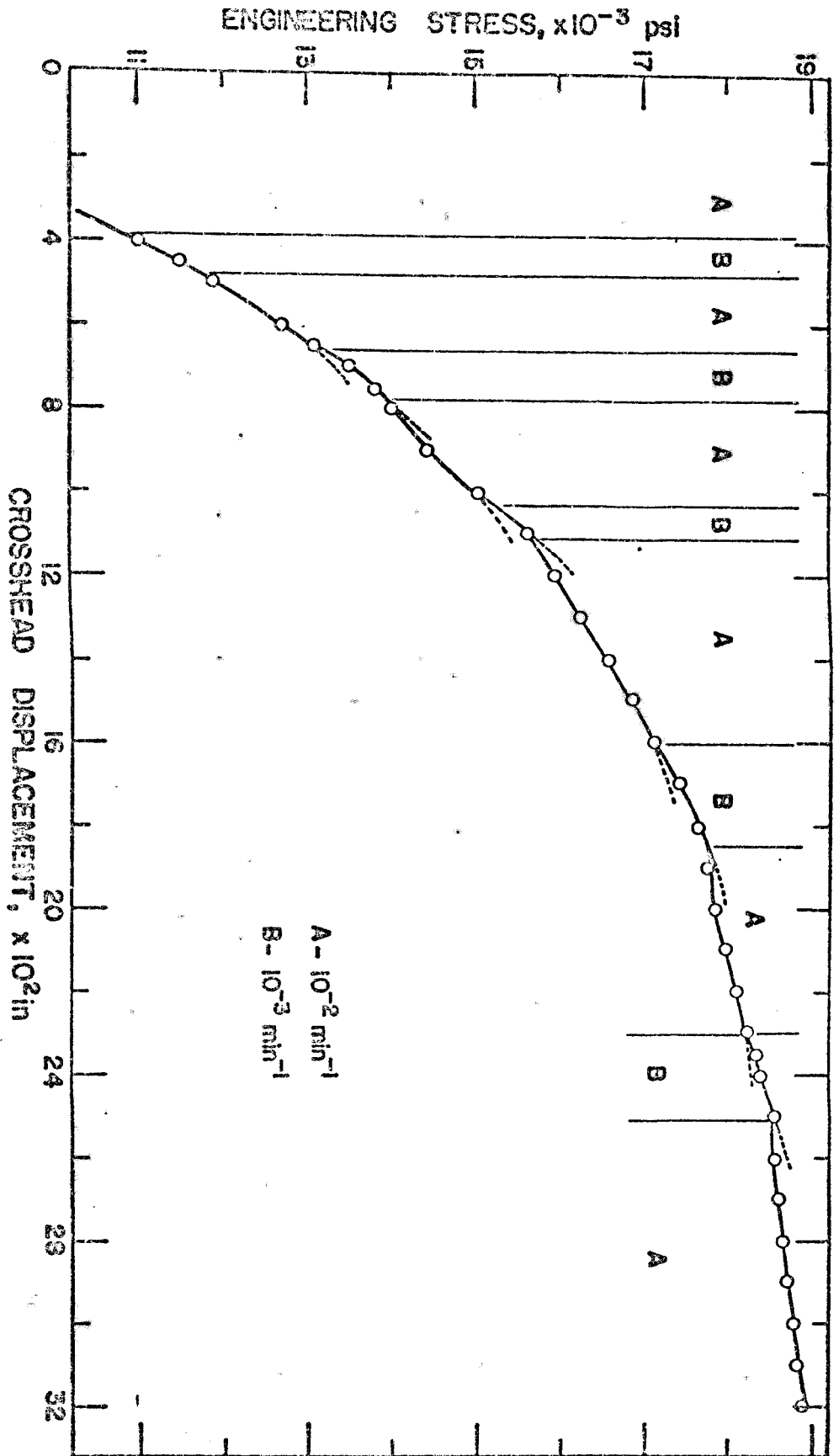
Fig. 64. Influence of changes in nominal strain rates on the stress-elongation curve for annealed, 70μ grain size material.
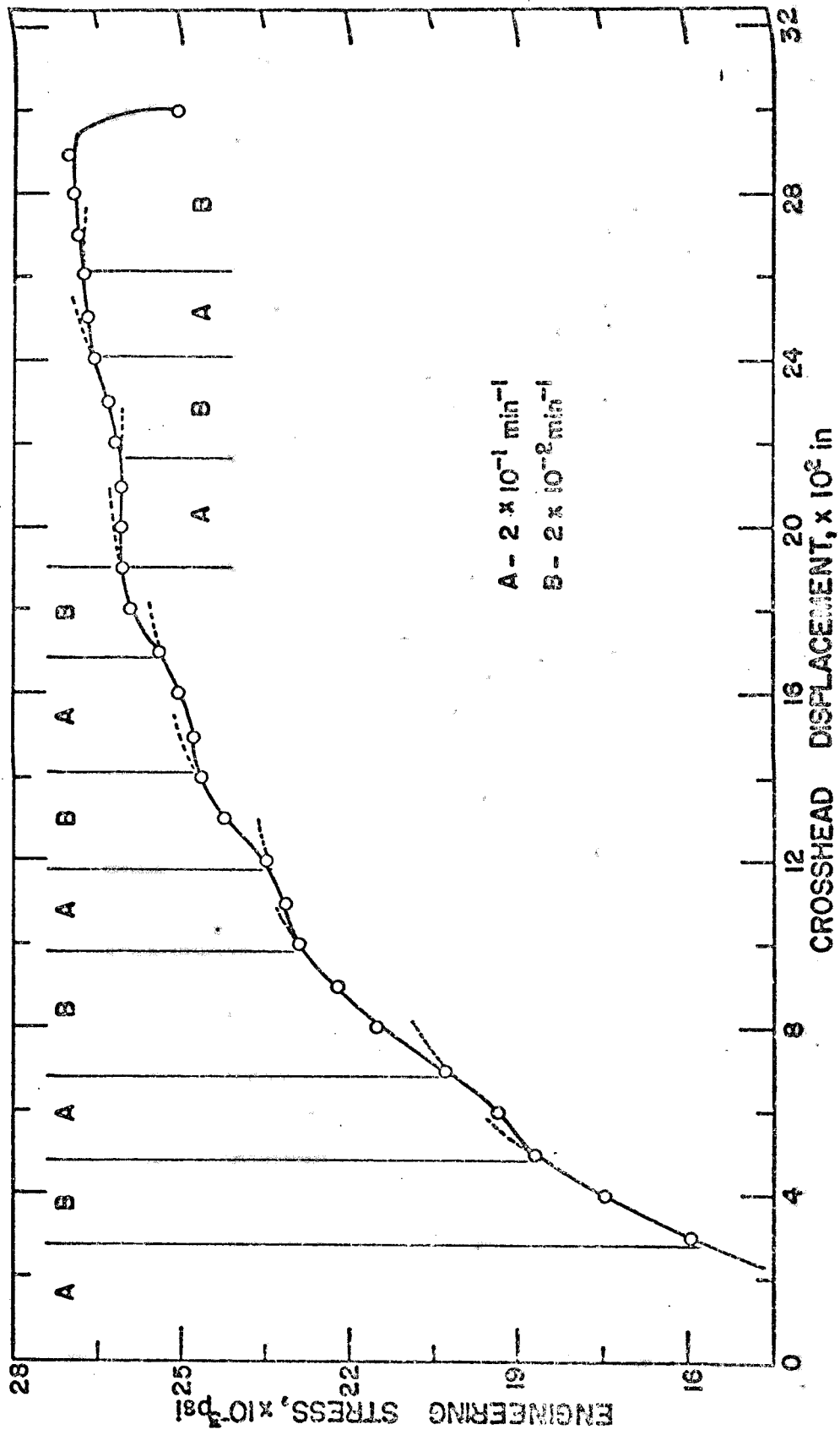
Fig. 65. Influence of changes in nominal strain rate on the stress-elongation curve for material solution treated at 535°C and quenched, grain size 10μ.
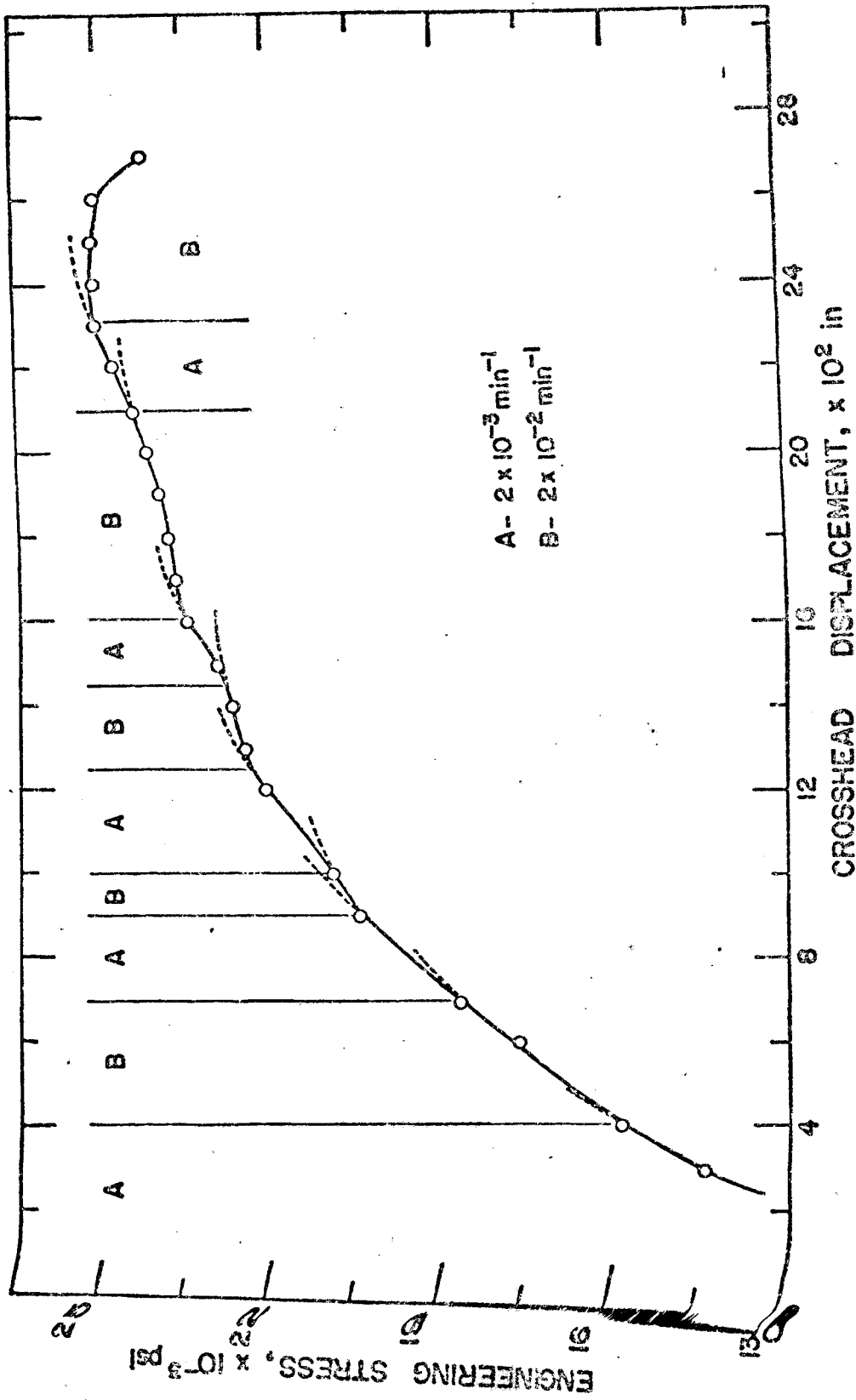
Fig. 66.

Influence of change in nominal strain rate on the stress-elongation curve for material solution treated at 535°C and quenched, grain size 10μ.
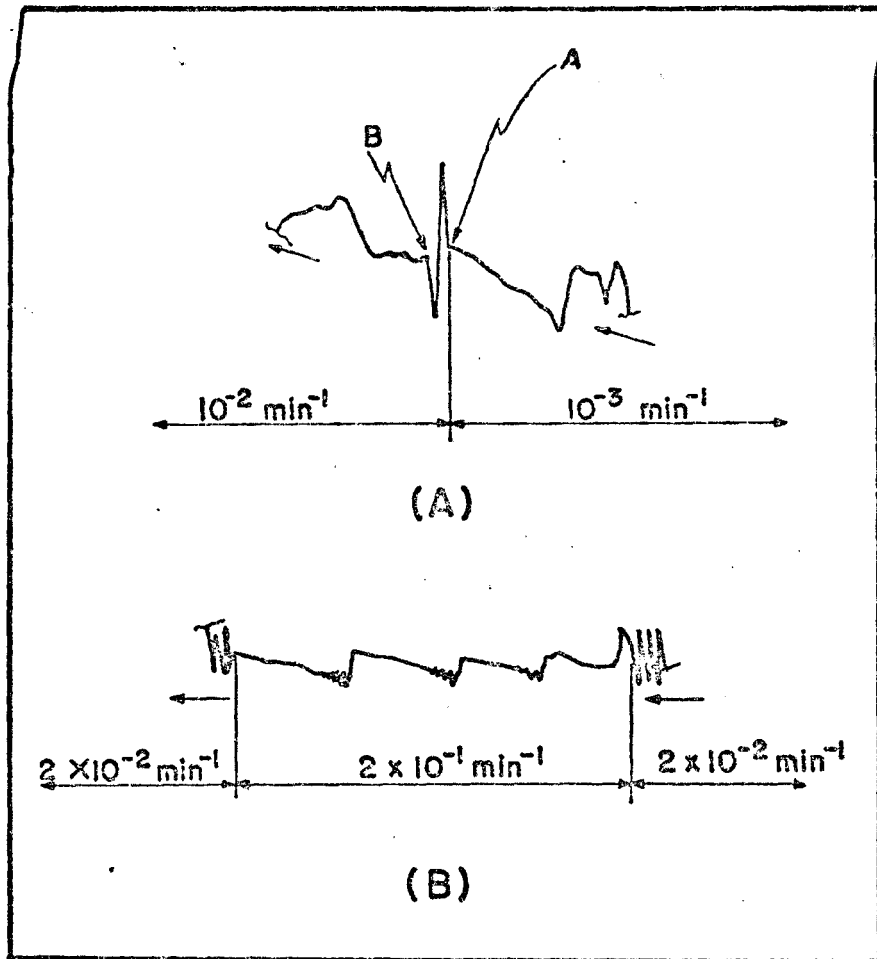
Fig. 67-A. Strain rate change effect during the propaga-
tion of a deformation band in Type A serra-
tions. Annealed material, grain size 70μ.
     -B. Strain rate change effect during Type B serra-
tions, at high strains. Material solution
treated at 535°C and quenched, grain size 10μ.

Considering Fig. 67-B, one can see that an increase in nominal strain rate changes the serrations from B to A and vice-versa. This was also observed in specimens solution treated from lower temperatures, where a strain rate change caused an immediate change in the character of the serrations.

Figure 67-A also shows that the load associated with point A is slightly higher than the load at point B. Since this strain rate change was performed during the propagation of a band, this means it is easier to propagate a band under higher nominal strain rates. Indeed, a decrease in strain rate brings point B a little bit above point A.

A few relaxation tests were performed, where the load was relaxed at constant strain, for different times, strain, and positions in relation to the Type A band nucleation peak, since the test in question was performed on annealed, 70μ grain size material, that presents profuse Type A serrations. After the relaxation, the curve always showed a peak upon reloading, as shown in Fig. 68-A. The height ΔP of the peak was then measured in relation to the load-time diagram extrapolated back to the peak region, as shown in the same figure. Since just a few of these tests were performed, we shall only report the general trend observed, without trying to get any quantitative results. According to our data, the height of the peak, for a given test, measured in pounds, depends only on the relaxation time,

(A)

(B)
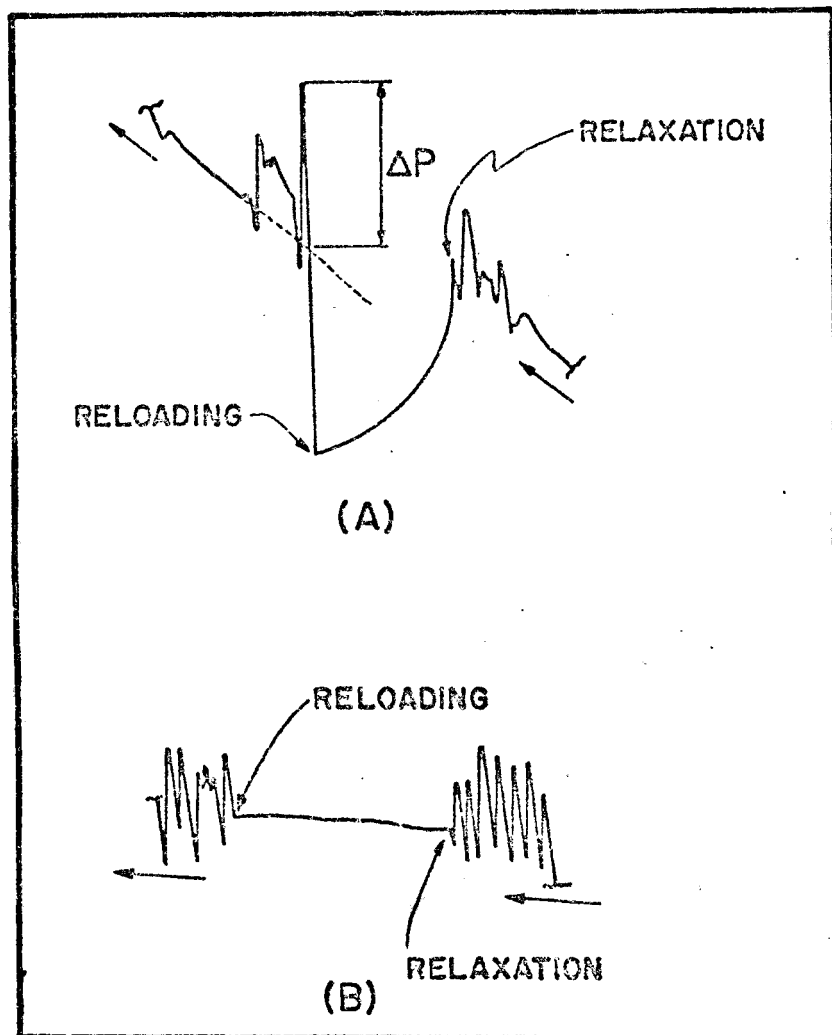
Fig. 68-A. Relaxation during Type A serrations. Annealed
            material, grain size 70μ, nominal strain rate
            10^{-2} min^{-1}.
      -B.   Relaxation during Type B serrations. Material
            solution treated and quenched, grain size 10μ,
            nominal strain rate 10^{-2} min^{-1}.

being independent of strain and position in the curve in relation to Type A band nucleation peaks. The value of this height seems to increase very quickly with time, and finally reaches a value approximately constant for very long periods of relaxation time (above 10 seconds).

One relaxation test was performed also during Type B serrations. No decrease in load was observed, and the aspect of the curve is shown in Fig. 68-B. Also note that no noticeably larger peak is observed upon reloading.

CHAPTER IV

DISCUSSION

4.1. Introduction

In Chapter I the current experimental results and the-
ories about serrated flow were discussed. In this chapter,
the present results will be compared with those obtained
in other works.

This shall be done by dividing serrated flow in its
general aspects, much in the way followed in the previous
chapters, and then the results obtained from tests with
photoelastic coatings, from local measurements of strain
along the gage length of specimens, and from other tests
will be discussed.

4.2. General Aspects of Serrated Flow
in Aluminum 6061 Alloy

4.2.1. The Effect of Strain

Concerning the effect of strain, the results obtained
resemble very much results obtained in other materials, like
α-brass,[5] copper-tin alloys,[17] etc. Actually, the similarity
between the behavior of solution treated and quenched alumi-
num 6061 alloy and copper-tin alloys[17] is remarkable. As

can be seen in Fig. 4, the amplitude of serrations of Type B in this material also tends to increase with strain, and the transition from Type A to Type B serrations is very similar (compare Fig. 4 with Fig. 37) to aluminum 6061 alloy.

Regarding the effect of strain on the strain between two successive Type A serrations ($\Delta\varepsilon$) and the load drop at Type A serrations ($\Delta\sigma$), the behavior is much the same as in Al 6063 alloy.[3] This can be seen by comparing Fig. 39 with Fig. 5, and Fig. 40 with Fig. 6. However, it seems that for aluminum 6063 alloy[3] the data scatter for values of $\Delta\sigma$ is much less than in the aluminum 6061 alloy.

The only theory that can offer any explanation for these phenomena is Cottrell's,[7] and would follow the rationale already presented in section 1.2.2.

4.2.2. The Effect of the Mechanical Characteristics of the Tensile Apparatus

The main consequence of a softening of the pulling apparatus is that the strain associated with each load drop was quite large at high strains. The spring constant was 300 lbs/in, and for an observed load drop of 7 pounds, this corresponds to an increase in length of ~0.023 in. As seen from the results with photoelastic coatings, in this case bands propagate very fast up to distances of about half a gage length. If this gage length is 2 inches, this load drop would correspond to about 2 percent deformation. On the other hand, the specimen usually fractured suddenly at

a load drop very soon after the load drop of the magnitude
discussed above was attained. This implies that most prob-
ably the strain caused by the band in the region of nuclea-
tion is much higher than the above calculated 2 percent.
For example, if the band associated with the load drop above
has a width of 0.1 inches when nucleated, the strain asso-
ciated with it would be about 23 percent, and a thinner band
could easily lead to necking and fracture. However, this
has to happen very quickly, for fracture occurs suddenly in
one load drop.

Thus, if the specimen does not fracture upon the nucle-
ation of the band, it propagates quickly and stops. As the
strain associated with the band increases, the specimen will
finally rupture at one load drop.

These phenomena are most probably associated with the
fact that in a softened machine, the load decreases very
little in comparison with a hard machine, for the same
strain in the specimen. Thus, in the soft machine, when a
band nucleates in the specimen, the load applied on it is
practically the same as before the nucleation, and this
should account for both the increase in strain in the band
and its propagation after nucleation.

4.2.3. The Effect of Temperature

The effect of temperature on the appearance of the
curves and on the critical strain for the onset of serra-
tions is perfectly consistent with the results for other

materials,[3,5,17] and the theoretical explanations given in section 1.2.2 could be applied accordingly.

It should be pointed out that a lower temperature not only raises the overall level of the stress elongation curve (see Fig. 43), but also increases the initial slope of the curve. Besides, lowering the test temperature by only roughly 20°C, completely eliminates Type B serrations in material solution treated at 485°C and tested at a nominal strain rate of 2×10^{-2} min^{-1}, which is a quite drastic change. This suggests that the range of temperatures over which one has serrated flow in this case must be quite small, of the order to 50-100°C.

4.2.4. The Effect of Nominal Strain Rate

Concerning the influence of nominal strain rate on the critical strain for the onset of serrations, Fig. 49 shows that the trend predicted by Cottrell's theory[7] is obeyed. However, based on data on aluminum 6063 alloy[3] and α-brass,[5] it just might be possible that at very low nominal strain rates, or equivalently at high temperatures, this trend would be inverted, following the tendency shown in Fig. 11 for low strain rates.

Regarding the overall shape of the serrations, aluminum 6061 alloy follows again the same tendency observed in other materials. The nominal strain rates used cover the limit below which one has serrations, in the case of annealed material, and is near to the same limit, for solution treated

and quenched material. In the case of solution treated
materials tested at low temperature, these strain rates
cover again the above-mentioned limit.

As stated in section 1.1.4, the effect of a large
change in nominal strain rate is equivalent to a small change
in temperature. Then, if strain rate changes of a factor of
10 can cause the changes discussed above and in section
1.1.4, the effect of a change in temperature ought indeed to
be large, as seen in the last section.

Again, in this case, Cottrell's theory predictions
agree with the results obtained: lower nominal strain rates
promote serrations, usually of Type B, while higher nominal
strain rates promote either smooth flow or Type A serrations.

Figures 45 and 46 show that both at room temperature
and at 1°C, solution treated and quenched material present
an inverse stress-nominal strain rate dependence, while Fig.
48 shows that annealed material has a practically nominal
strain rate independent stress-elongation relationship. Be-
sides, Fig. 45 makes clear that this difference is due to
an inverse slope relationship, where the material presents
a "steeper" curve at lower nominal strain rates.

4.2.5. The Effect of Heat Treatment

Section 3.2.5 made clear that heat treatment has a very
big influence on the kind of serrated flow observed. This
was also stated in section 1.1.5.

The results obtained in this investigation point out that at room temperature, solution treated and quenched specimens easily present Type B serrations, while annealed specimens tend to show Type A serrations or smooth curves. According to Cottrell's theory,[7] Type B serrations require a higher diffusion coefficient for solute atoms than Type A. This picture is coherent with the experimental tendency observed, since solution treated and quenched specimens have a higher vacancy concentration and thus, higher diffusion coefficient. Besides, as the solution treating temperature is decreased, one needs more and more strain to change the initial Type A serration into Type B. This is still coherent, for as the solution treating temperature is decreased, the concentration of vacancies at the beginning of strain decreases, and one needs more and more strain to reach the critical value for transition from A to B, since, according to Cottrell's theory, strain generates the necessary vacancies. However, the critical strain for the onset of serrations (ε_o) remains unchanged with a decrease in solution treating temperature, which is not coherent with the above model.

The effect of aging 24 hours at room temperature after solution treating, and its relationship with the solution treatment temperature is not understood. The material solution treated at 535°C and aged presented a very big increase in the critical strain for the beginning of serrations (ε_o),

in relation to the non-aged. The material' solution treated at 450°C presented no change at all in ε_o with aging. In this last case, there seems to be no reason why the initial Type A serrations should be more irregular after aging.

Figure 49 indicates that ε_o would be smaller for annealed than for solution treated specimens, which is in disagreement with data from similar material[3] (see Fig. 11 for aluminum 6063 alloy), and with what could be expected from Cottrell's theory.[7] However, data from Fig. 49 may involve errors due to the difficult determination of ε_o, since the amplitude of the initial serrations is extremely small.

Figure 50 shows that material aged 24 hours after quenching requires less stress to be deformed than the non-aged. This is most probably due to the higher effectiveness of dynamic strain aging in the freshly quenched material.

Figure 51 shows that as the solution treating temperature is lowered, the stress to deform aluminum 6061 alloy is decreased, until one goes down to 350°C when the trend is reversed. This is probably due to the fact that very little solution of the solute was obtained and since the material was originally in a T-6 condition, it just reflected its strength under this temper. Also note that for the same strain, the slope of the curves increases as we go up in solution treating temperature. If one compares the curve for 535°C in this figure with the curves for annealed

material (Fig. 48), one can see again that much of the difference in the level of the curves is due to higher slopes in the solution treated and quenched specimens.

4.2.6. The Effect of Grain Size

Regarding the influence of grain size on the critical strain for the beginning of serrations, Table 2 shows that our results agree with the general tendency discussed in section 1.1.6 -- it increases with grain size. This would be again coherent, within the framework of Cottrell's theory.[7]

Table 2 also shows that the stress for the beginning of serrations, σ_o, is practically independent of grain size, in a way very similar to α-brass.[5] In this case, the explanation for this would be the one given in section 1.2.2.

However, the tendency for Type A serrations to be preferred with increasing grain size is not understood, and no current theories account for this.

4.3. The Local Strain Behavior Associated with Serrations

The local strain behavior during Type A and Type B serrations, as well as this behavior for deformation in a "softened" tensile machine were presented in section 3.3. We shall now consider these results.

149

4.3.1. Type A Serrations

As seen in section 3.3.1, Type A serrations (see Fig.
3) indeed correspond to the nucleation of a deformation band
in one end of a tensile specimen, at each peak in the curve,
and the propagation of this band to the other end of the
specimen, in the region between load peaks. As seen, this
propagation is done under increasing load.

In the case of aluminum 6061 alloy, the propagation of
this band is usually not smooth, but can involve changes in
the direction of its movement and changes in its propaga-
tion speed. This is reflected in the load elongation curves
by irregularities between the nucleation peaks, as seen in
Fig. 38 and Fig. 52. We have called these irregularities
secondary serrations, and they probably are associated with
localized strains in the beginning of the test. It seems
that when a propagating band faces a region that is more
work hardened, it slows down, and more force has to be ap-
plied for propagation to go on. If the localized strain is
small, the load goes up until the band goes through this
region, usually in a burst forward, associated with a load
drop, since after the strain hardened region is overcome,
the band can propagate easily again. If the band actually
stops at this barrier, the load will go up elastically, as
seen in peak E', Fig. 52, for example. In this case the
band will start moving again at the region where it is
easier for it to move, and if the obstacle ahead of it is

too big, it may change its direction of propagation, as
shown schematically in Fig. 54. This is what happened at
point D', Fig. 52. On the other hand, it may also continue
moving forward under bursts, as seen in points B' and C',
Fig. 52. However, if the obstacle ahead of the band is
small, it may only decelerate temporarily the band, the load
will go up a little bit, and that is all. This can be seen
in the last secondary serration in the upper curve of Fig.
55.

Thus, it is no wonder that the deformation associated
with specimens strained with self-aligning grips (Fig. 55)
is simpler than that performed with screw grips (Fig. 52),
since in the last case it's much easier to produce high
localized strains in the beginning of the deformation, due
to misalignment effects. Besides, since each test has
slightly different gripping characteristics, it should be
expected that they present different secondary serrations.
However, in the same test, they should be quite regular and
repetitive, as has indeed been observed.

It has been stated before that secondary serrations
grow quickly and then disappear also quickly, as illustrated,
incidentally, in Fig. 55. Let us analyze this phenomenon,
that might be connected with the general parabolic shape of
face centered cubic metals stress-strain curve, where very
high work hardening occurs for low strains and then, as the
curve "flattens" down, small work hardening results for the

same increase in strain, as illustrated in Fig. 69. For
example, an increase $\Delta\varepsilon$ in strain at point A hardens the
material by $\Delta\sigma$. However, the same increase of strain from
point C hardens the material by only $\Delta\sigma'$. Due to this fact,
any initial localized strain in the gage length of a speci-
men causes very high work hardening in the deformed region;
the gage length may, for example, have some small regions
hardened to point C in Fig. 69, while almost all the rest of
it will be at point A, still quite soft. Thus, when a de-
formation band sweeps along the gage length of a specimen
in such a condition, it has to overcome quite a barrier.
The initial difference in work hardening between different
points in the gage section would be ΔAC, in Fig. 69.

When a band propagates along the gage length of a
specimen, it causes some small deformation everywhere (of
the order of 0.1-0.2 percent for the initial bands, accord-
ing to Fig. 39). Let us suppose that the strain associated
with the band is constant during its propagation. In other
words, all regions are strained $\Delta\varepsilon$ by the passage of the
band. Thus, in Fig. 69, regions previously at point A go
to point B, and points previously at point C go to point D.
Now the difference in work hardening between different
points in the gage section would be ΔBD, which is obviously
less than ΔAC, due to the shape of the stress-strain curve.
Thus, as successive bands sweep the gage length of the speci-
men, the work hardening gradient along the specimen decreases
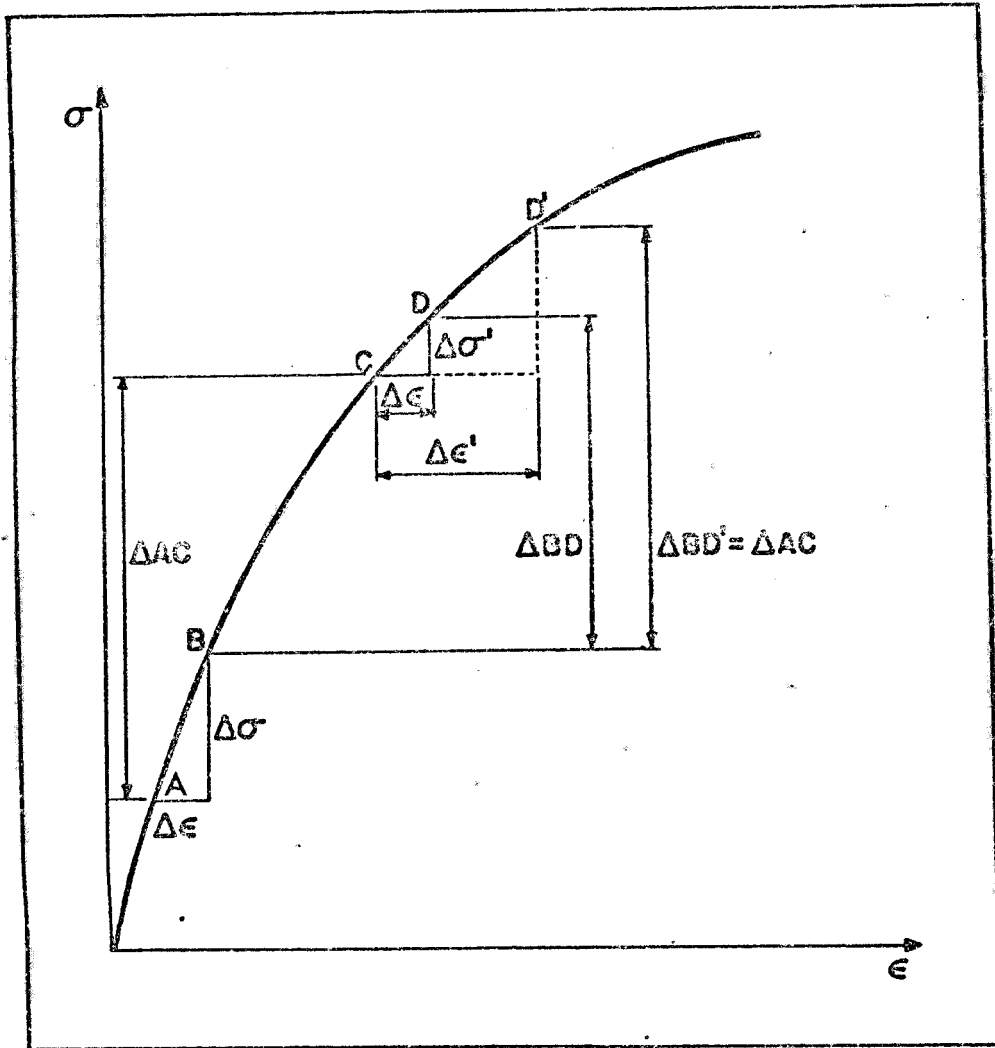
Fig. 69. The influence of the shape of the stress-strain
curve on the work hardening characteristics of
a material.

and the barrier to the movement of the band also decreases with increasing strain, until the whole specimen has practically the same work hardening. Then, the bands should propagate without any secondary serrations. This could account for the fading away of secondary serrations seen in the latter part of Fig. 38, and in Fig. 55.

However, how could one account for the initial increase in the secondary serrations? According to Fig. 69 and our earlier concepts, this would require an initial increase in the work hardening gradient with the passage of bands, or, in other words, ΔBD should be greater than ΔAC in Fig. 69. It can be easily seen that this could be accomplished if one had different amounts of strain associated with different positions of the band; for example, if the band somehow causes a deformation $\Delta \varepsilon'$ when it goes through the more work hardened region (point C in Fig. 69), it will work harden this region to point D', and now $\Delta BD'$ could be greater than ΔAC.

One could then imagine two processes occurring simultaneously: first, somehow the band causes more strain when it goes through more work hardened regions (point C, Fig. 69) than when it goes through less work hardened regions, thus tending to increase the work hardening gradient in the specimen. Second, an effect tending to decrease the work hardening gradient, due to the shape of the stress-strain curve, as explained before. In the beginning of the

deformation, the first process wins, and secondary serra-
tions grow. After some time, the processes compensate for
each other, and afterwards the second process wins the com-
petition, bringing down the secondary serrations. Let's
see how this could happen. The actual strains associated
with bands are much smaller than shown in Fig. 69. In the
beginning of the deformation, both points A and C are still
in a quite steep part of the curve, and a difference in $\Delta\varepsilon$
at these points may easily cause an increase in the work
hardening gradient, as shown in Fig. 70. However, as the
curve flattens down, $\Delta\varepsilon'$ would have to be increasingly bigger
than $\Delta\varepsilon$ to keep ΔBD greater than ΔAC, as shown in Fig. 71.
This is not likely to happen, and after some time the greater
value of $\Delta\varepsilon'$ cannot compensate anymore for the effect of the
shape of the curve. As a result, the work hardening gradi-
ents would start decreasing, in the way described before.

We shall discuss further the concepts above in section
4.4, where evidence is offered for the increased strain in
points where the initial strain is higher.

It has been observed that when a band has to face a
barrier caused by localized work hardening, it usually stops
or decreases its speed, depending on the magnitude of the
barrier. In section 4.4 we shall also discuss the possi-
bility of having a relationship between different velocities
of propagation and the strain caused by the band.
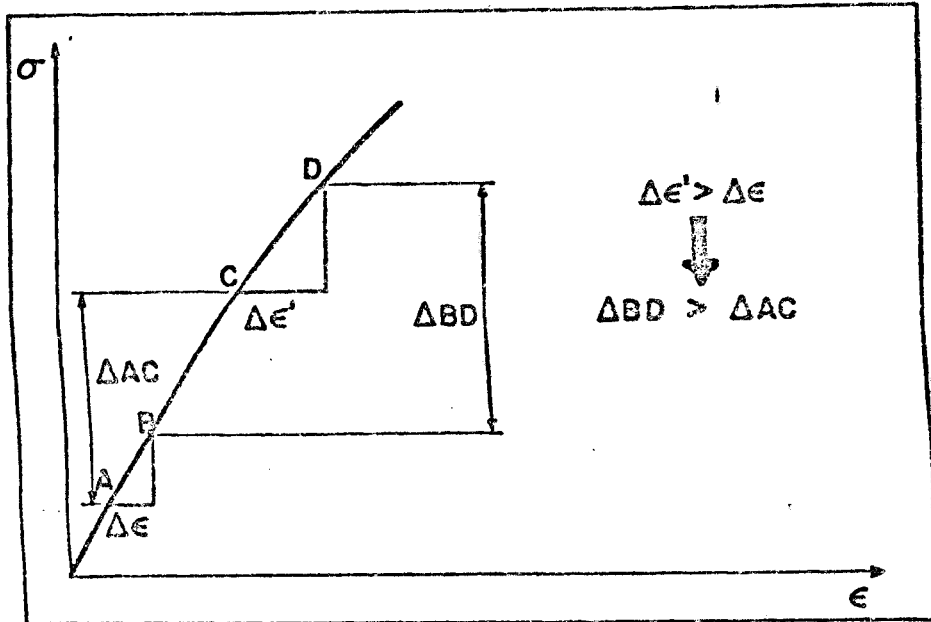
Fig. 70.   Initial work hardening behavior as
            bands sweep along the gage length.
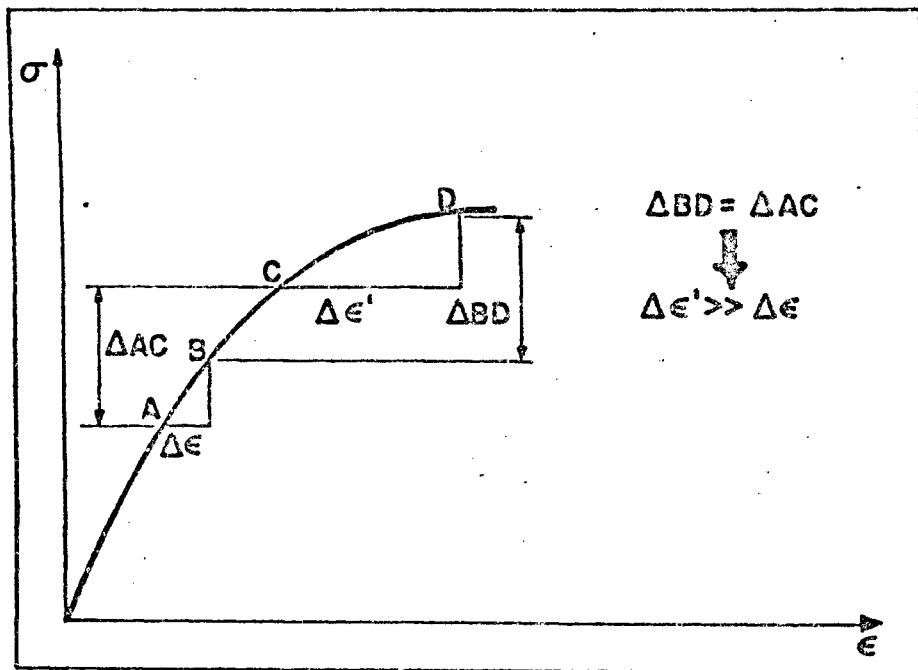
Fig. 71.   The effect of the shape of the stress-
            strain curve on the strain gradient
            along the gage length of the material.

It should be pointed out that the ideas presented above
cannot be definitely established only with the present ex-
perimental results. Much more evidence is obviously needed
to fully clarify the concepts in question. Besides, it is
not known if other factors besides work hardening gradients
are involved in the problem, and how far these gradients
can account quantitatively for the effects described.

Secondary serrations occur in other materials, and
actually may be more common than supposed, due to the fact
that most of the tensile tests are run without any scale
expansion, which obviously masks them out. However, they
may be seen very clearly in α-brass,[5] and Fig. 4 also shows
some irregularities between Type A load drops, for copper-
tin alloys.[17]

As stated before, the initial deformation by bands is
quite complex. However, after some strain, all the bands
start forming in the same end of the specimen and propagate
to the other end. This has also been observed in α-brass[5]
and aluminum 6063 alloy.[3] This is not well understood, and
we shall make some comments about it in section 4.4.

The propagation of bands associated with Type A serra-
tions is done under increasing load. Note that all the
bands nucleate in one end of the specimen and propagate to
the other end. However, when reloading was done in Fig. 52
a band nucleated in the middle of the specimen, at point L',
and propagated in the same direction others had propagated,

under an increasing load, to point M'. Then, from point N'
to O' the band propagated in the other direction under a
decreasing load! As stated before, this was commonly ob-
served, and suggests that whatever is causing the increase
in load during the band propagation has to do with some pre-
vious directional property of the material, as, for example,
a work hardening gradient, as indicated by McCormick.[3] If
this is indeed true, it should be expected that smaller
work hardening gradients should require less increase in
load. As discussed before, the work hardening gradients
tend to fade away at high strains, and indeed less and less
increase in load is necessary to propagate the band at high
strains, as seen in Fig. 38. On the other hand, according
to what was said before, in the beginning of the deformation
one ought to have higher local work hardening gradients,
that should cause higher local increases in load. Indeed,
the secondary serration in Fig. 38 really becomes higher and
steeper with strain, and this also can be seen in Fig. 52
(compare peaks X, Z with D', E'; they correspond to the same
phenomena).

It has also been observed experimentally that bands de-
crease their speed of propagation as the total strain in-
creases; this will receive more attention in section 4.4.
Besides, it is also observed that at high strains the nucle-
ation of bands is easier, without involving big peaks. This
is not understood.

None of the theories for serrated flow can explain many of the features above. For example, no explanation is given concerning the reason the bands propagate under an increasing load, why the bands always nucleate in the same end of the specimen, why their speed decreases with strain, and why their nucleation is easier at high strains. We shall try to cast some more light on some of these questions in the following paragraphs.

4.3.2. Type B Serrations

Although the current literature states that Type B serrations are associated with the formation of bands that do not propagate, there is some controversy among authors concerning the way these bands would form. Some authors state that they form successively ahead of each other, constituting what has been called discontinuous propagation of bands,[5,17] while others argue that they form at random along the gage length.[18]

The experimental results presented in section 3.3.2 show that Type B serrations indeed correspond to the formation of bands that do not propagate. Besides, they can form in three different ways during a test: they may form at random, they may nucleate successively ahead of each other, covering small distances, and they may nucleate exactly in the same region another band nucleated before.

This last nucleation mode is particularly interesting, because at times, four to five bands nucleate in the same

region, one after the other. This may imply that aging of
the freshly created dislocations is not that efficient in
this region, which might make easier further nucleation in
that point. On the other hand, it may be argued that the
stress is higher in this region, but it is also higher
where other bands had nucleated before. Anyway, the combi-
nation of a higher stress with a less efficient locking may
cause the phenomenon in question, until the region of nucle-
ation is so work hardened that further nucleation of bands
at that point isn't favored anymore.

The fact that random nucleation of bands during the
test can be at times associated with bigger load drops (see
points marked N' in Fig. 56) could be related to the fact
that these bands occur in regions where the material has
had plenty of time to age.

The concept that pinning after band formation might
not be as efficient as previously considered receives sup-
port from the behavior associated with the regions marked
"T" in Fig. 56. However, the reason why wedge-shaped bands
nucleate as shown in Fig. 58 is unknown. Anyway, the smooth
transverse or longitudinal propagation of bands can only
happen if an incomplete locking of dislocations is involved.

The fact that discontinuous propagation of bands seems
to be favored at higher strains is not understood. If
Brindley and Worthington's[18] extension of Cottrell's theory[7]
is valid, it may be argued that as the strain increased,

locking of dislocations will be more and more efficient,
and that this would somehow favor the discontinuous propaga-
tion, perhaps due to stress concentration at the fronts of
a nucleated band.

Another point of interest is the transition from Type
A to Type B serrations. This transition can be seen in Fig.
37, in Fig. 4, and in Fig. 44. As seen, Type B serrations
start as "damped oscillations" just after the load drop
associated with Type A serrations. Nothing has ever been
said in the literature about this transition, concerning
the strain behavior of the material, and it is our belief
that the use of photoelastic coatings can easily uncover
the phenomena involved in this transition, and perhaps give
more insight on why such a transition may occur merely as a
result of strain.

4.3.3. Serrations During Deformation in a Softened Machine

The material deformed in the soft machine was such that
it would present profuse Type B serrations in a stiff
machine. However, its deformation in a soft machine dras-
tically reduces the number of peaks in the curve, and prob-
ably increases the deformation associated with each load
drop, as discussed in section 3.3.3.

It should be pointed out that it takes a long time to
raise the load to a high level after the drop, as can be
seen in Fig. 41. This would give time for the material to
age completely before another band could be nucleated.

It has been observed that the magnitude of the load drops at high strain does not differ very much for deformation with the spring and without it. One might suppose then, that once a load drop starts, it will go down to a level where the driving force on the dislocations cannot move them anymore. If this is true, at each level of stress the magnitude of the load drops should be about constant for any mechanical characteristic of the pulling apparatus. However, the softer the machine, the more strain will be associated with the load drops, and the specimen is liable to neck and fracture earlier, as observed in this work. This does not necessarily imply in a loss of ductility, for it must be remembered that as the softness of the machine increases, the strain associated with load drops prior to the one causing the fracture also increases. Thus, it should be expected that the number of peaks will decrease in a softened machine, as stated previously, since the strain associated with each load drop increases, and the material has the same ductility, whether deformed or not in a softene pulling apparatus.

Another effect of softening the Instron is that once the band nucleates, it propagates very fast, in contrast to the stiff machine, where bands do not propagate. This is probably due to the fact that load falls much slower in a soft machine than in a hard one; when the initial band is formed, the load drop associated with only this nucleation

is obviously less than the total load drop, and there is plenty of driving force for the band to propagate, causing strain to a point where the load goes down an amount sufficient to stop propagation.

The discussion in section 4.2.2 shows that the deformation associated with just the nucleation of the band may be big. However, if it is not sufficiently big to cause instability and local necking, the final part of the load drop will be used in its propagation. On the other hand, if the strain associated with the nucleation is big enough to cause necking, the rest of the load drop will be used in fracturing the specimen. This is the reason why failure occurs suddenly in one load drop.

The complex strain patterns during the quick propagation of bands, that was shown in section 3.3.3, may be simply due to local differences in work hardening caused by earlier bands. Then, it would be easier to propagate a band in a softer region of the specimen than in a harder region. For example, in Fig. 59, the lower part of the specimen may be softer than the upper part. However, no experimental evidence is available about this.

4.4. Type A Serrations and Strain Gradients Along the Gage Length of Specimens

If one compares Fig. 60 with Fig. 7, it can be seen that in our case the variation of strain along the gage

length of a specimen is more complex than the ones indicated in this last picture. This may be due to the fact that Fig.7 is for aluminum 6063 alloy, while Fig. 60 is for aluminum 6061 alloy. Anyway, we did not obtain smooth strain gradients for different levels of average strain, but it should be pointed out that different curves in Fig. 60 correspond to different specimens, which may cause irregularities in these plots.

However, let's first consider the shape of the curves in Fig. 60. The curve for an average strain of 3.7 percent increases almost regularly, without any "bumps" in it, and the load-time curve corresponding to the deformation of the specimen presents no secondary serrations between the main peaks of Type A serrations. On the other hand, the curve for an average strain of 9 percent presents a huge peak about halfway along the gage length. If one observes now its load-time curve, it presents one big secondary serration. This trend, of associating any big irregularities in the curves in Fig. 60 with the presence of secondary serrations, is quite consistent. If should be pointed out that the strain peaks observed at both ends of the specimens do not seem to be associated with secondary serrations. Thus, secondary serrations can be associated with higher localized strains along the gage length of the specimen; we shall shortly point out that one has more strain in these regions than should otherwise be expected, which gives support to

our idea that somehow propagating bands cause more strain in regions where originally there was more work hardening.

The curves shown in Fig. 7 are quite smooth. Correspondingly, McCormick[13] reports absolutely no secondary serrations in the load-time curves for aluminum 6063 alloy. However, in an earlier paper,[22] he presents curves for the same material with mild secondary serrations!

This author[3] also attributes the presence of strain gradients to the sweeping of bands during Type A serrations, and has observed experimentally that the bands always nucleate in the less work hardened end of the gage length. This last fact can be easily understood, for it is easier for the bands to nucleate in a softer region. However, it is possible to establish strain gradients in a specimen without the sweeping of bands. If any part of the undeformed gage length of a smoothly deforming material is smaller to begin with, it is to be expected that more strain will occur at this region than in other regions, and even without serrations, one could end up with peaks in curves such as shown in Fig. 60.

Thus, a few tests were performed with commercial purity nickel, and the results are shown in Fig. 62. Although in this case the peaks are usually "flattened" down, the deformation is by no means strictly uniform. If one compares the original and final diameters in these specimens (see Fig. 63), one can see that the diameter profiles before and

after deformation are similar in shape, with strain concentrating in the smaller diameters, as explained above. Note that the differences in the original diameter for different parts of a specimen are very small (less than 0.001 in). Besides, if the specimens are strained past the necking region, it was observed that the necks always form in the regions of originally smaller diameter.

Thus, it could be safely stated that the peaks observed in Fig. 60 most probably start during the smooth initial part of the deformation, where smaller diameters in the original profile would bring forth localized strains. Due to the shape of the stress-strain curve for face centered cubic metals, these regions would work harden much more than other regions in the beginning of the deformation, constitute barriers to the propagation of bands, and cause secondary serrations. However, the peaks seen in Fig. 60 are bigger and more abrupt than the ones seen in Fig. 62. If indeed it is true that the propagating band can cause more strain in regions already more work hardened, the peaks in Fig. 60 should be higher and more localized than in Fig. 62, as it is indeed observed.

Now let us compare the diameter profiles before and after deformation for the aluminum specimens strained 3.7 percent and 9 percent. These curves are seen in Fig. 61.

The original diameter of the specimen deformed 3.7 percent changes practically uniformly, without any irregularitie

in it. This leads to no regions of localized strain in the beginning of the deformation, nor localized barriers to the propagation of bands, and consequently one has no secondary serrations in its load-time curve, and no peaks in its strain profile. However, it should be expected that this specimen should present a strain gradient along its gage length, because of its original shape. Figure 60 shows that this is indeed the case. Also note that the diameter profile for this specimen after strain is practically parallel to the original one, according to our predictions.

The original diameter of the specimen deformed 9.0 percent presents a smaller diameter in the middle. This will lead to localized strain in the beginning of deformation, to a barrier to band propagation, and to a secondary serration in its load-time curve, as indeed was observed. Thus, one peak at about the middle of its strain profile should be expected, and it can be seen in Fig. 60. If we consider the final diameter for this specimen, it can be seen that once again it is similar to the original one, as expected. If the work hardening barrier also causes more localized strain, as discussed before, this should increase the height of the peak in the strain profile.

It should be pointed out that the fact that more strain causes higher peaks in the curves in Fig. 60 does not imply that the barriers are increasing, but actually that they are decreasing. This is due to the shape of the stress-strain

curve, that at high strains will cause small differences in work hardening in different regions of the gage length. What causes the barrier are differences in work hardening, and not in strain.

Thus, if the suppositions made before are correct, at least a part of the rising load during the propagation of Type A serrations is used in overcoming local work hardening gradients. In the case of the specimen deformed 9 percent, in Fig. 60 a band will be nucleated at abscissa 0, and start propagating to the other end of the specimen. It faces increasingly hardened regions and the load goes up to keep it propagating. After it overcomes the region corresponding to the central peak, the load drops, because it is suddenly easier to propagate the band. After that, the band has to face another hardened region, and the load goes up again. In the case of the specimen deformed 3.7 percent, one has no peaks, and the load has only to keep increasing to keep the band moving.

The above picture is strongly supported by the propagation of a band under decreasing load between points N' and O' in Fig. 52. In this case, a band is propagating in the direction of softer material, and it should be expected that less and less load would be needed in its propagation.

If the model presented in indeed true, then one problem remains: to determine how far work hardening gradients are responsible for the discussed increase in load. It is

obvious that much more experimental results than the ones presented here are necessary in order to definitely ascertain the ideas introduced. It should also be pointed out that the curves shown in Figs. 52 and 55 represent the load necessary to propagate a deformation band along the gage length of a specimen, and have little to do with the actual flow stress of the material.

It should be stated that the initial geometry of the specimens seems to play a very important role in the deformation by bands. Besides, any external factors, like misalignments in the tensile apparatus, that affect the strain distribution in the specimen, also have great influence in the results obtained. The fact that some uniform deformation occurs before deformation by bands sets in is also of crucial importance, because it permits the establishment of initial work hardening gradients. It should be pointed out that in steel, where no deformation occurs before the yield point, Lüders bands propagate under a practically constant load. Besides, in body centered cubic metals, there is no big difference in work hardening for small differences in strain, at low levels of strain.

Another interesting point is how could a propagating band cause different strains in different regions of the gage length. A closer observation of Fig. 60 shows that strain peaks are associated not only with secondary serrations, but frequently also with both ends of the specimen

(see, for example, the curve for the specimen deformed 4.7 percent). On the other hand, these three points along the gage section (both ends and the more work hardened region causing the secondary serrations) are associated with changes in propagation velocity of a band: when the band forms in one end of the specimen, it nucleates very quickly and immediately slows down due to the load drop; when a band faces a more work hardened region, it slows down or stops, and then bursts forward; finally, as the band approaches the other end of the specimen, it has to slow down due to the increasing shoulder section. Thus, there is a possibility that the different strains mentioned above could be associated with these different propagation velocities. According to what was said before, the only change in speed present at all three points in question is a slowing down, and thus its quite attractive to associate a slowing down of the band with an increase in the strain caused by it. However, the experimental facts that we shall present now do not give any definite indication about this, and may even indicate a reverse trend, where a faster speed would correspond to higher strains. It is obvious that the experimental results presented here are not sufficient to definitely establish any such relationship.

The average velocity of a sweeping band can be calculated from plots such as shown in Fig. 38, if one assumes that the time between two successive nucleations of bands

is used to propagate a band over a known distance, namely
the gage length of a specimen. A test similar to the one
in Fig. 38 was run, but with nominal strain rate 1.54×10^{-1}
min^{-1}; then, both the velocity and the strain associated
with each band were calculated as a function of strain, for
this specimen and another tested at 0.77×10^{-2} min^{-1}.

Figure 72 shows that for a given test, the average
velocity of the band decreases as the strain associated with
it increases. This has been stated before, qualitatively,
as a result of the experimental observation that as the
strain increases, the band velocity decreases, and the strain
associated with it increases. This can also be seen in Fig.
73. Thus, it may indeed be true that a lower propagation
velocity is associated with higher deformation. Figure 73
also indicates that a higher nominal strain rate causes an
increase in the band velocity. Thus, it. should be expected
that at higher nominal strain rates, the strain associated
with a band would be smaller than at lower strain rates,
for equivalent positions along the curve. Figure 74, how-
ever, shows that this is not the case, at least at high
strains. The dashed line indicates that no serrations were
observed at low strains. Thus, the deformation history of
the two specimens in question are different, and it is prob-
able that a comparison between the two curves in Fig. 74
would be valid only for identical previous histories. For
example, strain rate changes during a test ought to give
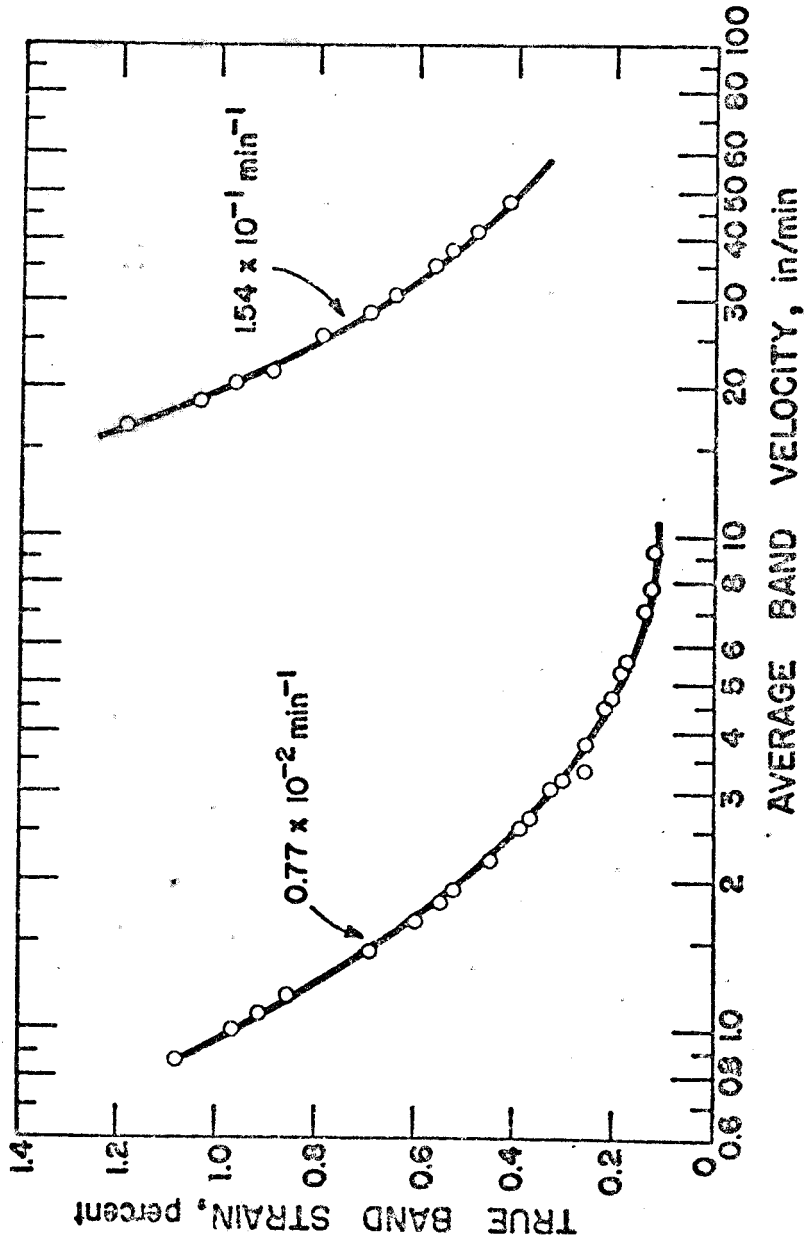
Fig. 72. Average band velocity as a function of strain associated with the band and of nominal strain rate.
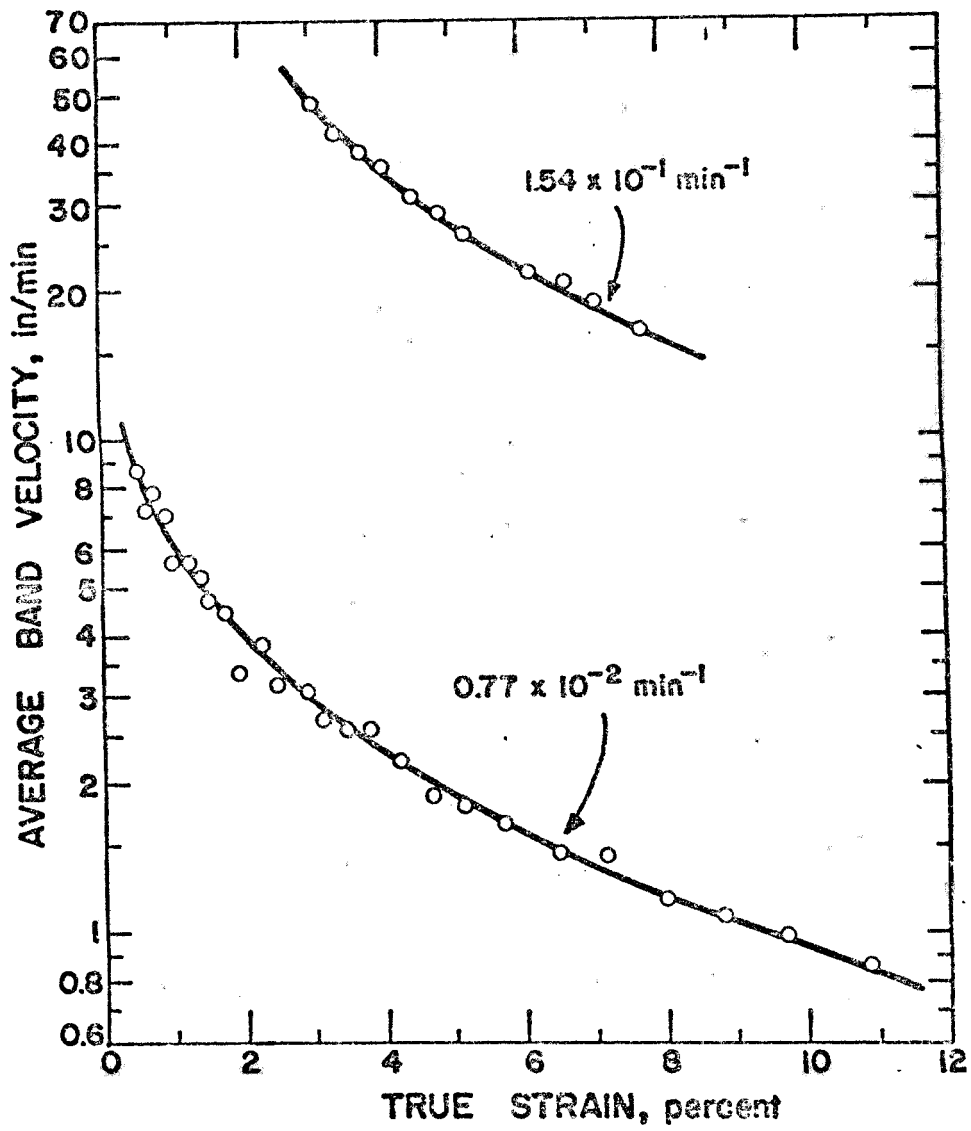
Fig. 73. Average band velocity as a function of total strain and nominal strain rate.
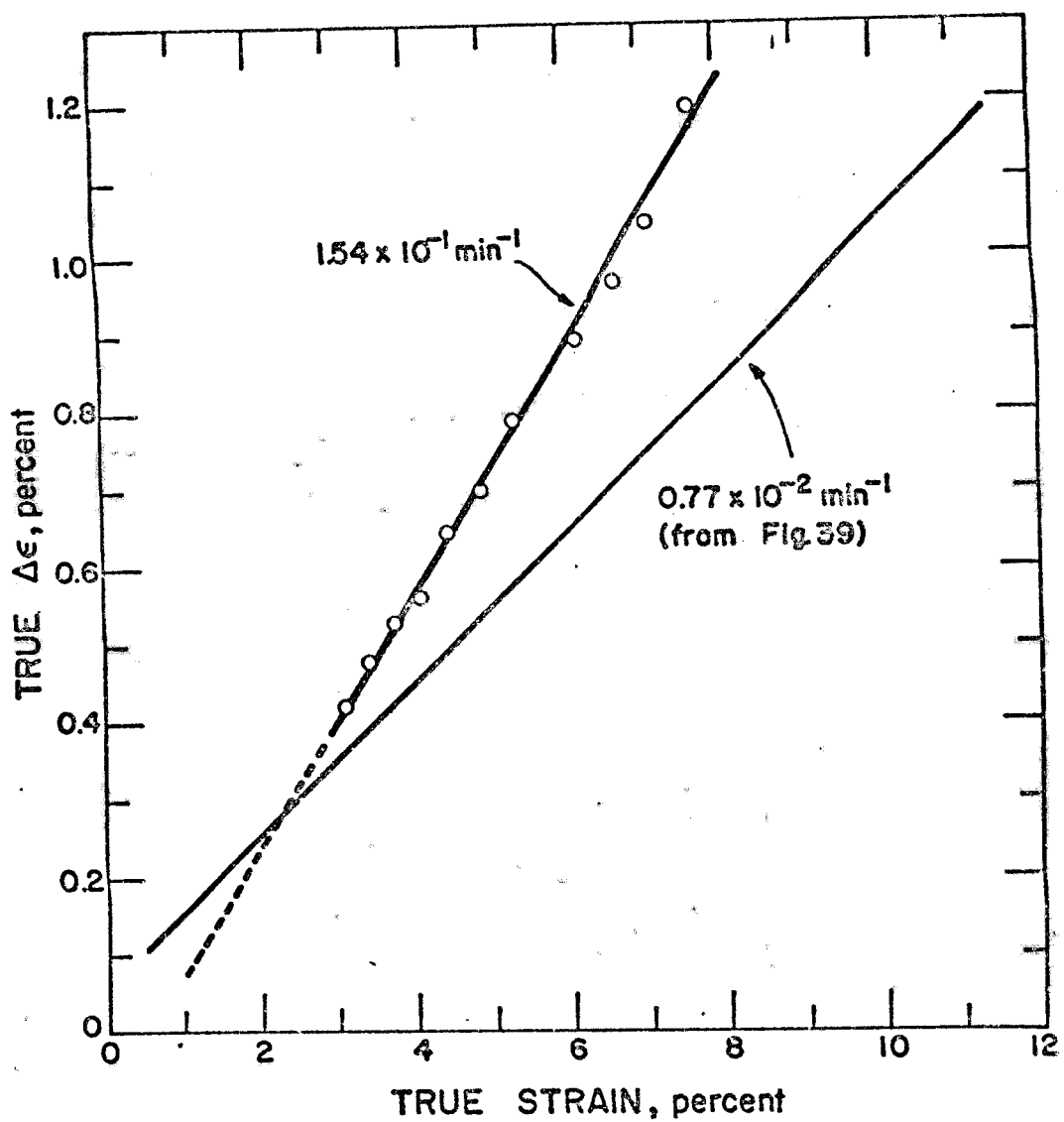
Fig. 74. Strain associated with bands as a function of total strain and nominal strain rate.

more accurate results than the ones presented here. Besides, McCormick[9] has reported a decreasing strain associated with bands for decreasing temperature (see Fig. 5), which is roughly equivalent to increasing strain rates.

Anyway, although the current results do not seem sufficient to establish a definite relationship between the band propagation velocity and the strain associated with this band, it seems quite possible that such a relationship may exist.

4.5. Tests Involving Relaxation and Changes in Nominal Strain Rate

In both theories seen in sections 1.2.3 and 1.2.4, a basic requirement is that the material presents a negative flow stress-strain relationship. As seen in Fig. 45 and Fig. 46, this is the case for solution treated and quenched materials; and Fig. 48 shows that in the case of annealed materials, there is an almost complete independence of the curves with nominal strain rate, although a small negative relationship may be noted.

However, as argued in the above-mentioned sections, the theories do not take into account the previous strain history of the material. In order to verify this, some strain rate change experiments were performed. In the case of solution treated and quenched specimens, the strain rate sensitivity was usually zero, as seen in Fig. 67-B (Chapter

3), even though the character of the serrations may be en-
tirely changed by the strain rate change. However, as seen
in Fig. 65 and Fig. 66, there is an inverse relationship
between the nominal strain rate and the slope of the curves,
where an increase in the strain rate causes a decrease in
the slope. Thus, the difference in level in the curves in
Figs. 45 and 46 is indeed due to differences in slope.

In the case of annealed material, a change in nominal
strain rate is seen in Fig. 67-A, and indeed a small nega-
tive strain rate sensitivity is observed, once the transients
associated with the change are over. In other words, point
A is below point B for an increase in strain rate, and A is
above B for a decrease in nominal strain rate. However,
when Fig. 64 is considered, one might conclude that in all
possibility any major difference in the level of curves
should again be due to an inverse relationship between nomi-
nal strain rate and the slope of the curve. It is difficult
to compare Figs. 48 and 64, because Fig. 48 is for specimens
with grain size 10μ, while Fig. 64 is for a specimen with
grain size 70μ.

However, in aluminum 6061 alloy, no drastic change in
the level of the stress elongation curve is observed with
changes in nominal strain rate, which makes the theories in
question of difficult applicability. Besides, it is doubt-
ful whether the load indicated by a serrated curve can be
really used to compute the flow stress of a material. In

the case of Type A serrations, for example, the part of the curve between serrations merely repnesents the load to propagate a deformation band along the gage length of the specimen. In the case of Type B serrations, the top of the peaks may be considered as the load necessary to nucle-ate bands in the gage length.

Thus, Fig. 64 simply shows that at higher nominal strain rates, the propagation of bands involves less increase in load than at slower nominal strain rates, and Figs. 65 and 66 show that the same happens for the nucleation of Type B serrations at higher strain rates.

Figure 67-A also shows that slightly less load is required to propagate a band under high nominal strain rates than at slower nominal strain rates (point A is lower than point B). However, nothing is known about what is happening during the transient caused by the change in strain rate.

Concerning Rosen and Bodner's theory (explained in Chapter I), two points should be brought out: these authors base their conclusions on flow stress-strain rate plots, usually obtained from serrated curves. It remains to be proved that a serrated curve really shows the flow stress of a material, or just the load necessary to propagate or nucleate deformation bands in the specimens. Besides, the true strain rate in the band is most probably much higher than the nominal strain rate.

Concerning the relaxation tests, the dependency of ΔP (see Fig. 68-A), only on the relaxation time, discussed in section 3.5, suggests that the aging rates involved with Type A serrations may be smaller than considered up to now. Besides, if a relaxation is made during Type A serrated flow, just after a band is nucleated, one wonders if the dropping load would not be associated with further propagation of the band down the gage length.

Figure 68-B suggests that during Type B serrations the whole gage length is aged, and does not deform on relaxation Thus, aging would be very quick and complete in this case, in agreement with Cottrell's theory. However, this is not in agreement with the possible smooth propagation of bands discussed in section 3.3.2. On the other hand, it should be considered that only a few relaxation experiments were made during Type B serrations, and a more thorough investigation of the relaxation behavior, with regard to strain level and t the moment of crosshead stopping in relation to the peaks, seems necessary before any conclusion may be reached.

4.6. A Tentative Schematic Explanation of the Phenomena Involved in Type A Serrated Flow

Let us consider a specimen whose initial profile is similar to that of the specimen in Fig. 61-A. It is almost perfectly tapered, and after some deformation in tension it

will present a reasonably regular work hardening gradient, as shown in Fig. 60 (specimen strained 3.7 percent).

If we consider a plot of stress vs distance along the gage length, it is safe to assume that before any deformation, the initial long range component of the flow stress, σ_0, is constant along the gage length. However, after some strain one shall have a work hardening gradient along the specimen, as discussed previously. This is shown schematically in Fig. 75.

Let us suppose that a band has nucleated in the left end of the specimen, and is propagating to the right. The band causes some work hardening also, and the work hardening profile at time t in the propagation should have the appearance shown in Fig. 76, supposing that the band causes a fixed amount of strain. The applied stress should be approximately σ_{app}, disregarding any aging effects, because of the following reasoning: at point B, the mobile dislocation density starts increasing. At point A, it has gone back to zero, because we have no deformation behind the band, the dislocations don't move, and the applied stress should be sufficient to equilibrate the work hardening at this point. It follows immediately that the applied stress should increase as the band sweeps along the gage length (see Fig. 76). The stress necessary to propagate the band has to be σ^*. Note that as one goes from point B to A, σ^* decreases, due to the work hardening in the material. At point A, σ^* is zero.
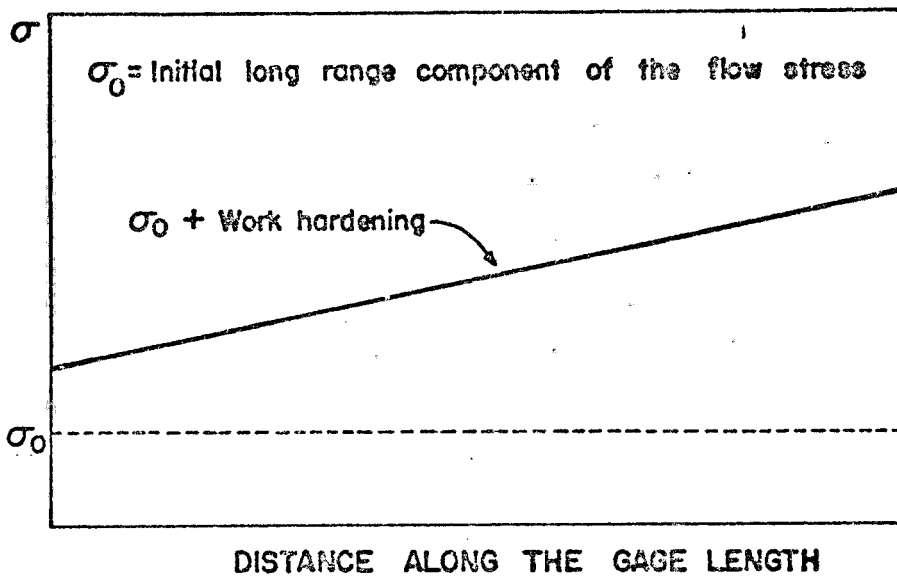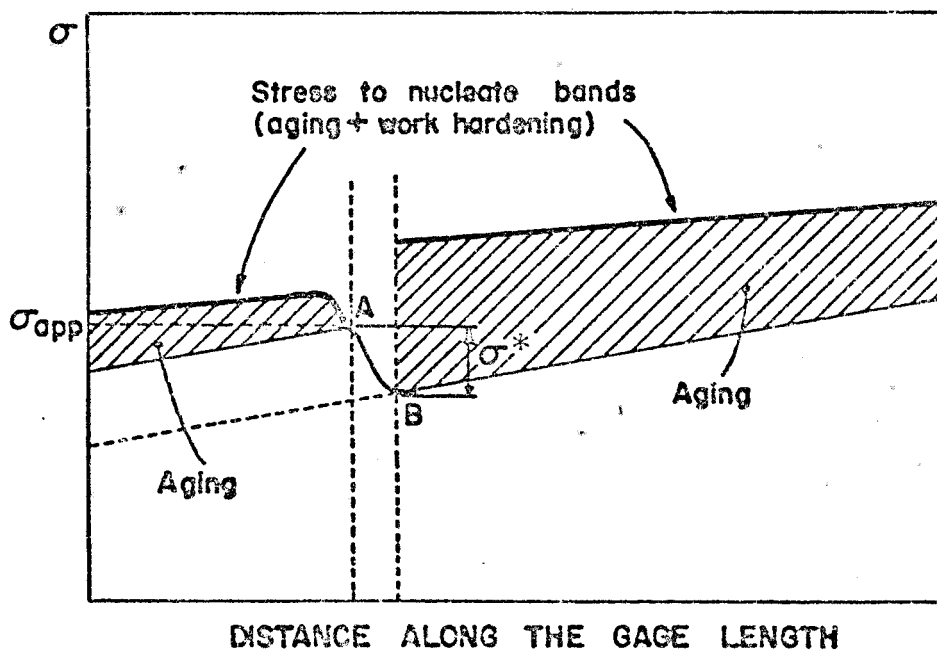
Fig. 75. Work hardening pattern along the specimen.

Fig. 76. Propagation of the band at instant t_1.

Since experimental results indicate it is easier to
move a band faster, one should expect σ^* to depend on the
band velocity, and thus on the nominal strain rate.

Deformation does not occur in other points in the gage
length because these regions are aged, and should deform
only by the formation of bands. One might say then that
the stress to nucleate bands is the result of the work
hardening and the aging, and should obey the curve shown in
Fig. 76. The shaded part is due to aging. This curve is
obviously time dependent, and at a later time, t_2, one has
the configuration seen in Fig. 77. Finally, Fig. 78 shows
the configuration at the moment the propagating band has
covered the whole gage length. Since no further propaga-
tion of the band is possible, σ_{app} will rise elastically to
point C. At this point, a band is nucleated at the same end
the first one formed. This would obviously correspond to
the peak and ·load drop in the formation of bands in Type A
serrations. Note that the curve showing the stress necessary
to nucleate a band is the sum of the work hardening and the
effect of aging (shaded area, Figs. 76, 77 and 78), and in-
deed accounts for more aging in the regions where more time
is available for age hardening. One could then explain why
the bands keep nucleating at the same end of the gage
length.
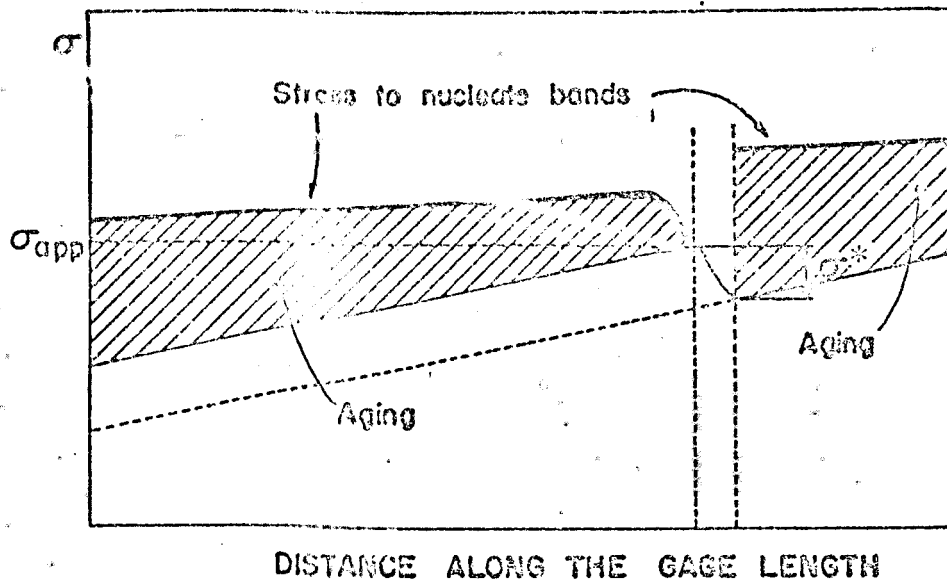
Fig. 77. Propagation of the band at instant $t_2 > t_1$.
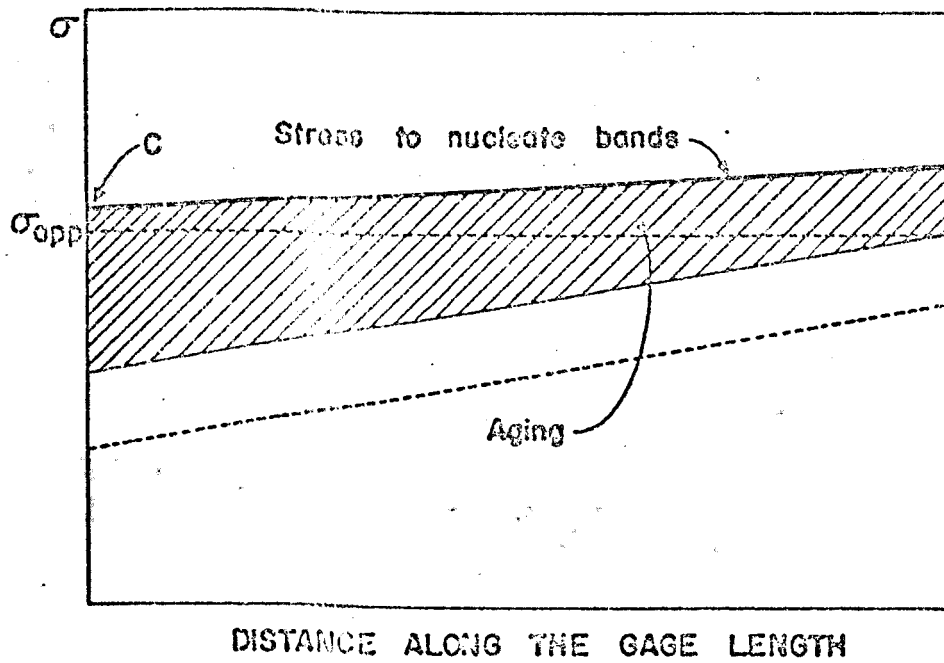
Fig. 78. A new band nucleates.

4.7. Summary

Concerning the generality of our results with aluminum 6061 alloy, and the possibility of extending the results obtained here to other materials, we would like to point out that many other materials present a behavior astoundingly similar to aluminum 6061 alloy, concerning the characteristics of serrated flow, and we can see no reason why our results could not be extended to these materials.

Other metals presenting this behavior are: aluminum 2024 alloy,[32] α-brass,[6] aluminum 6063 alloy,[3,22] copper-gold alloys,[33] copper-tin alloys,[17] and copper-indium alloys.[6]

As seen in this last chapter, there are still many points to be clarified concerning serrated flow. Actually, there are very few definitely established experimental observations. It is our hope that this work has brought some contribution to clearer understanding of the phenomena associated with serrated flow.

CHAPTER V

CONCLUSIONS

1. Cottrell's theory[7] for serrated flow describes reasonably well the qualitative aspects of serrated flow in aluminum 6061 alloy. However, there are quite a few aspects neither this theory or any other can account for.

2. Photoelastic coatings proved to be a powerful tool in the study of serrated flow. Besides, quantitative information about the phenomena involved could also be obtained, if desired.

3. Serrated flow was commonly observed in aluminum 6061 alloy. The irregularities observed included jerky flow, Type A and Type B serrations. .The character of the serrations depends on the level of strain in the material, temperature and strain rate of the tensile test, mechanical characteristics of the tensile apparatus, grain size and heat treatment of the material being tested.

4. .Type A serrations do indeed correspond to the nucleation of deformation bands always in one end of the specimen and their propagation to the other end of the gage length.

a. The load increases during this propagation, and it seems that at least a part of this increase is

183

used in making the band move against a work hardening gradient.

b. Secondary serrations are commonly present during the propagation of a band, and are most probably associated with localized work hardening in the gage length during the early stages of the deformation.

c. Secondary serrations grow quickly in the beginning of the deformation and then fade away rather quickly. This is most probably due to different work hardening caused by a propagating bond in different points along the gage length.

d. This position-dependent work hardening may be associated with different propagation speeds of the band.

e. The initial geometry of the specimen and misalignments in the tensile apparatus are very important in that they seem to determine secondary serrations.

f. The sweeping of bands along the gage length of specimens during Type A serrations seems to enhance the peaks in the strain profile of these specimens.

5. Type B serrations do indeed correspond to the formation of bands along the gage length of a specimen. However, these bands do not propagate. Besides, the bands may form in three ways during a given tensile test: at random along the gage length of the specimen, in the same region other band had nucleated before, or successively ahead of each

other, constituting what has been called discontinuous propagation of the band.

  a. There seems to be no way to identify what kind of nucleation of band is taking place merely by the appearance of the load-time curve for Type B serrations.

  b. The relatively smooth regions that appear during Type B serrations are associated with the smooth transversal propagation of a wedge-shaped band or with the smooth longitudinal propagation of a band over small distances.

6. The load drops observed during deformation in a soft machine of material that would present Type B serrations in a stiff machine are associated with the nucleation and very fast propagation of a deformation band in the gage length of the specimen.

  a. Very complex strain distribution may be associated with the above propagation of a band.

  b. It seems that the deformation associated with each band is far bigger than in the case of a hard machine. Actually, this could cause the observed sudden fracture of specimens during a load drop.

7. As a rule, the strain rate sensitivity of aluminum 6061 alloy is small, and under certain circumstances has some negative tendency.

a. The slope of the load-time curve increases for decreasing nominal strain rate and inversely. This means that at high nominal strain rates one needs less increase in load to keep propagating a band or to keep nucleating bands, in the case of Type B serrations. Propagation of bands during Type A serrations requires less stress for fast bands and more stress for slower bands.

8. It seems that pinning of dislocations during Type B serrations is more efficient than in the case of Type A serrations.

9. The results obtained in this investigation should apply to a wide variety of other substitutional alloys, due to the striking similarity between serrated flow in these alloys and aluminum 6061 alloy.

APPENDICES

APPENDIX I

DESIGN OF A LEAF SPRING
OF SPRING CONSTANT 300 lbs/in

The type of spring chosen is shown in Fig. I-1a; the design conditions are the following:

    Maximum load - 300 lbs

    Spring constant - 300 lbs/in

    Material - Al-2024-T4

This material was chosen because it presents a very good elastic behavior. Its yield stress is

$$\sigma y = 25,000 \text{ psi, with a safety factor of } 1.88[34]$$

The system chosen consists of two springs in series, and actually the design involves only one of the leaves, for a spring constant of 600 lbs/in. This leaf may be considered as a beam with built-in edges, as shown in Fig. I-1b. If a load P is applied at the center of the beam, one may write

$$\frac{P}{y} = 192 \frac{EI}{\ell^3} \qquad (A-1)$$

where y is the deflection at the center of the beam, ℓ is the span of the beam, I the inertia moment of the cross section, and E is the Young's modulus of the material

P
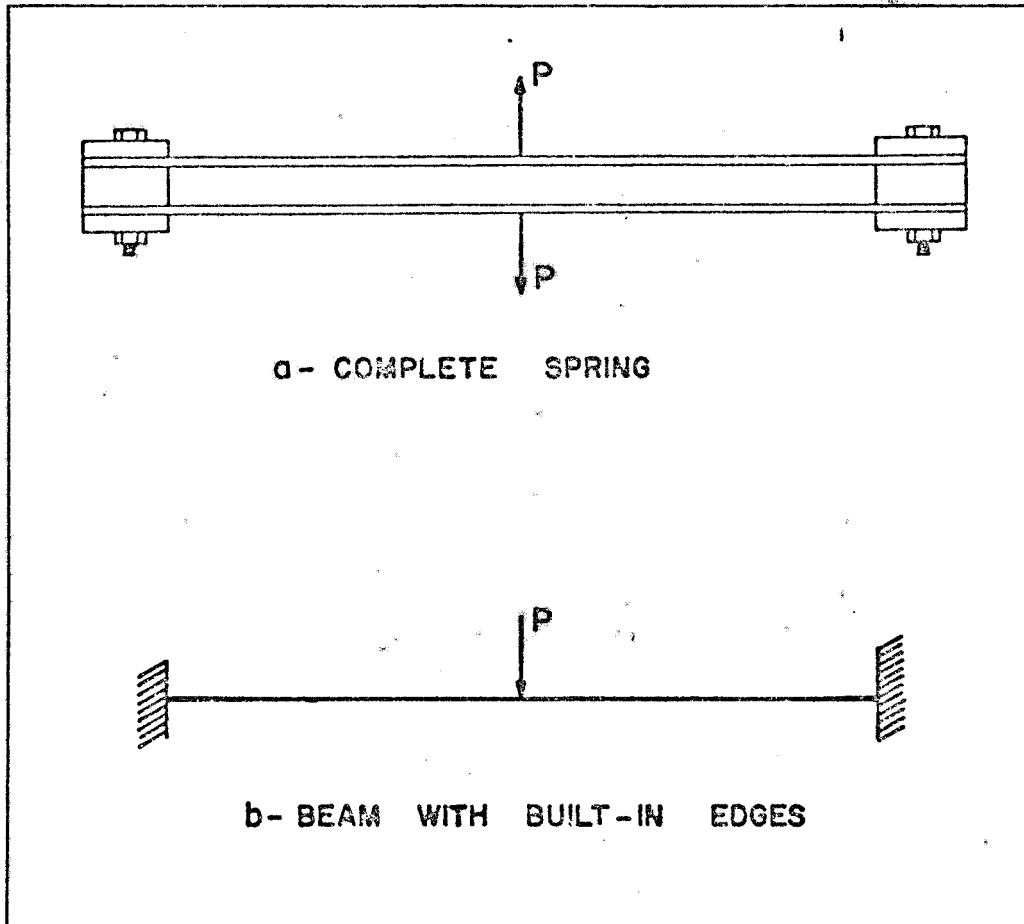
a- COMPLETE SPRING

P

b- BEAM WITH BUILT-IN EDGES

Fig. I-1. (a) Type of spring used for decreasing the
spring constant of the Instron machine.
(b) Ideal beam used for design purposes.

$(10.5 \times 10^6 \text{ psi})$.[34] For $P/y = 600$ lbs/in, one shall have then

$$I = \frac{6\ell^3}{2,016 \times 10^4} \text{ in}^4 . \tag{A-2}$$

Strength of materials requires that

$$\sigma_y = \frac{P\ell}{16} \frac{h}{I} \tag{A-3}$$

where h is the thickness of the rectangular section that shall be used.

Making $\sigma_y = 25,000$ psi, $P = 300$ lbs, and inserting in (A-3) the value of I given by (A-2), one has

$$h = (3.97 \times 10^{-4})\ell^2 \text{ in} \tag{A-4}$$

If b is the width of the cross-section, it may be written that

$$I = \frac{bh^3}{12} . \tag{A-5}$$

Comparing (A-5) and (A-2), one has

$$b = \frac{57,078.9}{\ell^3} \text{ in} . \tag{A-6}$$

Using equations (A-4) and (A-6) as guides, the following values were chosen:

$$\ell = 26 \text{ in}$$

$$h = 1/4 \text{ in}$$

$$b = 4 \text{ in} .$$

APPENDIX II

ELEMENTARY CONCEPTS OF PHOTOELASTICITY[35,36]

Photoelasticity is an experimental technique for stress and strain analysis. In our case, interest is focused on qualitative strain analysis. This method presents the advantages that it gives whole field information, and not point to point; besides, it is particularly useful for members having complicated strain behavior.

A2.1. Photoelastic Behavior

The photoelastic method is based upon a unique property of some transparent materials, in particular, certain plastics. Let us first consider the situation where a polarized, monochromatic ray of light passes through a piece of photoelastic material, along one of the directions of principal stresses. The plastic divides the light into two component waves, each with its plane of polarization parallel to one of the principal planes. Furthermore, the light travels along these two paths with different velocities, which depend upon the magnitudes of principal stresses in the material, or, correspondingly, upon the strains along these directions.

191

Figure II-1 illustrates this phenomenon. Since the
two waves traverse the body with different velocities, they
emerge with a new phase relationship, or relative retarda-
tion. This phenomenon is called double refraction, and it
is produced artificially in photoelasticity, where it is
controlled by the state of stress at each point in the body.

In the case of reflection photoelasticity, there are
some different aspects from transmission photoelasticity,
that has been discussed up to now. In this case, a sheet
of photoelastic material is glued to the part to be studied,
and a reflective backing is put between the plastic and the
part. When the plastic is now illuminated with monochro-
matic polarized light, the split beam is reflected back by
the reflective backing instead of passing through the plas-
tic, as was the case in transmission photoelasticity.

One of the advantages of reflection photoelasticity is
that the retardation of the waves is doubled, because the
light traverses the plastic twice. This enhances the sensi-
tivity of the results. Since this method was the one used
throughout this work, we shall refer only to it from now on.

A2.2. Analysis of Results

The two reflected split waves are brought together in
an apparatus known as photoelastic polariscope and per-
mitted to come into interference. Since there is a rela-
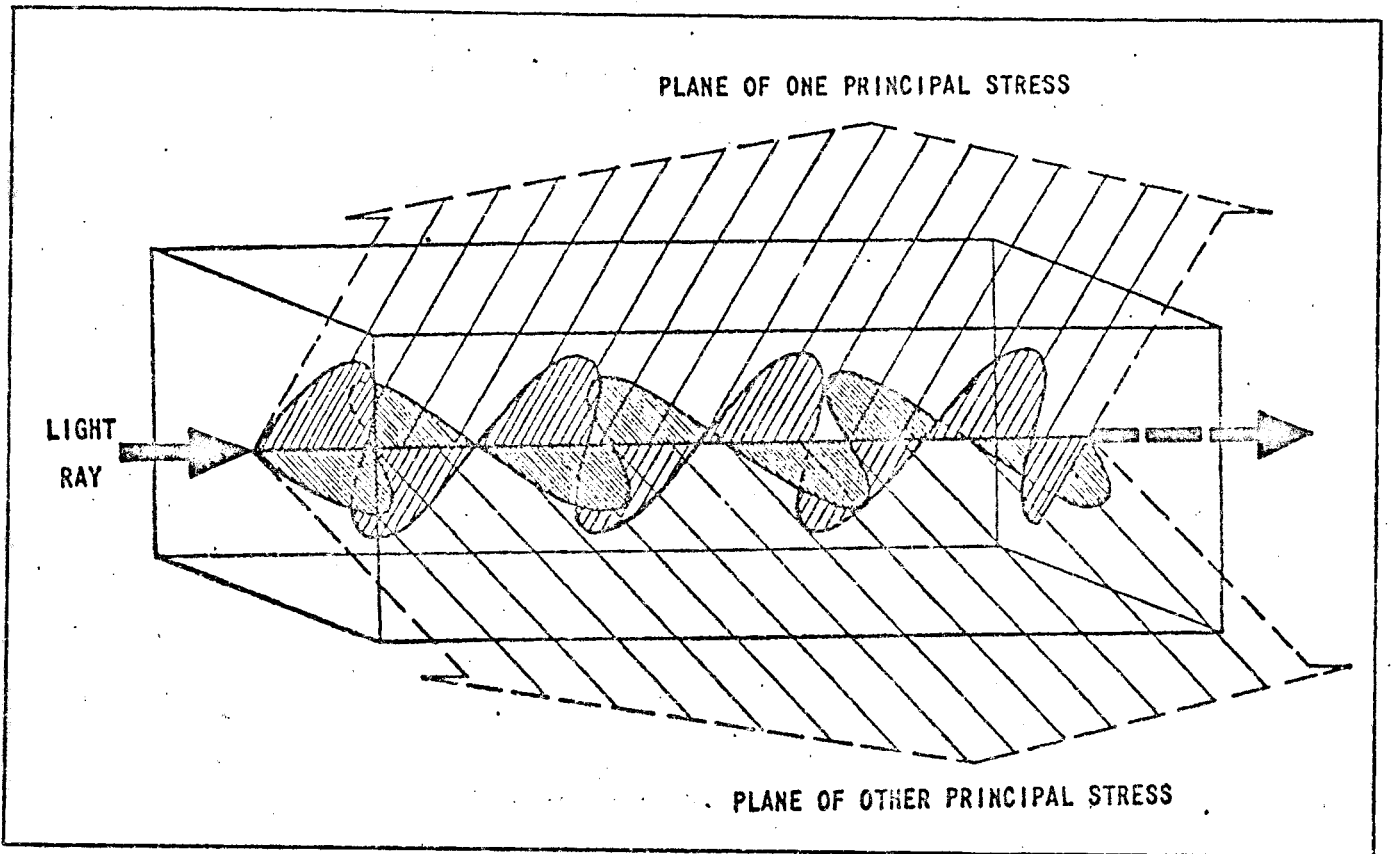tive retardation in the waves, and this retardation changes

Fig. II-1. The phenomenon of double refraction.[35]

from point to point, in some regions these waves will rein-
force each other, while in others they will interfere
destructively, causing zero light intensity. One shall end
up then with an overall pattern of black fringes and white
regions, as shown in Fig. II-2. However, when white light
is used instead of monochromatic light, one has a pattern
of colors besides the fringe color.

With the use of white light, one has simultaneous
illumination by all the wavelengths of the visible spectrum;
however, waves of different wavelengths do not interact,
and each wavelength displays its own intensity pattern in
its own color. The result is a superposition of patterns
for all wavelengths employed, and at any point in the plastic
the resulting color is a unique function of the stresses, and
points equally stressed comprise a band in a colorful iso-
chromatic pattern. This also presents the advantage that
the human eye perceives more easily variations in color than
maximum or minimum intensity points in a monochromatic pat-
tern. Fringes can still be observed easily, as regions
where colors suddenly change, for example, from red to green,
in a narrow, purple band, for the first three fringes formed.

If the fringes are observed as tightly grouped loops
confined to a single area (see contact points in the wrench
in Fig. II-2), it means that the strain varies rapidly from
one point to another, resulting in a stress concentration.
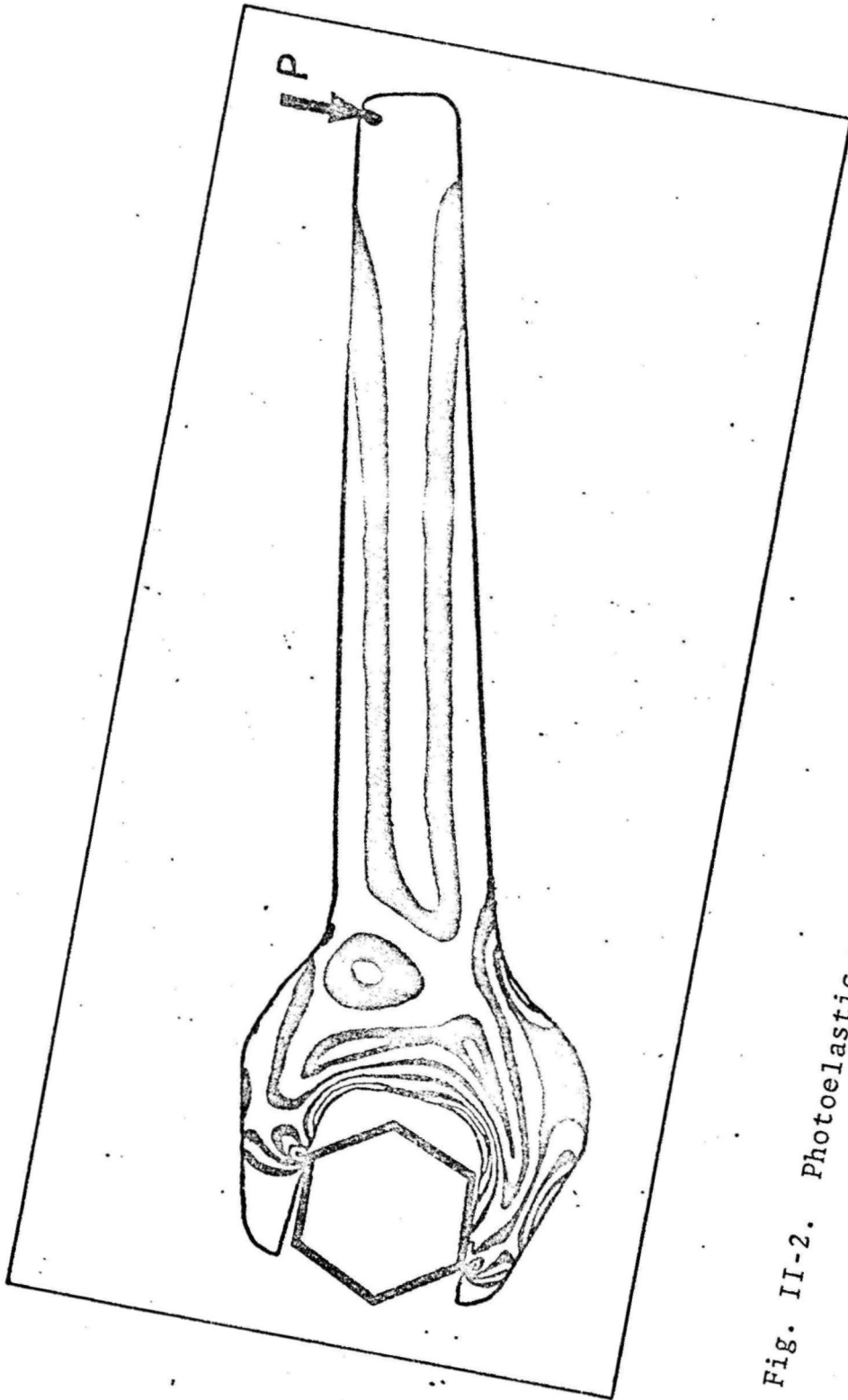On the other hand, a single uniform color, as in the case of

P

Fig. II-2. Photoelastic pattern for a wrench model. 35

a tensile specimen ideally aligned, indicates that the strain is behaving uniformly over the entire area, neither increasing nor decreasing from one point to another.

A2.3.   The Reflection Polariscope

This instrument is shown schematically in Fig. II-3. In practice the obliquity of illumination is small, normally less than 3 degrees, and conditions of normal incidence are assumed.

Basically, the polariscope operates the following way: the light leaves the light source and goes through a polarizer P, that divides the incident light waves into vertical and horizontal components, absorbs for example all the vertical components and transmits only the horizontal components. Next, this ray of light goes through a quarter-wave plate, that behaves exactly like a photoelastic material that retards one of the split waves by a constant quantity of a quarter of a wave. It is oriented with its principal planes at an angle of 45 degrees to the axis of the polarizer P. This quarter-wave plate serves to supply equal quantities of light along each of the two planes of polarization at every point in the photoelastic coating. After the ray of light is reflected by the reflective backing in the plastic, it goes again through another quarter-wave plate and through the analyzer A, which actually is another polarizer. This is necessary for the waves to develop
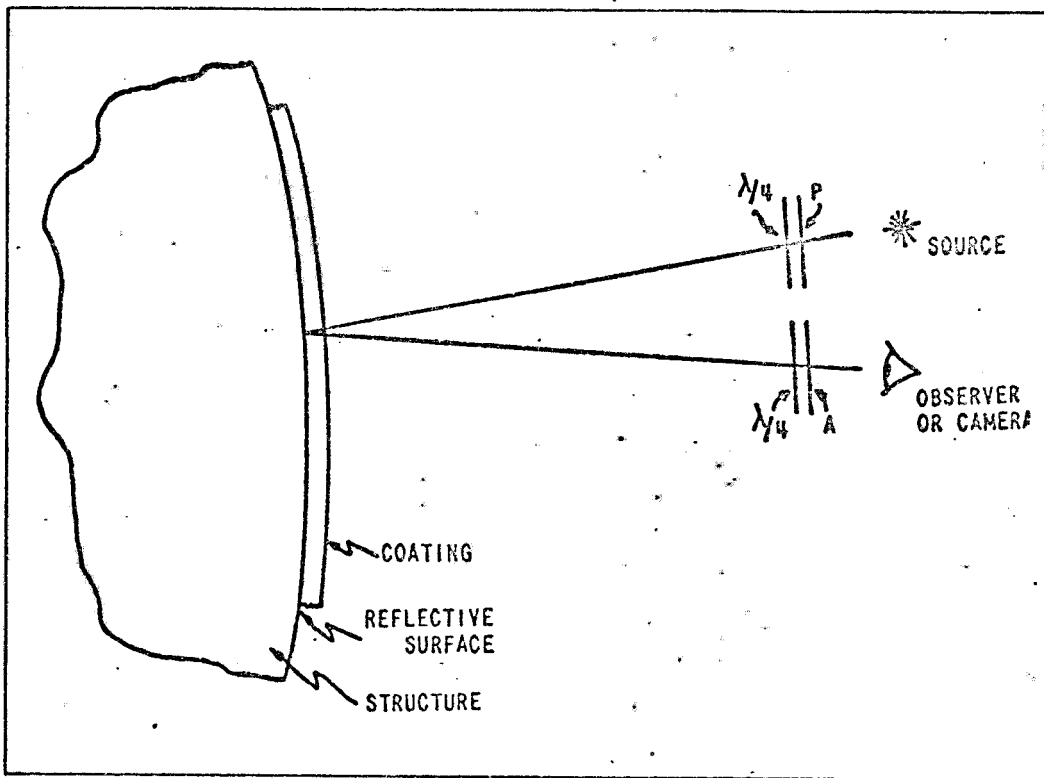
Fig. II-3. Reflection polariscope arrangement for photo-
elastic coating observations.[35]

interference patterns. The observer then is able to observe or photograph the pattern obtained.

The instrument described is the so-called circular polariscope; a plane polariscope does not have the quarter-wave plates in the light path, and the reflected light intensity will depend on the direction of the principal stresses.

A2.4. Photoelastic Material

In our case, we have dealt with extremely low modulus plastic (1,000 psi). This has greatly decreased any reinforcement effects. The plastics are characterized by a strain-optical coefficient, k, similar to the "gage factor" of resistance strain gages. However, the sensitivity of the material used depends very much on its thickness, and one may lump together in a constant, "f," both the effects of material and thickness. This constant gives the strain, in microinches/inch, necessary for the formation of a fringe in the material, and can be easily used in the selection of the most appropriate coating for a certain purpose.

Since the sensitivity is proportional to coating thickness, the question of how thick the coating can be has gained attention. It can be shown that the strain in the coating exactly matches that at the structure coating interface when no shear forces are developed at the interface. Then, there is no direct limitation on thickness.

In the case of a flat tensile specimen of any shape, if the coating is merely clamped at its ends to the tension bar, the two elements will experience identical displacements and strains everywhere, except in the immediate vicinity of the clamps. Even when the coating is bonded along the entire surface, shear forces are developed only near the ends previously clamped, and no forces are developed in the adhesive in the remainder of the sandwich. The strain is constant through the thickness of the coating and equal to the interface strain. Under these conditions, the photoelastic results provide an accurate account of the surface strain in the structure.

This argument holds exactly when Poisson's ratio of the structure and coating are exactly equal. Since Poisson's ratio is nearly the same for most structural materials and common coating materials, there has been no evidence of significant discrepancies associated with this mismatch.

LIST OF REFERENCES

1. A. W. McReynolds, Trans. AIME, 185 (1949) 32.

2. A. Rosen and S. R. Bodner, Mater. Sci. Eng., 4 (1969) 115.

3. P. G. McCormick, Acta Met., 19 (1971) 463.

4. J. D. Lubahn, Trans. ASM, 44 (1952) 643.

5. E. Macherauch and D. Munz, Zeit. Metallke., 57 (1966) 552.

6. B. J. Brindley and P. J. Worthington, Central Electricity Research Laboratories, Lab Note No. RD/L/M 265, February 1970.

7. A. H. Cottrell, Phil. Mag., 44 (1953) 829.

8. A. W. Sleeswyk, Acta Met., 6 (1958) 598.

9. A. Rosen and S. R. Bodner, J. Mech. Phys. Solids, 15 (1967) 47.

10. J. D. Lubahn, Metals Transactions, 185 (1949) 702.

11. A. T. Thomas, Acta Met., 14 (1966) 1363.

12. F. LeChatelier, Rev. de Met., 6 (1909) 914.

13. A. Portevin and F. LeChatelier, C. R. Acad. Sci., 176 (1923) 507.

14. Sutoki, Sci. Rep. Tohoku Imp. Univ., 29 (1941) 673.

15. Lüders, Dinglers Polytechnisches Jnl., 156 (1860) 18.

16. Hartmann, Distribution des Deformations dans les Metaux Soumis a des Efforts, Berger Levrie (1896).

17. B. Russel, Phil. Mag., 8 (1963) 615.

18. P. J. Worthington and B. J. Brindley, Phil. Mag., 19 (1969) 1175.

19. P. R. Cetlin, unpublished data, Univ. of Florida, 1971.

20. A. Rosen and S. R. Bodner, J. Mech. Phys. Solids, 15 (1967) 63.

21. A. Rosen, Mater. Sci. Eng., 7 (1971) 191.

22. P. G. McCormick, Scripta Met., 4 (1970) 221.

23. W. Charnock, Phil. Mag., 18 (1968) 83.

24. R. K. Ham and D. Jaffrey, Phil. Mag., 15 (1967) 247.

25. S. R. Bodner, Mater. Sci. Eng., 2 (1967) 213.

26. R. E. Reed-Hill, Mechanical Metallurgy course, Univ. of Florida, Winter 1971.

27. R. E. Reed-Hill, Physical Metallurgy Principles, 1st ed., D. Van Nostrand, 1964.

28. W. P. Longo and R. E. Reed-Hill, Scripta Met., 4 (1970) 765.

29. Metals Handbook, Vol. I, 8th ed., 1969, p. 946.

30. ASTM standard E8.

31. Instructions for Bonding Flat and Contoured Photoelastic Sheets to Test Part Surfaces, Photolastic Company, Bulletin IB-P-320.

32. A. S. Gülec, Univ. of Florida, unpublished data.

33. A. Wijler and J. Schade van Westrum, Scripta Met., 5 (1971) 159.

34. Metals Handbook, Vol. I, 8th ed., 1969, p. 940.

35. D. Post, Photoelasticity, Manual on Experimental Stress Analysis, Society for Experimental Stress Analysis, 2nd ed., chapter IV, p. 29, 1965.

36. Introduction to Stress Analysis by the Photoelastic Coating Technique, Photolastic Company, Inc., Technical Bulletin TDG-1 (1971).

BIOGRAPHICAL SKETCH

Paulo Roberto Cetlin was born on December 12, 1946, in Belo Horizonte, Brasil, where all his studies, up to his B.S. degree in Mechanical Engineering, were completed. After finishing elementary school in a private institution, he was graduated from a state high school and admitted to a federal engineering school, the Escola de Engenharia da Universidade Federal de Minas Gerais. He received his B.S. degree in December, 1969.

The author was admitted to the University of Florida in September, 1970, when he began to pursue studies for the degree of Master of Science in Engineering. He was a Graduate Research Assistant during his time at the University of Florida.
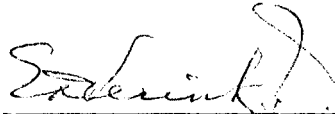
The author is a member of Alpha Sigma Mu, American Society for Metals, and National Association of Corrosion Engineers.

I certify that I have read this study and that in my
opinion it conforms to acceptable standards of scholarly
presentation and is fully adequate, in scope and quality,
as a thesis for the degree of Master of Science in Engi-
neering.

R. E. Reed-Hill, Chairman
Professor of Metallurgical
and Materials Engineering

I certify that I have read this study and that in my
opinion it conforms to acceptable standards of scholarly
presentation and is fully adequate, in scope and quality,
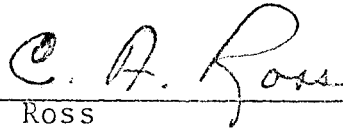as a thesis for the degree of Master of Science in Engi-
neering.

E. D. Verink, Jr.
Professor of Metallurgical
and Materials Engineering

I certify that I have read this study and that in my
opinion it conforms to acceptable standards of scholarly
presentation and is fully adequate, in scope and quality,
as a thesis for the degree of Master of Science in Engi-
neering.

C. S. Hartley
Associate Professor of
Metallurgical and Materials
Engineering

I certify that I have read this study and that in my opinion it conforms to acceptable standards of scholarly presentation and is fully adequate, in scope and quality, as a thesis for the degree of Master of Science in Engineering.

_____
C. A. Ross
Assistant Professor of
Aerospace Engineering

This thesis was submitted to the Dean of the College of Engineering and to the Graduate Council, and was accepted as partial fulfillment of the requirements for the degree of Master of Science in Engineering.

March, 1972

_____
Dean, College of Engineering

_____
Dean, Graduate School